This project has received funding from the European Union's Seventh Programme for research, technological development and demonstration under grant agreement No [308417]".

New Directions in Seismic Hazard Assessment through Focused Earth Observation in the Marmara Supersite

Grant Agreement Number: 308417
Co-funded by the European Commission within the Seventh Framework Programme THEME [ENV.2012.6.4-2]-[Long-term monitoring experiment in geologically active regions of Europe prone to natural hazards: the Supersite concept]

D8.3 Synthesis report on spectral and statistical analysis of marine multi-parameter time series

Project Start Date	1 November 2012
Project Duration	42 months
Project Coordinator /Organization	Nurcan Meral Özel / KOERI
Work Package Number	WP8
Deliverable Name/ Number	Synthesis report on spectral and statistical analysis of marine multi-parameter time series/ D8.3
Due Date Of Deliverable	29/02/2016
Actual Submission Date	29/04/2016
Organization/Author (s)	Ifremer / Louis Géli & Gaye Bayrakci – CEREGE / Pierre Henry, Ben Hepburn –ITU / Sinan Ozeren

Dissemination Level		
PU	Public	
PP	Restricted to other programme participants (including the Commission)	
RE	Restricted to a group specified by the consortium (including the Commission)	
CO	Confidential, only for members of the consortium (including the Commission)	

CONTENTS

Abstract

Using datasets collected in the Sea of Marmara (Western Turkey), the following work has been done:

Within Task 1 ("Simulate multi-parameter acquisition using the available datasets"), different datasets have been found and made available to the project. These include data acquired by Ifremer in 2009 and 20011: seismological data from Ocean Bottom Seismometers (OBS), pore pressure data from deep seafloor piezometers, seabottom temperature and acoustic data from a Buble Observatory (BOB). A specific software (Visumultiparameter) has been developed to visualize, to process and to analyze seismograms, sea-bottom temperature and sediment pore pressure simultaneously. Sea floor pressure records from KOERI observatories and from Marnaut cruise (2007) were also examined.

Within Task 2 ("Implementation of pre-processing procedures"), pre-processing procedures have been applied to the different datasets (e. g. data reduction, reformatting, time drift correction, amplitude and gain correction, offset removal, etc).

Within Task 3 ("Analysis of BOB data"): automatic, but separate, procedures have been developed: i) to apply echo-integration for the computation of acoustic backscatter amplitudes; ii) to represent echo-integration results in a geo-referenced frame; iii) to compute the flow rates of the identified gas sources. The work within Task3 is fully reported in *Leblond et al (2014)* and in *Bayrakci et al (2014).*

Within Task 4 ("analysis of OBS data"), procedures for the analysis of background noise and event characterization from OBS recordings have been developed. Most particularly, a specific tool was developed and tested to detect and characterize the short-duration, non-seismic signals that are known too commonly occur at the seafloor.

Within Task 5 ("Base-line characterization"), the real significance of the non-seismic, short duration events (SDE) was studied.

Within Task 6 ("Multi-parameter data cross-correlation"), the BOB data was analyzed jointly with the OBS data and the piezometric data, following a deterministic, direct approach.

Within Task 7 ("Bottom pressure records"), a spectral analysis of available pressure records was performed.

The analysis conducted in the present study shows:

1. BOB is a powerful tool to detect gas bubble emissions, within a radius of a few tens of meters that directly depends on the acoustic frequency. The echo-integration method allows the characterization (flow rate, source location, etc) of gas emissions.

2. Collocated OBS (and acoustic gas bubble recorders (BOB) represent a very promising

way to directly monitor gas related processes within the uppermost sediment layers:

- Numerous Short-Duration Events (SDEs), having a duration of less than 1 second, are commonly observed on the OBS records.
- The common analysis of OBS data and BOB data confirms previous interpretations, that SDEs are directly related to gas emissions from the seafloor.
- Crisis of SDEs may occur remotely (at distances of up to 10 km), in response to earthquakes of moderate magnitude (M ~ 3 - 4). Seismic ground shaking may thus trigger gas outbursts from the seafloor.
- The real significance of SDEs for geohazards monitoring is still not understood.

3. The piezometers have clearly recorded variations in sediment pore pressure, triggered by transient, seismic signals. One case of correlation was also observed between the occurrence of SDEs and pore pressure decrease recorded at 5 m below seafloor. The quantitative relation between ground motions and pore pressure variations requires further investigation, through additional data acquisition and numerical modelling.

4. The present study suggests the following recommendations:
    - Gas bubble emissions at a given site may be continuous (over the duration of the survey) or transient, at a variety of time scales (minutes, hours, days). Hence, multibeam, bathymetric surveys -on a regular, monthly or yearly basis- are strongly recommended to complement local BOB surveys, not only to determine the geographical distribution of gas emissions sources beyond the BOB acoustic range, but also to assess the continuity of gas emissions at the scale of months or years.
    - Sea-bottom currents may strongly affect the acoustic energy that is backscattered by the gas emission sources. Hence, current measurements are very much needed to help interpret the BOB echo-integration results.
    - With the present version of BOB, flow rates can be computed accurately only if the gas bubbles emitted by the source are all located within the insonified area of 7°. An acoustic system allowing the continuous insonification of a volume larger than the actual 7° is needed to compute the flow rates of wider sources. This may be done by replacing the actual split-beam echosounder of BOB with a multi-beam echo-sounder. Or, several split-beam echo-sounders may be used to insonify a larger area. *Either solution will also greatly improve the joint analysis of acoustic and seismologic data*.
    - Precise positioning is needed for BOB and OBS deployments.
    - Bottom pressure recorders with digiquartz type sensors should be deployed in

the deep basins in order to better understand the hydrodynamics in the Sea of Marmara in relation with tsunami modelling and early warning, and also as pressure variations in the water column may influence pore pressure in the sediment and gas emissions fluxes.

1. Task 1. Simulate real-time acquisition using available, multi-parameter data

1.1 Overview of the available datasets

1.1.1 Survey area

The dataset used in the present study was collected in the Sea of Marmara Sea (Fig 1.1.1.1), in NW Turkey. This area is one of the most adapted site worldwide to study the predictability of earthquakes, for at least 4 reasons: i) there is a high probability that an earthquake of Mw > 7.0 will strike within the next decades along the NAF in the Sea of Marmara, directly affecting the heavily populated Istanbul area; ii) the segment having the highest probability to rupture is relatively well determined [e.g. Parson, 2004]. The two other reasons are less known, both resulting from recent findings: iii) recent work has reported that the observation of the nucleation phase of the Mw 7.4 Izmit earthquake, which devastated part of northwestern Turkey in 1999, was accompanied by tremors for at least 44 minutes before the main shock [Bouchon et al., 2011]; iv) gas emissions were found in the water column near the seabed expressions of known active faults [Géli et al., 2008]. The finding that thermogenic gas is expelled through the North Anatolian fault zone opens new perspectives that were not even imaginable a few years ago, and supports the necessity to monitor gas emission activity along with seismicity. If seismic tremors or other anomalous seismic activity are found to be associated with anomalies in gas emission activity, then we could have more criteria for characterizing and identifying transient slip events on the offshore fault segments.

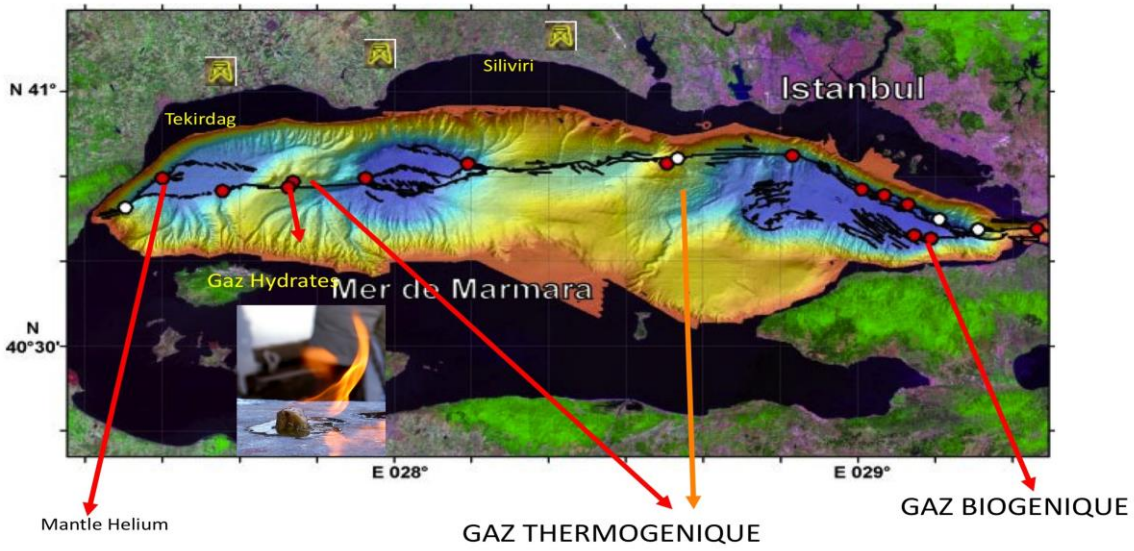

Figure 1.1.1.1 In 2007, the North Anatolian Fault (indicated as black lines) has been shown to cut thermogenic gas reservoirs within the Sea of Marmara.

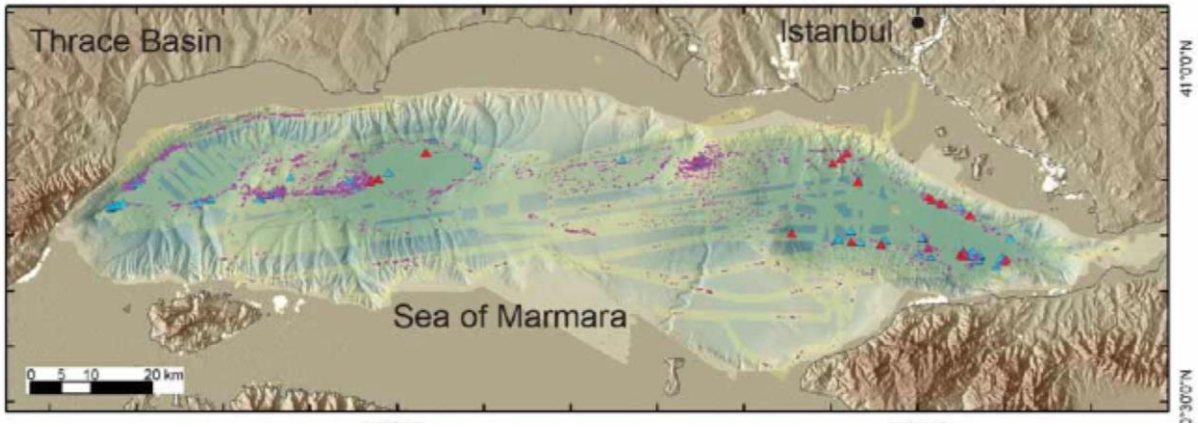

Figure 1.1.1.2, from Dupré et al., [2012], in prep. : Violet dots indicate the gas emissions sites that were detected in a variety of environments within the Sea of Marmara, using the multibeam echosounder SIMRAD EM-302 of R/V Le Suroit in 2009. Yellow stripes indicate the trace of the swath coverage of EM-302 on the seafloor. Red and blue triangles indicate gas emission sites identified in 2000 and 2007 using non-systematic, acoustic coverage in specific places [Géli et al, 2008].

1.1.2 Instrument description

In the present study, we will use data collected with 3 different types of instruments: a Bubble OBservatory (BOB) for acoutic bubble dectetion (BOB), Ocean Bottom Seismometers (OBSs), and piezometers.

BOB

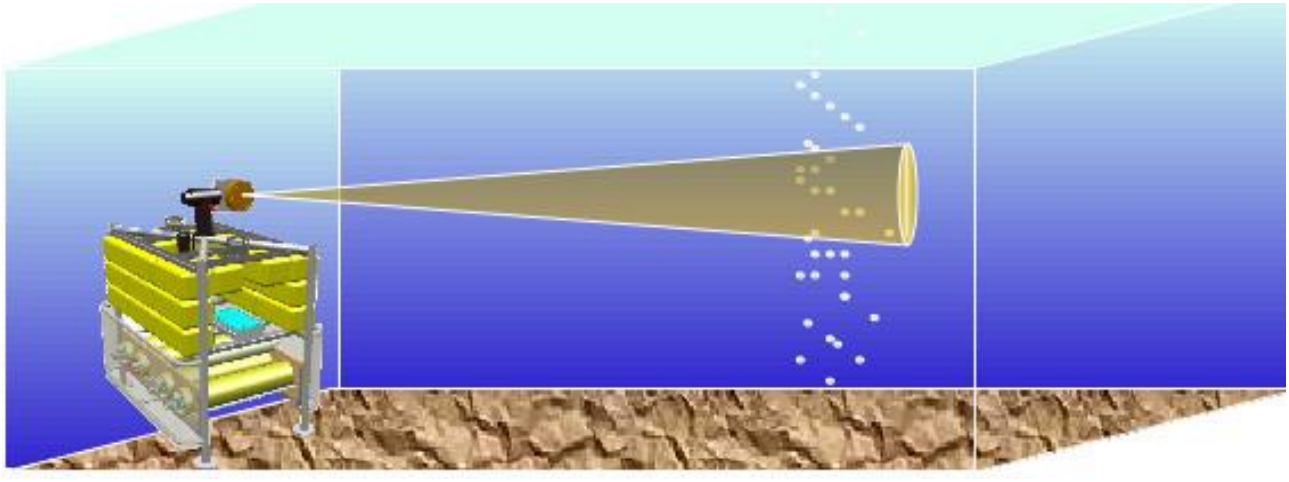

Figure 1.1.2.1: Schematic representation of the Bubble Observatory Module (BOB).

BOB is a module (Fig 2.1.1) designed to provide short time series data of gas seeps flow rates. It is a standalone acoustic lander which is deployed on the sea-floor to insonify horizontally the water column and to record continuous data BOB, in its standalone version, must be seen as a demonstrator device before the installation of cabled versions in the framework of a sea-floor observatory.

The system is equipped with a single beam echosounder (active acoustics) running on battery with a nominal autonomy of 25 days. The choice of the frequency was dictated by the compromise among several features such as target size detection versus pulse resolution and useful detection range versus mechanical system dimensioning for ease of deployment. The 120 kHz split-beam transducer allows the insonification of a water volume bounded by the circular opening of the 7° directional beam over a horizontal distance of 100 m.

Since the transducer is mounted on a pan & tilt system (about 1.5 m above the seafloor), the insonification volume can be sequentially increased by horizontally rotating the transducer with 7° pan steps. Thereby, the echosounder insonifies an angular sector of 7° during a given interval of time, then it rotates 7° clockwise to insonify the next sector. The tilt angle is typically 5° upwards, in order to avoid reflections from fixed obstacles (e.g. topography).

OBSs

The seismological data discussed in the present study were recorded by short-period (4.5 Hz) OBSs equipped with one hydrophone and three velocity sensors : one vertical and two horizontal. The orientation of the horizontal components is provided by a compass, with an accuracy of ± 2,5°. The characteristics of the instruments are described in the table below.

General	Depth maxi. Weight in air Total weight in air with anchor Weight in water Total weight in water with anchor Dimensions (H / L / I)	5 000 m 50 kg 75 kg -8 kg 17 kg L 550 x l 550 x H 700 mm
Sensors	4 components Sensibility hydro Hydrophone LF-3dB Hydrophone signal full scale Geophones Geophone central frequency Geophone sensibility Geophone full scale Orientation	1 hydro et 3 géophones - 160 dB ref. 1 mV/microPa 2 Hz 70 Pa 3 axes 4,5 Hz (-3 dB) 22,4 mV/mm.s-1 +/- 0,38 mm.s-1 Compas 3 axes
Acquisition	Seismic channels Resolution Sampling Frequency Band width Preamp Gain Clock Clock drift correction Synchronisation Interface Data Storage Configuration Interface	4 24 bits 25 à 250 Hz DC to 0,40 x f échantillonnage Variable, from 1 to 64 5.10^{-8} Linear correction DCF 77 (signal GPS) 32 Go (disk IDE SSD) RS232 (9 600, 1, 1)
Energy	Battery pack Alcaline or Lithium Electric Consumption Autonomy	Li-ion 0,7 W recording, 0,3 W low power 1 to 12 months
Release	Release Unit Acoustics Depth maxi	Minirelease titanium + imbedded electronics Hydrophone 5 000 m
Localisation	Flash Gonio VHF	Novatech (ST 400-A) Novatech RF700A-1VHF 156,625 MHz

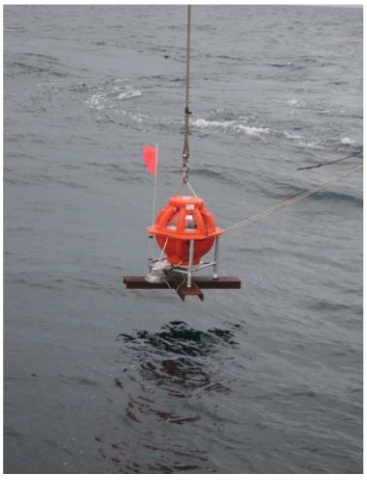

Figure 1.1.2.2: Ifremer's OBS at launch, off-board R/V Urania in 2009.

Piezometers

During the Marmesonet 2009 experiment, 5 piezometers were deployed to measure the in situ pore pressure within the Cinarcik Basin, within the neighborhood of the OBSs Piezometers are made of an expandable part, which consists in a 9 m long needle which penetrates into the sediments, and a recoverable part that contains data storage and batteries (Fig. 2.3.1). The needle is equipped with 6 differential pore pressure sensors and 6 temperature sensors collocated at at 0.79, 3.84, 5.39, 6.94, 7.74 and 8.54 m respectively. Differential pore pressure sensors measure the difference between hydrostatic pressure and in situ pore pressure at various levels via porous stone filters. The sensors measure a current which depends on the deformation of a quartz fixed on a membrane. A positive excess pore pressure corresponds to a higher pressure compared to hydrostatic pressure. Piezometers have one sensor per monitored depth, with separated clocks and electronics. Sensors are inside the soil, in contact with sediments. A cable filled with seawater connects the sensor with the reference pressure up to the seafloor. Sensors are inside the soil, in contact with sediments. A cable filled with seawater connects the sensor with the reference pressure up to the seafloor.

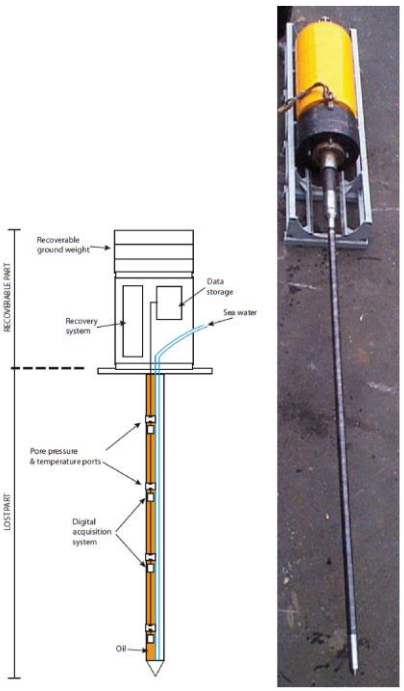

Figure 1.1.2.3 Ifremer's piezometer.

Piezometer	Lat. (deg.)	Long. (deg.)	Depth (m)	Duration	Recording period (at 1 s sampling interval)
PZ-A	N40.758417	E 28.797767	1199	153 days	27/09/2009 - 27/02/2010
PZ-B	N 40.719317	E 29.117067	1248	3 days	28/09/2009 - 01/10/2009
PZ-C	N 40.734083	E 29.120033	1265	106 days	28/09/2009 - 12/01/2010
PZ-D	N 40.728217	E 29.385950	168	147 days	29/09/2009 - 23/02/2010
PZ-E	N 40.833383	E 28.937050	1219	11 days	29/09/2009 - 10/10/2009

Sensor	P1	P2	P3	P4	P5	P6
Depth (m)	0.79	3.84	5.39	6.94	7.74	8.54

Table 2.3.1: Coordinates, recording period and sensors depth of piezometers that were deployed during the Marmesonet cruise (sampling frequency: 1 Hz).

Bottom pressure recorders

Few records of absolute pressure are available in the deep basins of the Sea of Marmara. A Paroscientific Digiquartz bottom pressure recorder had been deployed for one year (2007-2008) near a fluid emission site located on the fault in Tekirdag basin (Tryon et al., 2012). The sensitivity of this instrument is less than 10 Pa, even when operating at ambient pressures of more than 10 MPa, corresponding to the depth the Sea of Marmara deep basins. This corresponds to variations of water height of less than 1 mm. These instruments are subject to drift, but can reliably record small pressure oscillations in a broad frequency range.

The KOERI Sea Bottom Observatories were equipped with deep sea Differential Pressure Gauges (Cox et al., 1984). These instruments have a very low noise level (5×10^{-3} Pa^2 /Hz at a period of 100 seconds) but their band width is limited between 2 Hz to 500 seconds (8.3 minutes). Data acquired between April and August 2011 are available from the KOERI archives. Instruments were deployed in Tekirdag Basin, Central Basin and Imrali Basin.

1.1.3 Summary of the different datasets

The multi-parameter datasets that were used during the present study were collected in the Sea of Marmara in 2007, 2009, and 2011, respectively:

Marnaut 2007: During Marnaut cruise of *R/V L'Atalante*, instruments were deployed at fluid

emission sites with Nautile manned submersible, in collaboration between CNRS, Ifremer and Scripps Institution of Oceanography (SIO, La Jolla, CA, USA). Six Chemical and Aqueous Transport (CAT) meters provided by SIO were deployed for one year at three locations (Tekirdag basins, Cinarcik Basin, Western High) in order to measure water fluxes through the sea floor and variations in aqueous fluid chemistry. This deployment showed that aqueous fluid emission is episodic, with flow rates varying in time from background values of mm/yr to cm/yr to peak values exceeding 1 m/yr (Tryon et al., 2012). These variations resulted mostly from local hydrodynamic processes (e.g. convection around gas vent and around brackish water springs) A pulse of high salinity fluid of deep origin was also observed at a gas hydrate and carbonate mound on the Western High but could not be correlated with recorded seismicity (Tryon et al., 2012). During this experiment, a bottom pressure recorder had been deployed in Tekirdag basin. The time series obtained with a sampling rate of about 300 s have been analysed as part of Marsite activities.

Marmara 2009 surveys: These surveys were carried out with *R/V Urania* and *R/V Le Suroit* respectively, as a part of the « Marmara Demonstration Mission Program (MDMP) » supported by the European project ESONET (European Seafloor Observatory Network).

- During the *R/V Urania* 2009 cruise, 10 Ocean Bottom Seismometers (OBS) covering the North Marmara Trough and 5 Piezometers covering the Cinarcik Basin were deployed (Fig. 3.3). The work on this dataset is presented in this final report.

    - During the Marmesonet 2009 cruise of *R/V Le Suroit* the Bubble Observatory module (BOB) was deployed at the southern part of the Cinarcik Basin providing acoustic data between 07/11/2009 and 12/11/2009. Acoustic data from the water column have also been acquired using the SIMRAD EM302 multibeam system of *R/V Le Suroit.* Volume backscattering coefficients were stored along more than 4500 km-long acoustic tracks (Dupré et al., in prep.).

M**armara 2011:** During this survey of *R/V Yunus* from *Istanbul Techncial University*, 10 OBSs from Ifremer were deployed on 15 April 2011 within the North Marmara Trough (Fig.1.1.3). The BOB module has been deployed at the Central High providing data between 12/04/2011 and 20/04/2011. The OBSs were recovered late July 2011. The combined study of OBSs and the BOB module data will be discussed in this report.

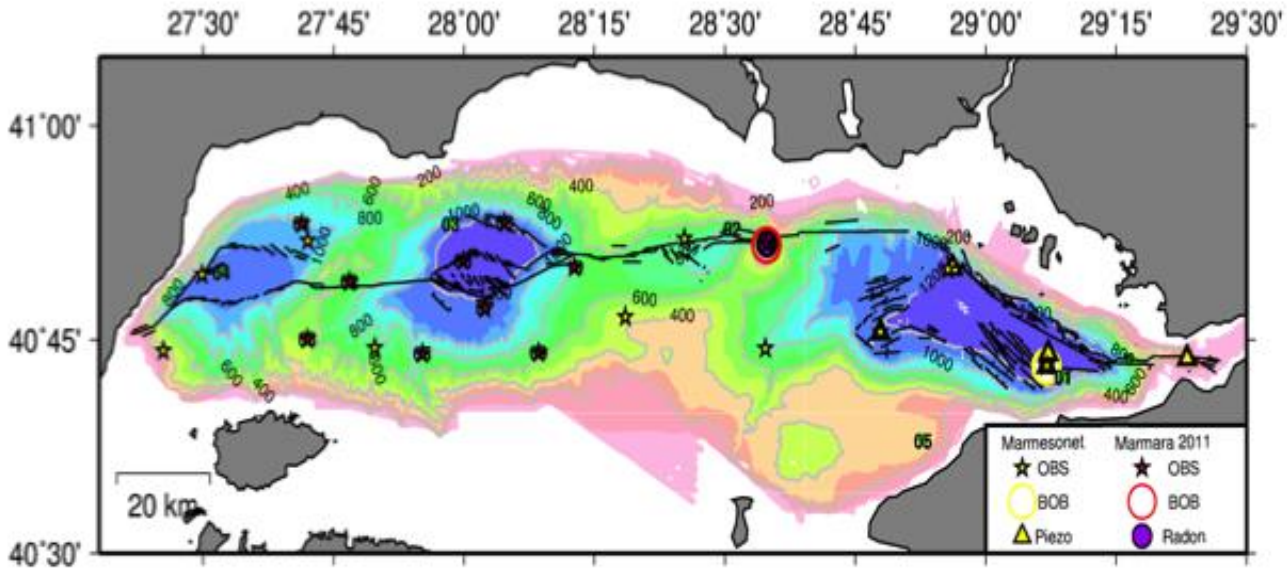

Figure 1.1.3.1: Position of the different instruments deployed during the Marmesonet 2009 (yellow) and Marmara 2011 (red) surveys.

	Acoustic BOB	Acoustic EM 302	Seismologic	Piezometric	Temperature
Marmesonet 2009	07/11/09 15:00 to 12/11/09 00:27 4 complete days of acquisition => 4 cycles	More than 4500 km-long acoustic tracks 21 days of acquisition	01/10/09 to 15/03/10 10 OBSs were deployed OBS 08 is lost	5 piezometers were deployed **PZA** 27/09/2009 to 27/02/2010 **PZB** 29/09/2009 to 01/10/2009 **PZC** 28/09/2009 to 12/01/2010 **PZD** 29/09/2009 23/02/2010 **PZE** 29/09/2009 24/12/2009	Recorded at piezometers Record periods are same as piezometric data
Marmara 2011	12/04/11 to 20/04/11 7 complete days of acquisition => 7 cycles bad raw data on some sectors of 4th, 5th and 7th cycles	None	15/04/11 31/07/11 10 OBSs were deployed. OBS02 stopped recording after 01/07/2011	None	None

Table 1.1.1: Table summarizing the different datasets used in the present study.

1.2 Simulate multi-parameter acquisition using the available, single-parameter time-series: the Visumultiparameters software

A specific software was developed internally by Ifremer to visualize, simultaneously and

synchronously, the data that were collected by the different equipments. Doing so, it was possible to simulate multi-parameter acqusition, using the available, single-parameter time-series collected by the different instruments. The software, called *visumultiparameters.m (matlab code)*, is based on the Graphical User Interface which enables the display of different datasets, simultaneously on the same screen, at any selected dates, asshown in Figure 1.2.1.

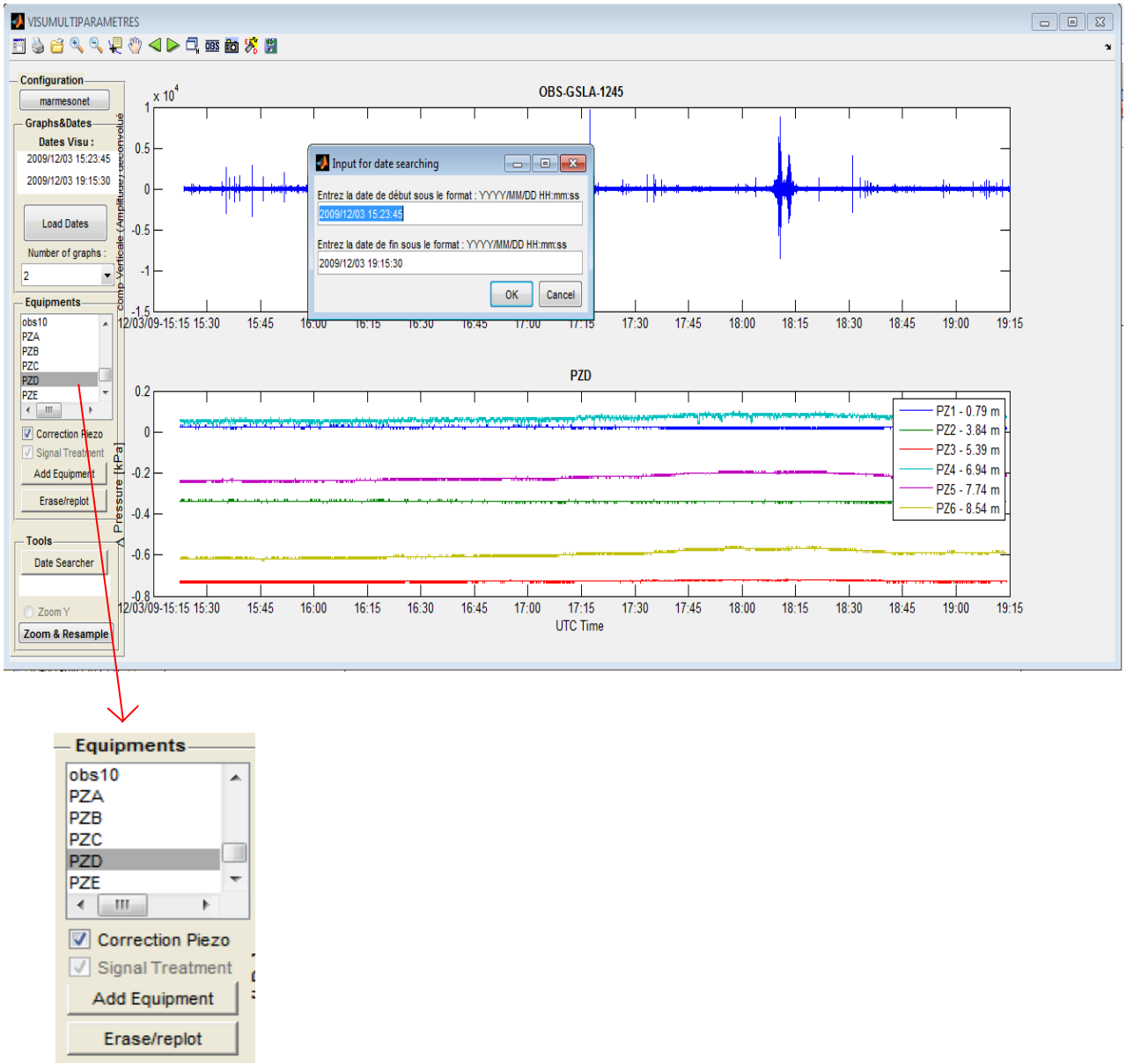

Figure 1.2.1 Screen shot showing an example of data. Here above the data collected by piezometer D and OBS 10 are displayed for a duration of 6 hours (March 12, 2009, from 15:15 to 19:15).

Up to 8 different time-series collected at different sampling rates with different instruments (OBS, temperature, pore pressure, methane concentration, turbidity, etc) may be displayed on the screen using the button "Add Equipment". At any time, the button "Erase/replot", enables the user to choose the plot he wants to replace. The user may also use predefined tools, by

clicking on the icons drawn on the different GUI's panels and following instructions on the screen :

GUI's improved toolbar

ICON	DESCRIPTION
	Launch another VISUMULTIPARAMS application
	Print the current figure
	Open a new figure
	zoom on the data (in and out, on different axes) NB: The graphs are linked by Matlab so when the user zoom on a specific graph the identical zoom is applied to the others to guarantee the simultaneity of the representation.
	DataCursor : a matlab tool to get values at a particular point of the curve plotted
	Pan : move the current curves.
	Move to the previous or next period. The soft calculate the delta between the beginning and ending dates and shift all graphs of this gap, the user does not have to reload the dates every time to review the data.
	Hide ans show main pannels
OBS	**Read and load** a specific .sac file defined by the user
	Take a picture or open a new figure to save datas
	µevents detector : launch a stalta algorithm in order to find all the µevents on the period of time previously setted
	Move and save : combined function of move and save figure automatically

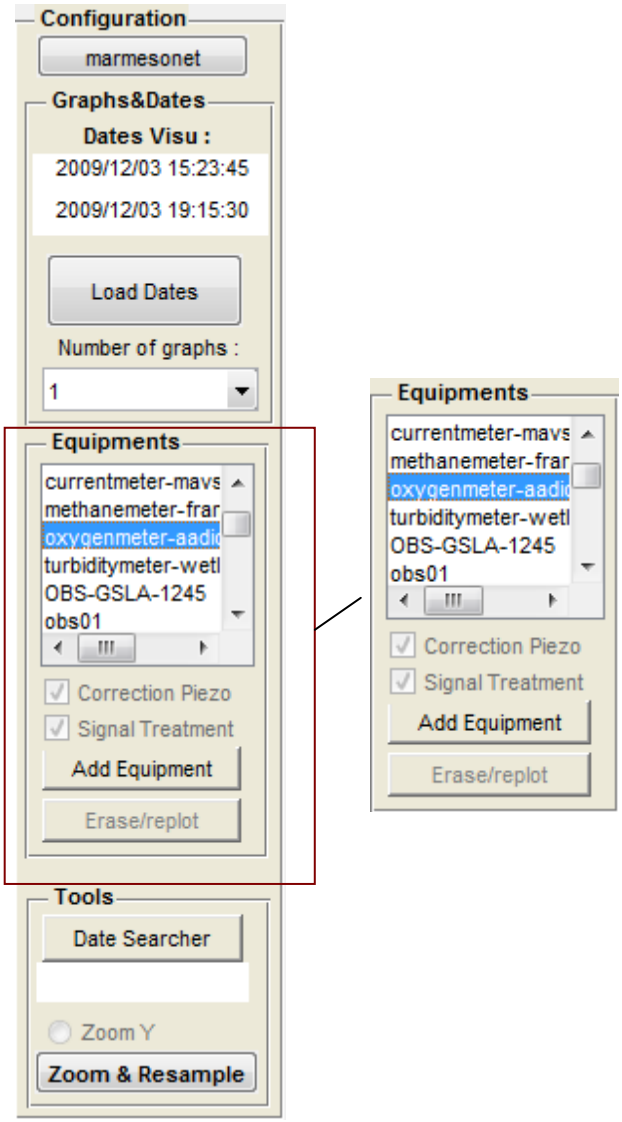

*Figure 1.2.1: Display of the main command panel, as it appears on the screen. The list Box contains the available equipments for the configured project. Ticking the **"signal treatment"** box enables the options **LowPass Filter** and **Deconvolution** for the visualisation period. Ticking the **"Correction Piezo"** box allows the user to set a corrective offset to the piezo dataset if it exists. The "**Add Equipment"** button the user adds a new graph and with **Erase/replot** button he can choose which one of the graphs he wants to replace by the new selected parameter.*

TOOLS	DESCRIPTION
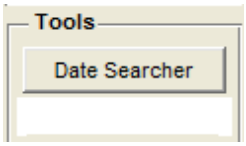	**DateSearcher**: the user gets the current date at the position of the mouse on the graph and prints in the white screen below the Date Searcher's button.
	**Zoom on the vertical axis** on separate figures
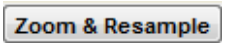	**Rezoom** into a smaller period : the software calculate a new number of points to plot and resample the seismic signal.

Figure 1.2.3: Available "Date searcher" and zooming tools.

The software automatically finds and loads the data requested by the user. But if it finds nothing, it returns an error with an explicative message to the user, thanks to a warning dialogue box. This detection depends on how the data is stored in folders so the user must read the ReadMe file beforehand and know which types of equipments are already supported by the software. The following equipments are supported by the software:

- **Seismometer** (4 components).
- **Piezometer** (2 components : pore pressure and temperature) at 6 different depth levels.
- **Multi-parameter data** stored in csv files, including methane and oxygen concentrations, salinity, sea-bottom temperature, turbidity, etc (not used in this study).

Resampling algorithm. The software is based on Object Oriented Programming, thus each project is internally managed by a predefined driver. Other functionalities can easily be added in order to support new types of equipments by programming new Matlab scripts and updating the driver's process. Due to the differences in format from an equipment to another, the software applies an automatic re-sampling on the data. In fact the great size of the seismic data represents the main obstacle that restricts the range of time scales. For instance, a computer can hardly plot 2 days of raw seismic data (sampled with 125 Hz) because of the millions of points the software has to cope with. Consequently this software has in memory a specific value for the number of points it can plot without sending an internal error (*Out of Memory*). This value comes from the resolution of the computer's screen : the software does not load more data than the maximal amount of points it is able to print . So it always applies a detection algorithm before plotting data.

Plotting long time-series. Plotting data for each equipment on a wide range of time is nearly

impossible and require an upstream treatment. To simplify the simulation, an automatic detection algorithm has been written in order to reduce the number of plotted points without loosing any useful piece of information of the original signal. So, what the user can see depends on the length of the period of the visualisation : with a sampling frequency of 125 Hz (125 samples per second), the data is far much too heavy to be integrally plotted. We admit that an earthquake with a period greater than 2 or 3 seconds can be detected even if the sampling is divided per 2 or even 15. So, with all due respect to Shannon theorem, even if we partially loose the form of the signal, we still see the seismic event. In practice, for instance: 3 seconds represent a small part of the graph, and when the user zooms on the algorithm calculate new series of points more adapted to the size of the visualisation window. Consequently long time-series may be analyzed without loosing resolution while zooming in.

STA/LTA algorithm. The STA/LTA (Short Time Average/Long Time Average) option tool is included in the VISUMULTIPARAMS pack. It allows the user to apply an automatic detection of µevents. The file *eventDetector.m* specifies how this function is applied and which default parameters are taken into account for the internal detection.

Signal processing options. The **deconvolution** of the output signal by the instrumental response is recommended for the Broad-Band Guralp seismometer. For all .sac files, the **lowPass filter** option was included for practical purposes. But this option requires the Matlab **signal processing toolbox**.

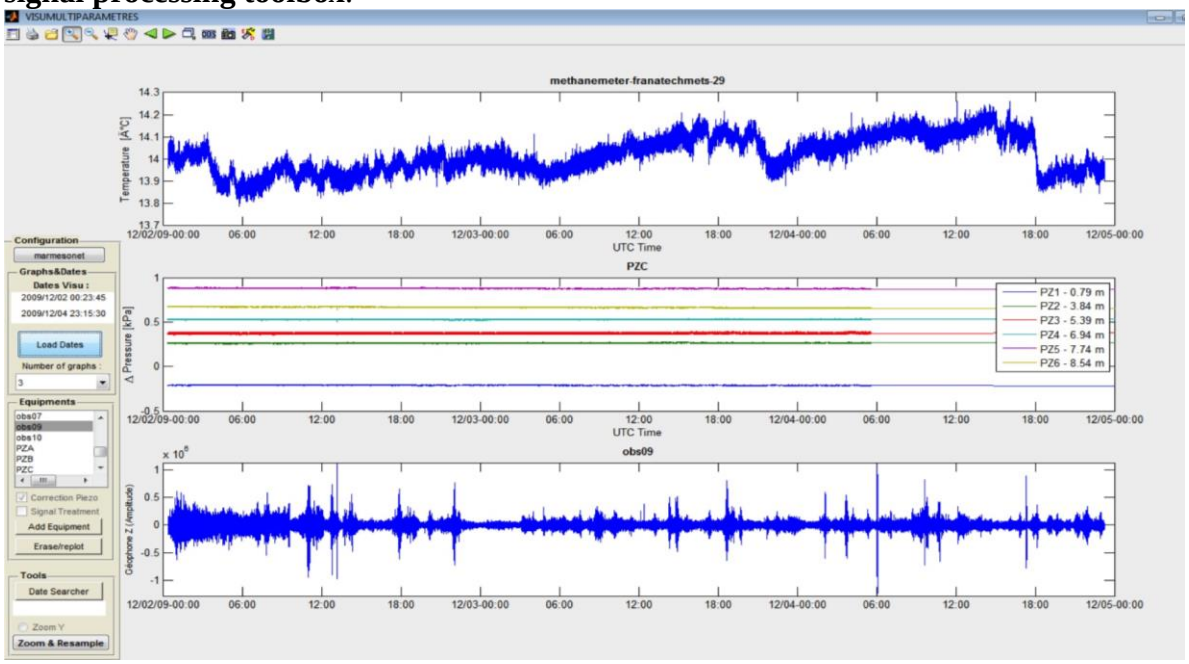

Figure 1.2.4: Example of a 72 hours-long time series of seabottom water temperature, piezometer and vertical displacement velocity.

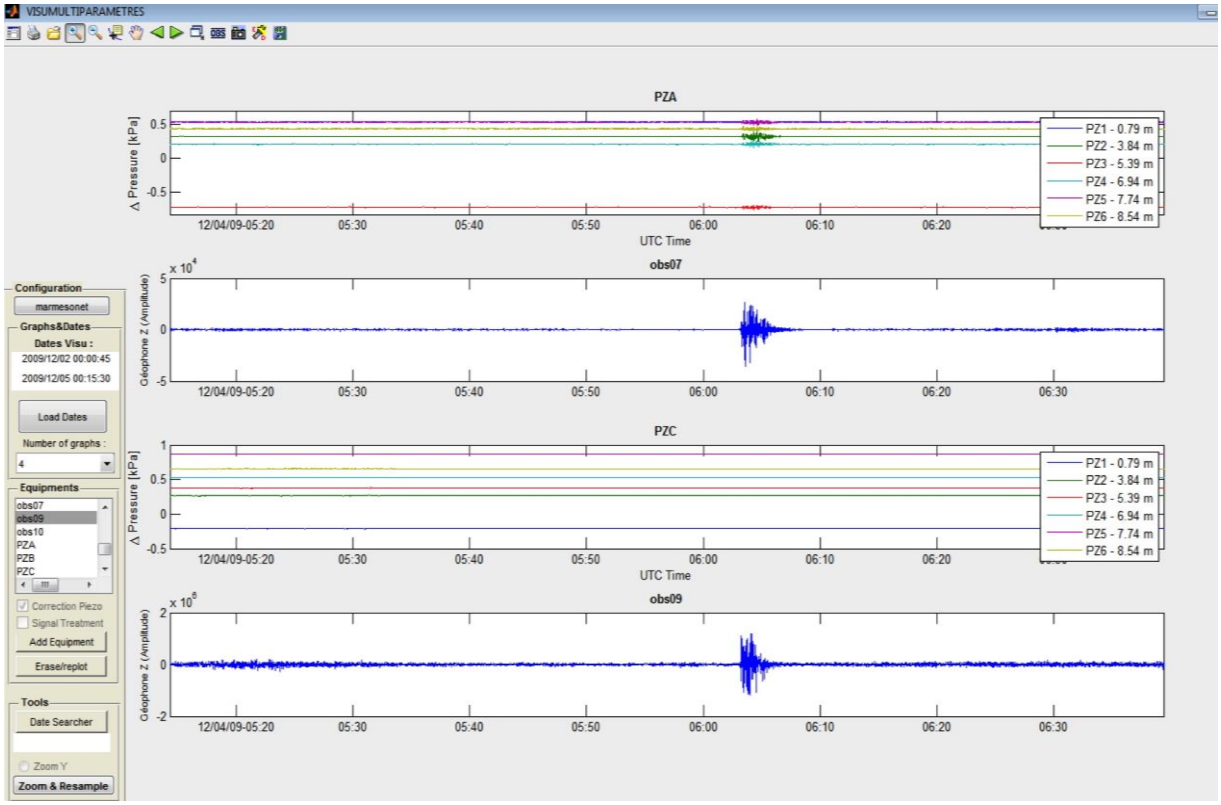

Figure 1.2.5 : Piezometer and vertical displacement velocity recorded at 2 different sites in the Sea of Marmara in 2009.

2. Task 2: Implementation of processing procedures

2.1 BOB

The data processing, as well as the implentation of the processing procedures are detailed in Section 3.1.

2.2 OBS

Based on laboratory results and on *in situ* tests in comparable pressure and temperature, the OBSs' internal clocks are known to drift almost linearly. The time drift of each instrument was thus linearly corrected, based on the total drift that was measured after the recovery of the instrument by comparison with a GPS-synchronized clock.

Classical, on-the-shelf, automated procedures were implemented to detect anomalous data peaks (using STA/LTA-type algorithms) and sequences of missing data (due for instance to low-voltage incidents, which turned to occur at the end of the 3-months recording period on a few OBSs). The "cleaned" OBS data were then converted into the standard, seismological "sac" format, ready for use for the ***Visumutiparameters*** application described in Section 1.3.

2.3 Piezometers3

The piezometric data were first corrected for clock drift. The clock drift depends on the temperature and range from 1.1 s/day at 0°C to –0.3 s/day at 20°C. Assuming a linear variation of the clock drift with temperature, the clock drift is 0.1 s/day on the Sea of Marmara seafloor (14.5 C). The pore pressure and temperature sensors are calibrated for pressure and temperature conditions ranging from 0 to 350 kPa and 0 to 50 C. Pore pressure sensors precision alone is ± 0.2 kPa, however, because of electronics, various oil behavior depending on in situ conditions, homogeneity of the system (possible presence of gas inside sea-water filled cables), and calibration difficulties, the real measure precision is about ± 0.5 kPa.

The analysis of the piezometric data was carried out by visualizing long time series of pressure and temperature measurements (see table 1.1.1 for recording periods). Anomalous values (peaks) were detected and removed from the time series. Missing records were also indentified and listed. Pressure variations exceeding the pressure sensor precision were identified on each piezometers. The correlations between different piezometers were checked. Then the relationships between pressure variations and seismic events on the

neighboring OBSs were analyzed. Eventually, the corrected data were transferred for visualization using the **Visumultiparameter** software.

The main difficulty in the simultaneous visualization of seismologic and piezometric data-sets lies in the memory requirement for the visualization of the seismologic dataset, which has a much higher sampling rate, comared to the piezometric data. We are on a early stage of learning about the phenomenology behind the relationships between the seismologic events related to the gas emission and the pressure and the temperature variations. Hence the importance of **Visumultiparameter,** which allows the visulaisation of longer duration (several days) pressure and temperature variations together with the corresponding seismologic data in reasonable loading times.

3. Task 3: Acoustic data analysis

3.1 General background

Refer to Leblond et al (2014) and to Bayrakci et al (2014)

3.2 Estimation of gas bubble abundance and geo-localisation of sources

Refer to Bayrakci et al (2014)

3.3 Computation of flow rates

Refer to Leblond et al (2014)

3.4 Processing work flows

The different steps of the processing work flow are summarized here after.

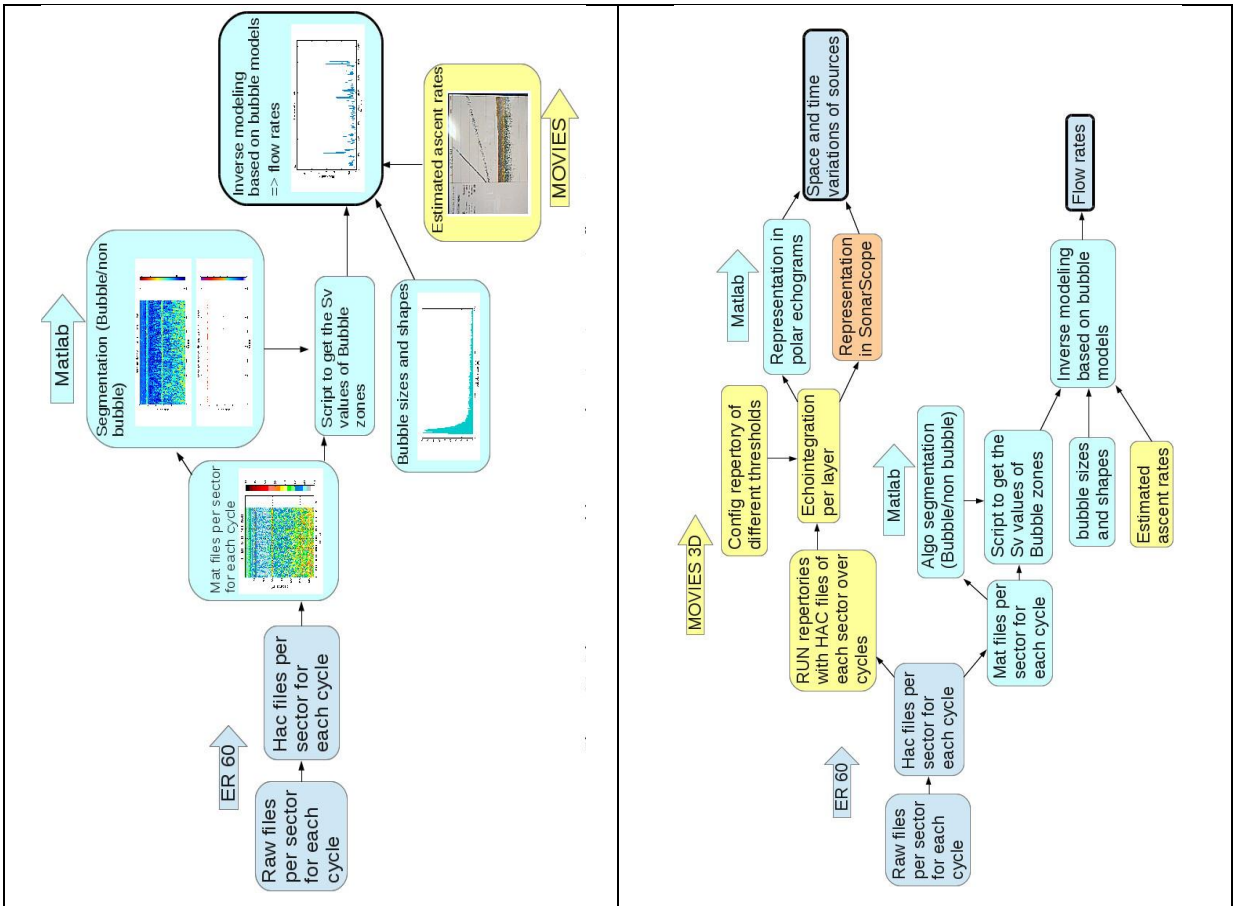

Figure 3.4.1: Workflow summarizing the different processing steps to compute flow rates.

Figure 3.4.2: Workflow summarizing the different steps required for processing the acoustic data recorded by BOB.

3.5 Analysis of BOB data, from Marmesonet-2009 and from Marmara-2011

Refer to *Bayrakci et al [2014]*

3.6 Comparison between near-bottom and ship-borne water column acoustic data

Refer to *Bayrakci et al [2014]*

3.7. Discussion

The analysis carried out on echograms and echointegration results of the Marmesonet and Marmara 2011 acoustic data shows that:

- The gas bubble sources may be continuous or transient.
- Gas emissions exhibit spatial and temporal variations. The Marmesonet echo integration results show that a new source appears on the third cycle which then disappear on the 4th one.
- In the case that all emitted gas bubble are located within the insonified conical volume of 7°, flow rates can be inverted from the Sv values observed on the echograms.
- Within the Cinarcik Basin, gas bubble sources seem to be aligned with a NW orientation. This orientation is coherent with the orientations of the bathymetric features and faults orientations.
- Some improvements may be brought into the precision of the location of the BOB module and the other instruments by using a DP equipped vessel during the instrument deployment. This will allow to approach precisely the places of the gas bubble sources.
- Three continuous gas bubble sources have been imaged within the area insonified by the BOB module, on the Central High. Echograms and echo-integration results suggest that a fourth continuous source is located just beneath the OBS.
- Small variations (from one sector to another or from one layer to another) in places of observed sources may be due to changes in the location of gas emission. Alternatively, this may be due to the current direction. For a given cycle changes towards same direction for all sources supports the second possibility.
- This current effect should be more easily observable for sources located at the border of the insonified sector.
- The ascent rate approached by Leblond et al., (2014) by the analysis of the target strength (TS) values of the isolated gas bubbles is 15.4 cm/s. A similar current velocity would be enough to deviate the bubble train 45° from the vertical.
- Some improvements in the acoustic data analysis may be brought by adding a current meter on the BOB module

- For a given source, in the case that the ascension is affected by currents and thus all gas bubbles emitted at a time t are not located within the conic volume of 7° diameter (one sector), the flow rates cannot be approached by considering only the Sv values of this sector.
- To improve the accuracy of the flow rate estimation, a calibrated multi-beam echo-sounder is necessary so that a larger volume could be insonified.
- The maximum flow rate observed on three continuous sources is 0.018 L/min. It is thus comparable with the maximum flow rate observed by Leblond et al., (submitted to Mar. Geophys. Res., 2013) for the Marmesonet data (0.011 L/min).
- Unlike the echoes from the Katerina rad on meter which appears flat like a fix reflector, the echo of the OBS appears pixallated like the gas bubble sources.
- The spatial and temporal variations observed on the echo of the OBS over cycles suggest that the OBS is located on a gas bubble source.
- The multi-beam data acquired in 2009 confirms the accuracy of the locations of the gas sources observed on the BOB data.
- The combined analysis of multi-beam data acquired in 2009 and BOB data acquired in 2011 shows that gas flares may be continuous over several years.
- Located on the sea-floor the BOB module improves the identification of gas flares with respect to a multi-beam echo-sounder, whose footprint becomes much larger than the bubble size with the increasing depth.

4. Task 4: Analysis of OBS data: short duration events detection and characterization

4.1 Characterization of short duration events

The OBSs deployed within the Marmara Sea have recorded earthquakes, but also unconventional, non-seismic, micro-events *[Tary et al, 2012]* hereafter called "short duration events" (SDE). SDEs are commonly found on OBS records, in a variety of geological environments *[Buskirk et al., 1981; Diaz et al., 2007]*. Because SDEs are not observed at more than one single station, they are not detected by automatic procedures used for locating micro-earthquakes (algorithms for earthquake detection require the identification of first arrivals on at least 3 distant stations). Hence, SDEs have for long remained undetected or simply disregarded, because considered as noise. A recent study *[Tary et al., 2012]* has shown that SDEs from the Marmara seafloor present the following characteristics:

- the duration of each SDE is less than 300 to 400 msec.
- SDEs have a monochromatic frequency content ranging between 10 and 30 Hz.
- SDEs peak amplitudes are highly variable, comprised between 0.5 and 20 μm/s.
- SDEs exhibit no clear P and S (body waves) arrivals.
- SDEs are detected by all geophone components (x, y, z); only those micro-events that have the largest amplitudes are detected on the hydrophone.
- There is no correlation between distant (> 1 km) OBSs.
- SDEs are frequent appearently occur as part of swarms, each swarm being made of a few tens of individual events.

Based on OBS recordings in various geologic contexts, Buskirk et al. [1981] and Diaz et al., [2007] proposed two explanations for the origin of the observed SDEs. Following the observations of SDEs distribution with depth, which could mimics the repartition of biomass in oceans, and observations of eggs of unknown biologic organism fixed on the frame of several instruments, Buskirk et al. [1981] proposed that SDEs could be produced by some living organisms "bumping" on the instruments. On the other hand, Diaz et al. [2007] suggested that SDEs could be produced by pressure transients involving the resonance of fluid-filled cracks, based on modelling [*Chouet, 1988, 1996*].

More recently, based on the observations of the presence of gas in superficial sediments and on the analogies with laboratory experiments, *Tary et al. [2012]* proposed that SDEs could be produced by the collapse of fluid-filled conduits induced by gas migration throughout superficial layers.

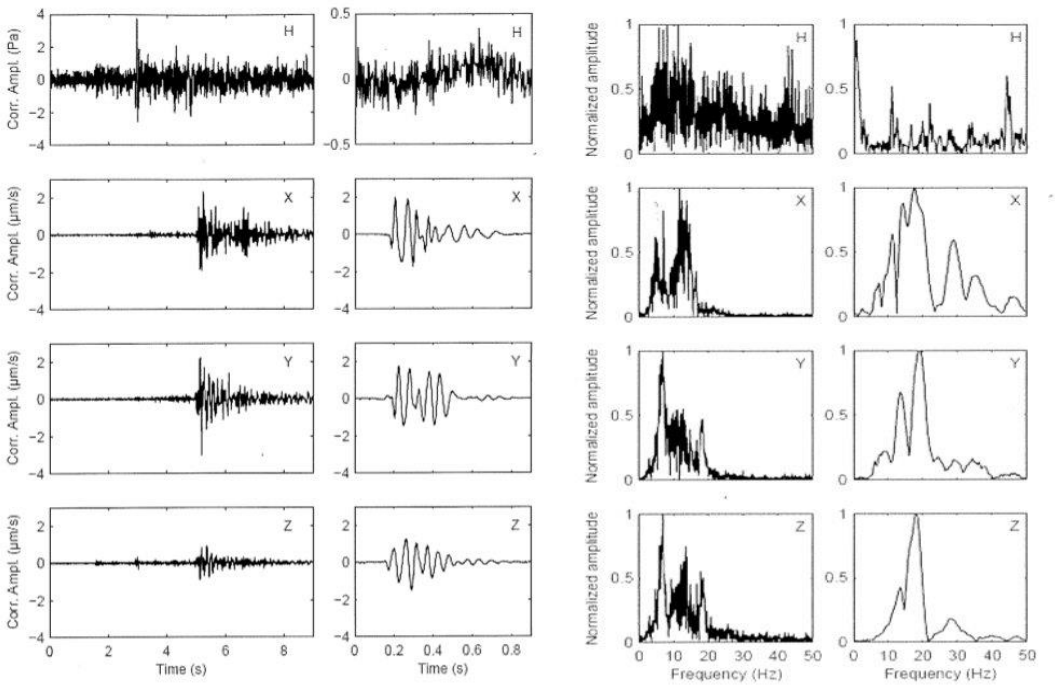

a) b)

Figure 4.1.1 ***a)*** *An OBS recording (H: hydrophone, X and Y: geophone horizontal components, Z: geophone vertical component), showing a micro-earthquake (Mw 1.98, May 14, 2007, 22:23:32) on the left and a micro-event on the right (May 14, 2007, 14:01:57).* ***b)*** *Frequency spectrum of the micro-earthquake (left) and the micro-event (right) shown in a (H: hydrophone, X and Y: geophone horizontal components, Z: geophone vertical component) After Jean-Baptist Tary PhD thesi(2012) .*

4.2 Tools for detecting micro-events

Presently available softwares for the automatic determination of earthquake epicenters (eg SAC, Seisan, Sytmis...) do not allow the detection of SDEs. On the contrary, the softwares dedicated to earthquake studies have some criteria to prevent the detection of unconventional micro-events. They only consider the events identified on several stations (usually three so that the earthquake relocation could be done) or with longer durations than the micro-events.

In this study a Matlab script was developed for the automatic detection of SDEs. Within this script the STA/LTA (short term average over long term average) algorithm is used to identify the amplitude peaks. The moving average of a large LTA window and a small STA window is computed and when the ratio between STA and LTA becomes greater than 5, the corresponding time is labelled as the arrival time of the event. The time when the ratio becomes 1 again is considered as the end of the event. To discriminate SDEs vs micro-earthquakes, a criteria is applied, based on event duration.

The automatic picking of SDEs was validated manually (e.g. through manual picking). This

validation process shows that our tool is effective to detect SDEs when the LTA time window does not contain signals from other origins such as micro-earthquakes, unconventional signals from human activities or electronic spikes. In the case of earthquakes and signals from human activities, the detection tool may not be effective either because the STA/LTA ratio may temporarily become equal to 1 before the end of the signal, or because SDEs may be buried beneath high amplitude signals.

On some OBS types (e.g. Guralp), short duration electronic signals with known waveforms may be sent in order to correct the temperature or the current effect on the OBS recordings. These electronic signals are similar to the SDE's with their short durations and their frequency content. The presence of such electronic signals may also decrease the effectiveness of the automatic detection. In some cases, electronic signals are sent with constant time intervals and are easy to remove. In some other cases, they occur at random time intervals (e.g. when produced by variations in temperature or dip). This second type of electronic signals may be detected as SDE's.

For the above reasons, visual checking is necessary for a reliable SDE identification. Alternatively, a principal component analysis (PCA) may be used to classify the automatically detected SDEs into families, based on their waveforms.

5. Task 5 Base-line characterization

5.1. Acoustic data (BOB)

At this stage, it is difficult to establish a general baseline on the background, gas emissions escaping from the seafloor. The analysis of the BOB data presented in Section 3 however provides useful indications:

- Gas bubble sources may be continuous or transient. Ship surveys, conducted on a regular basis, using surface, multibeam echosounders, are highly recommended to assess temporal variations.
- At the scale of the Sea of Marmara, gas emissions are controlled by different factors, including active faulting, the nature of the sediment cover and the connexion to buried gas sources.
- At the local scale (of a few tens of meters), gas emissions also exhibit spatial variations, as documented by BOB.
- Small spatial variations (from one sector to another or from one layer to another) may be due to small changes in the location of gas emission. Alternatively, it could also be due variations in sae-bottom current direction.

Additional work is required to know if the observed gas emissions are really significant or if they are simply a part of the background gas emission activity. The combination between OBS and BOB data is a promising approach to address this question (see section 6).

5.2 Spatial and temporal distribution of automatically identified SDE's

5.2.1 Introduction

Micro-earthquakes and short duration events were both detected in the Marmara 2011, OBS network. In 107 days (between 15th of April and 31th of July 2011), more than 50 000 SDEs per OBS in average were automatically detected, using a STA/LTA based matlab code specifically designed for this purpose (See section 5.1 *"Tools for detecting micro-events").* SDEs were plotted and saved as 1s window length as *.PNG* and *.MAT* files. A visual checking has been carried out on random time intervals, as a systematic visual cheking could not been carried out due to the very large number of SDEs. The checking showed that some electronic events of very small amplitudes were also detected by the STA/LTA code (Fig. 5.2.1.1). In order to remove electronic events, only events with amplitudes larger than $\pm 10^3$ units have been considered.

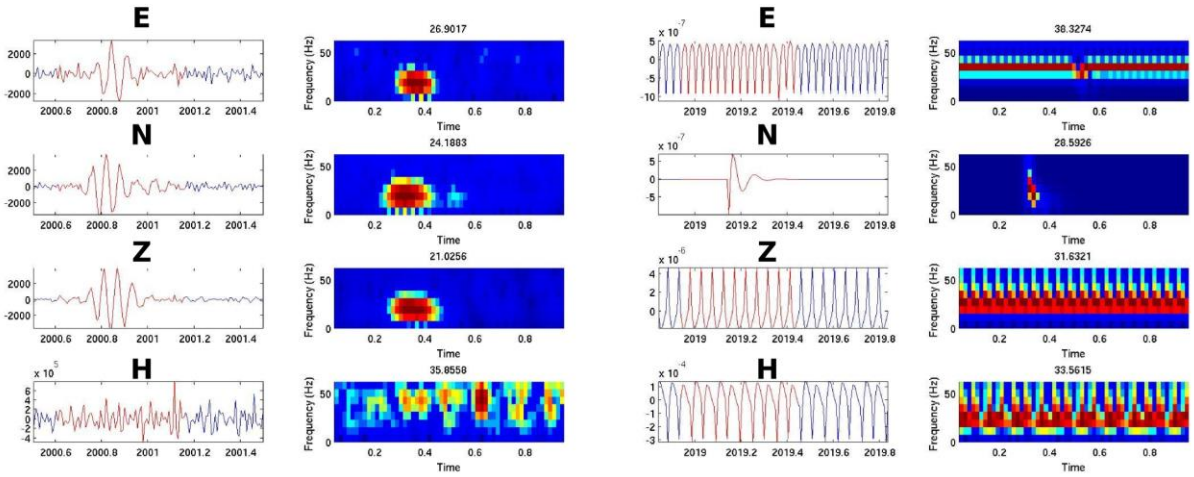

Figure 5.2.1.1: ***a)*** *Example of SDE redorded by OBS 07.* ***b)*** *Example of electronic event recorded by the same OBS.*

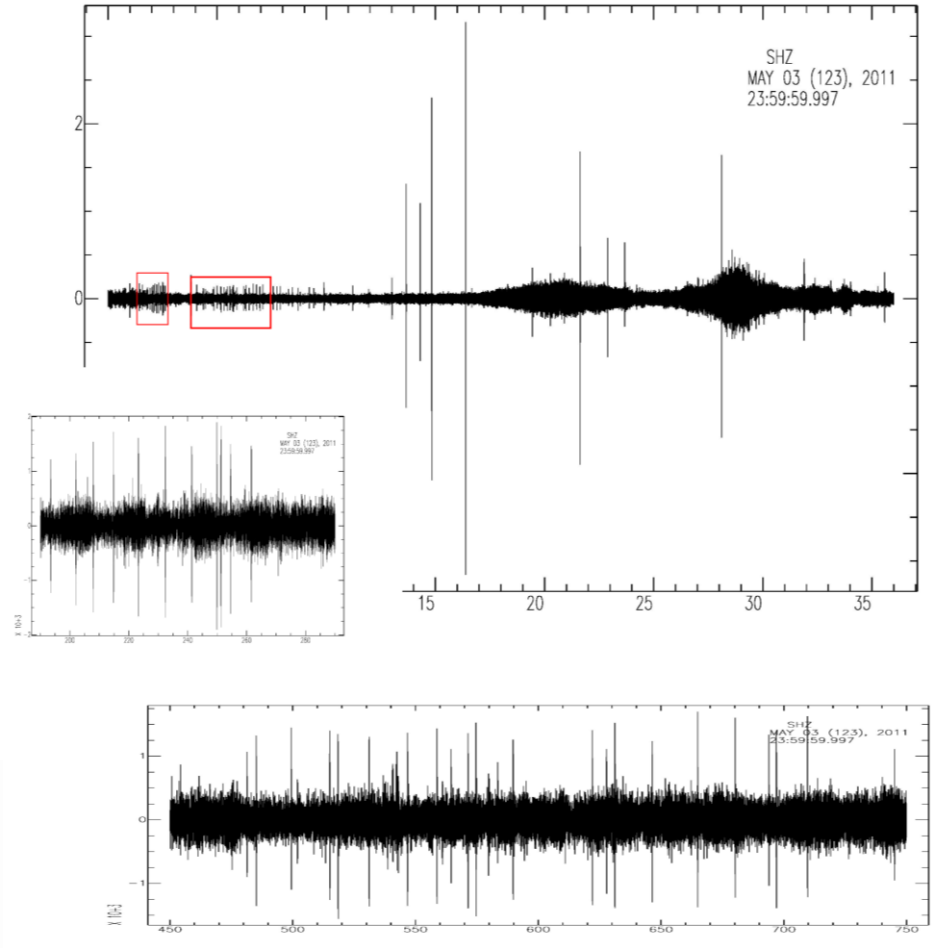

*Figure 5.2.1.2****:*** *One hour record section from 04th of May 00h to 01h on OBS 07. The red frames show zoomed time intervals. The SDE's may have a periodicity during the crisis (red frames), but it is difficult to quantify this periodicity since more than one source may have been recorded by the OBS. Larger amplitude events seems to happen with larger intervals than the ones constituting the crisis.*

5.2.2 Spatial and temporal distributions of SDE's

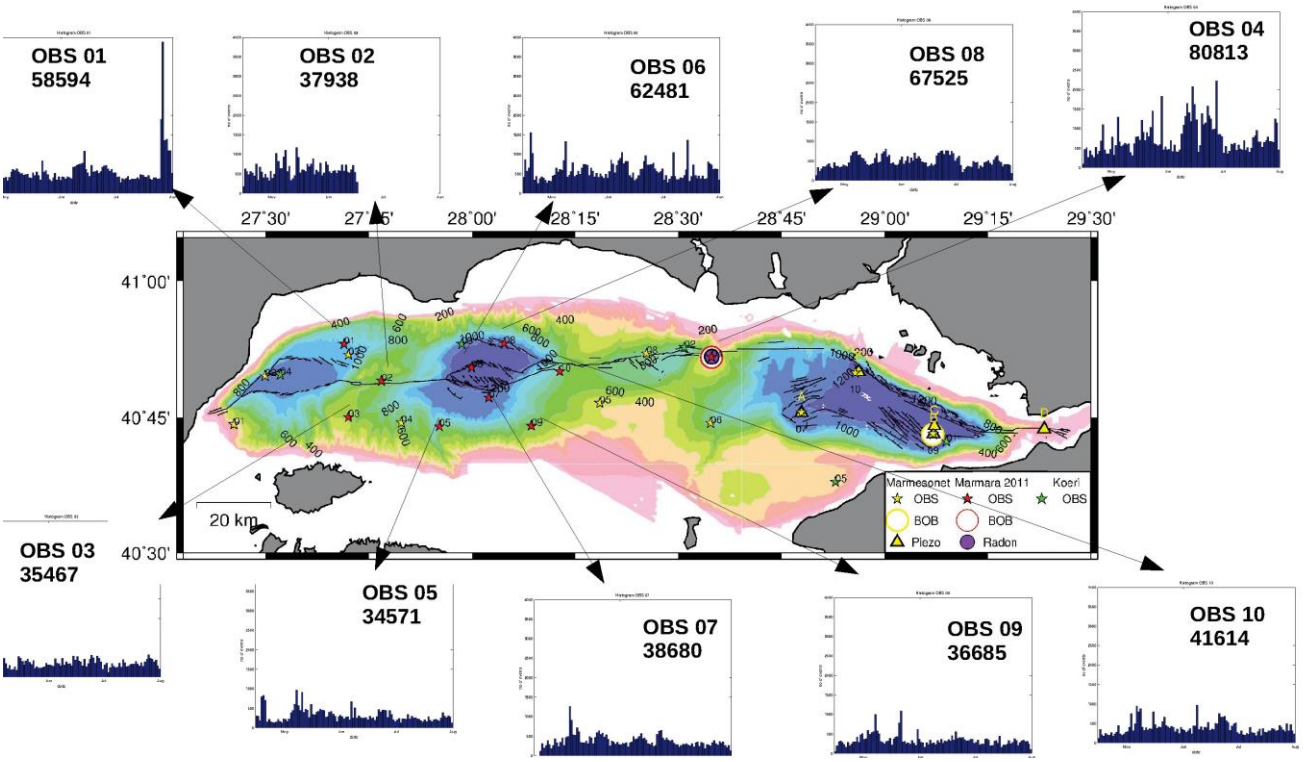

Figure 5.2.2.1: Daily distribution of SDE's on the 10 OBSs of the Marmara 2011 network;

Figure 5.2.2.1 shows the daily SDE ditribution on the 10 OBSs of the Marmara 2011 network. During the 107 days period, in average, 50 000 SDE's per OBS were recorded.

The number of detected SDE's is systematically higher on the northern OBSs. OBS 02 was located on a well known gas emision site, but it stopped recording on June 16th, at 09 am, before the end of the survey (31th of July 2011), possibly due to the high bubble activity of its surroundings. OBS 05, located at the southwest of the Central Basin recorded the lowest number of SDE's (34571). In contrast, OBS 04, which was located at the eastern edge of the Kumburgaz basin, near by the sea-floor trace of the North Anatolian Fault and at the neighborhood of the BOB module recorded the maximum number of SDE's (80813). The fact that the maximum number of SDE's has been recorded on the OBS 04 supports also the hypothesis that this OBS was located near a gas bubble sources.

Individual SDEs are not recorded by distant OBSs (e.g. for OBS spacing greater than a few tens of m). During the Marmara 2011 survey, OBSs were spaced by 20 km. Hence, there can be no correlation between individual SDEs. In contrast, some SDE crisis appear to have been recorded by different OBS simultaneously (or sligthly shifted in time) as shown in Figure 5.2.2.2.

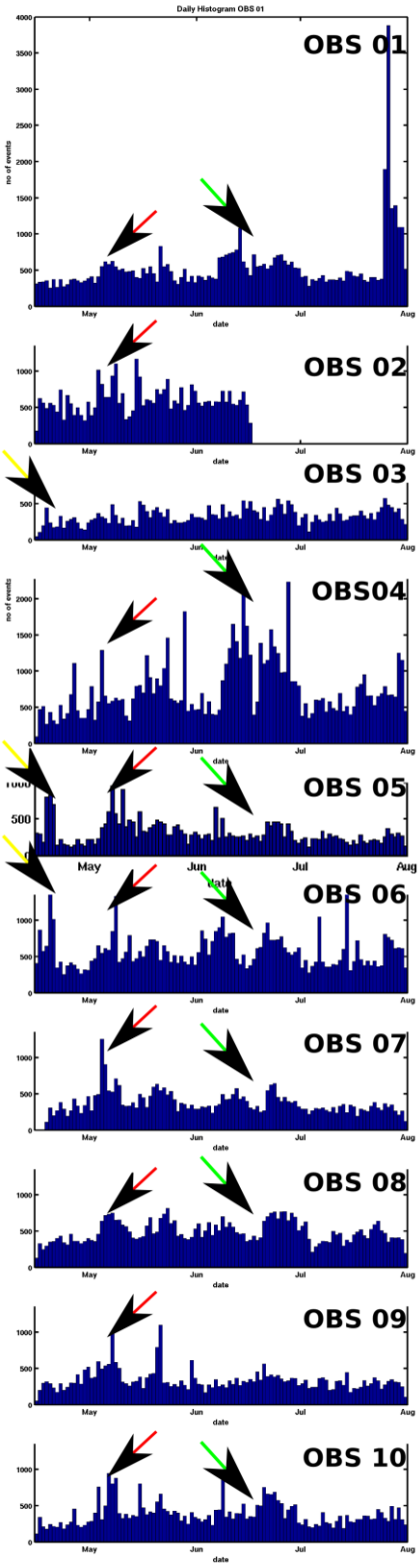

*Figure 5.2.2.2**:** Visual correlations between the SDE's recorded on different OBSs of the Marmara 2011 network. Collored arrows show different crisis observed on more than one OBSs. Notice that the crisis periods are retrieved by visual analysis. That means they may not be exacly at the same moment.*

Indeed, a first crisis is observed on OBSs 5 and 6, from 18th to 20th April (yellow arrows on Figure 5.2.2.2). This crisis is also observed on OBS 03 but the number of recorded SDE's is significanty smaller (> 500 event /day) on this OBS.

A second crisis is observed between 3rd and 8th of May (red arrows on Fig. 5.2.2.2) on almost every OBSs of the network besides OBS 03. The detailed analysis of daily and hourly histograms of all OBSs showed that the peak number of SDE's occurs at different times, from one OBS to the other (see Table 5.1). The difference of the peak days between the OBSs shows the necessity to analyse the distribution of the SDE's on different OBSs visually. Since the peak periods do not happen on the same day, the mathematical correlation between the OBSs which recorded this second crisis is not necessarily high. The reason of the difference between visual and mathematical correlations is that the mathematical correlation is very sensitive to the peaks with values significantly different from the average value.

3rd of May	4th of May	5th of May	6th of May	7th of May	8th of May
OBS 02	OBS 04	OBS 07	OBS 10	OBS 03	OBS 06
OBS 10	OBS 07			OBS 05	0BS 10
				OBS 09	
				OBS 10	

*Table 5.2.2.2**:** Correspondance between days of activity and OBSs having recorded the SDE activity, during May, 3-8, 2011 crisis.*

The occurence of micro-earthquakes from the 1st to 10th of May (Fig. 5.2.2.3) was analysed in order to see if there is a relationship with the increase of SDEs. The earthquakes recorded by the Mamara 2011 network have been used for this analysis. Earthquakes have been relocated by *Cros et al., in prep.*, using the SYTMIS software developed by *Ineris*.

From May 1st to May 10th 2011, a total of 11 earthquakes have been identified and relocated within 1.5°x1° frame centered aroud the Central Basin (Fig. 5.2.2.3). Seven out of eleven earthquakes are located within the Central Basin and one of them is about 20 km southeast of the basin. This observation suggests a relationship between the earthquake occurence and the increase in SDEs.

The relationship between earthquake and SDE occurences was further analysed by plotting hourly distributions of SDE's and by comparing them with the origin time of relocated earthquakes. A direct relationship between the occurece time of the earthqaukes and SDE pick periods is not found.

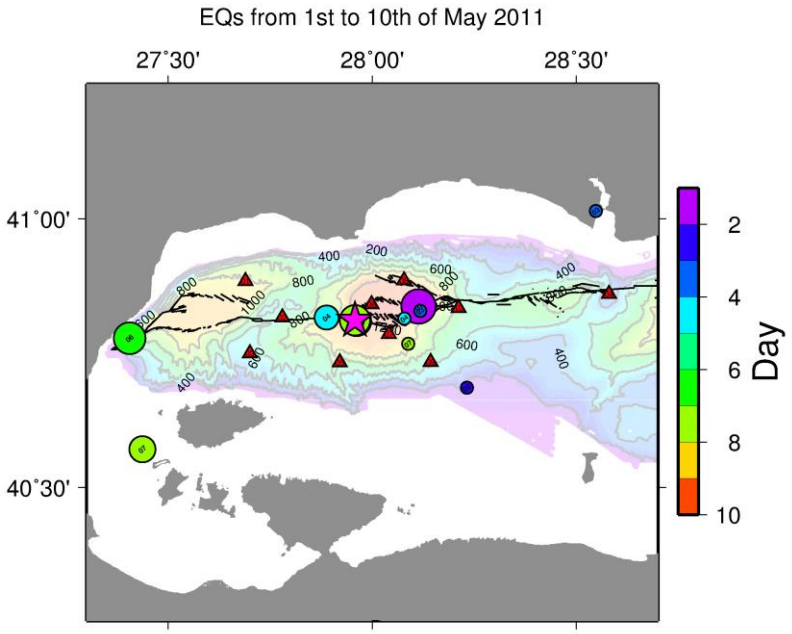

Figure 5.2.2.3: Positions of earthquakes recorded by the Marmara 2011 OBS network between the 1st and 10th of May after the relocation study carried out by E. Cros. Circles represent earthquakes. The size of the circles represent the magnitudes of earthquakes and the colours represent the dates. The pink star represents the Mw 3 event of 7th of May at 05:27:55 pm.

Peak hours on the hourly histograms do not necessarily correspond to the peak days observed on the daily histograms since the peak day may also correspond to several hours of high SDE activity. Figure 5.2.2.4 shows two example of hourly histograms (of OBS 05 and 07). Both OBSs recorded an increase of SDE during the crisis of 3 to 8 May, which is observed on the daily histograms (Fig. 5.2.2.1). A clear peak is observed on the hourly histogram of the OBS 05 on the 7th of May at between 04:00 and 05:00 pm with ~ 150 SDE's happining in one hour. This may be interpreted as being related with the Mw 3 event of 7th of May at 05:27:55 pm (Fig. 5.2.2.3). However, a similar peak is not observerved on OBS 06, which is closer from the hypocenter. On OBS 07 which is also located near the hypocenter, high SDE activity occured for several hours, between 3 to 8 May (Fig. 5.12). However no simultaneous peak periods are observed on OBS 05 and OBS 07.

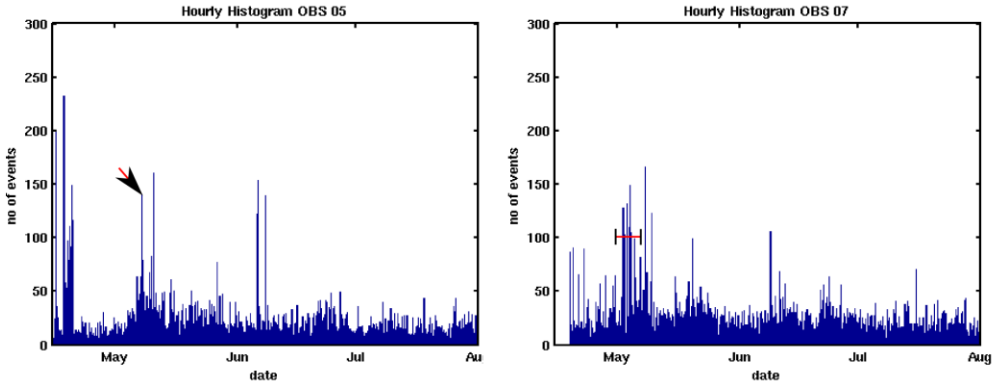

Figure 5.2.2.4: Hourly histograms of OBS 05 and 07. Both OBSs recorded an increase of SDE during the crisis of 3 to 8 May which is observed on the daily histograms (Fig. 5.2.2.1).

A third crisis is observed on OBSs 1, 4, 5, 6, 7, 8 and 10 from mid-june until the end of June (green arrows on Fig. 5.2.2.3). On some OBSs (1, 4, 6 and 7) this third crisis is preceded by another crisis which happens during the first half of June.

Figure 5.2.2.5 displays the earthquake occurrence from June 15th to June 30th. A total of 12 micro-seismic events have been identified and relocated during 15 days. Some of them occur on the North Anatolian Fault segment cutting across the Western High and others occur on the Biga peninsula or at the area located between the Western High and the Biga Peninsula.

OBS 02 is the nearest OBS to the earthquakes observed on the Western High. Unfortunately OBS 02 stopped recording on the 16th of June, possibly due to SDE or micro-earthquake crisis. OBS 03 is the nearest OBS to the earthquakes observed on the Biga peninsula, on the southern platform and the Western High. But no significant increase in SDE occurrence is observed on OBS 03.

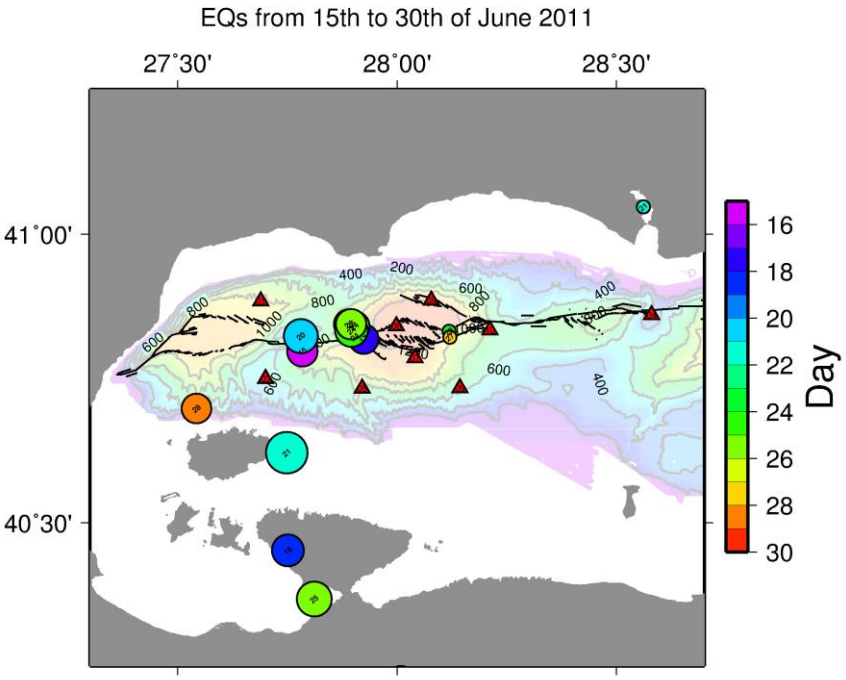

Figure 5.2.2.5: Locations (circles) of earthquakes recorded by the Marmara 2011 OBS network during June 15-30 after the relocation study carried out by E. Cros. Circle size is proportional to magnitude . Colors represent earthquake dates.

5.2.3. Correlations between OBSs

The mathematical correlations between the temporal SDE distributions observed at different OBSs were computed by considering histograms as vectors. Figure 5.2.3.1 shows a visual example of an histogram transformed to a vector. Correlations were computed with a Matlab® script in a pseudo-automatic way for all OBSs. The correlation matrix is shown in Figure. 5.2.3.2a.

- Correlation coefficient is greater than 0.5 between OBSs 03 and 04, which are separated from each other by more than 100 km. Correlation coefficients are highly dependent on the peak values, which may be very different from the average. The correlation between OBS 04 which recorded the highest level of SDE activity and OBS 03 with very smooth values without significant peaks is likely to result from a mathematical artefact.

- Correlation coefficient is also greater than 0.5 between OBSs 05 and 06. These two OBSs are separated from each other by less than 20 km. OBS 06 is located within the Central Basin and OBS 5 is located on the canyon southwest of the Central Basin. Both OBSs have recorded all three crisis identified previously by the visual analysis of the daily SDE distribution histograms. One hypothesis which would explain the

correlation between these two OBS is the pressure diffusion along a high permeability layer. Such hypothesis, however, is very unlikely, due to the presence of the North Anatolian Fault which probably acts as permeability barrier between the 2 OBSs. An alternative explanation is proposed in the next sections.

- OBSs 07, 08, 09 and 10, which are all located near or within the Central Basin appear to be correlated. Figure 5.2.3.3 shows the daily histograms of these OBSs plotted all together. These OBSs have recorded the SDE crisis of May 3-8 and June 15-30, which were identified by visual analysis of daily histograms. They also recorded the SDE crisis on the first half of june (with a peak on June, 8) and the crisis which happens around May 21 (May 21 on OBS 07 and May 23, on OBS 08).

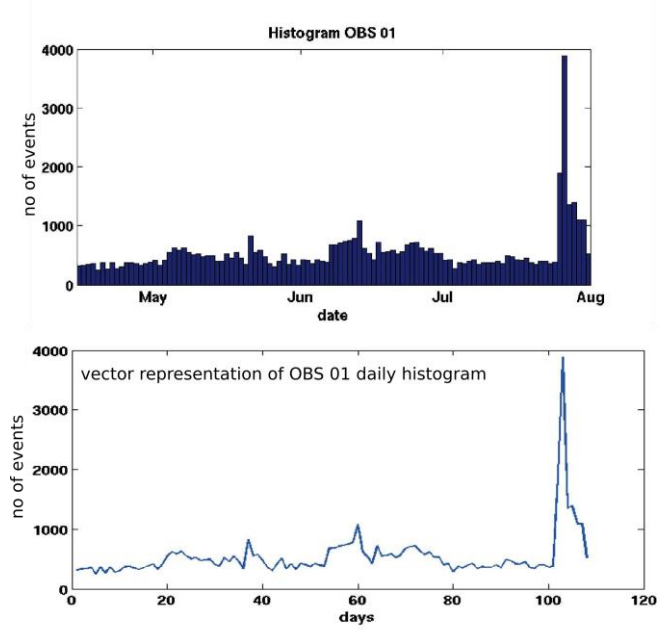

Figure 5.2.3.1: The vector representation of the daily SDE's distribution histogram of the OBS 01.

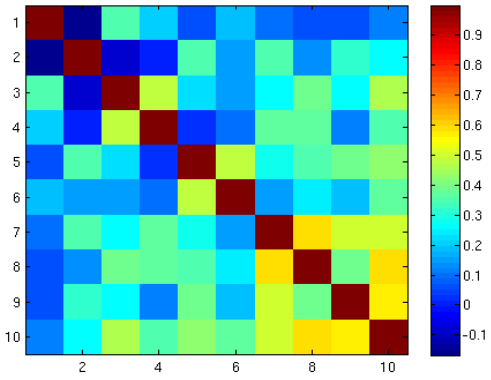

a)

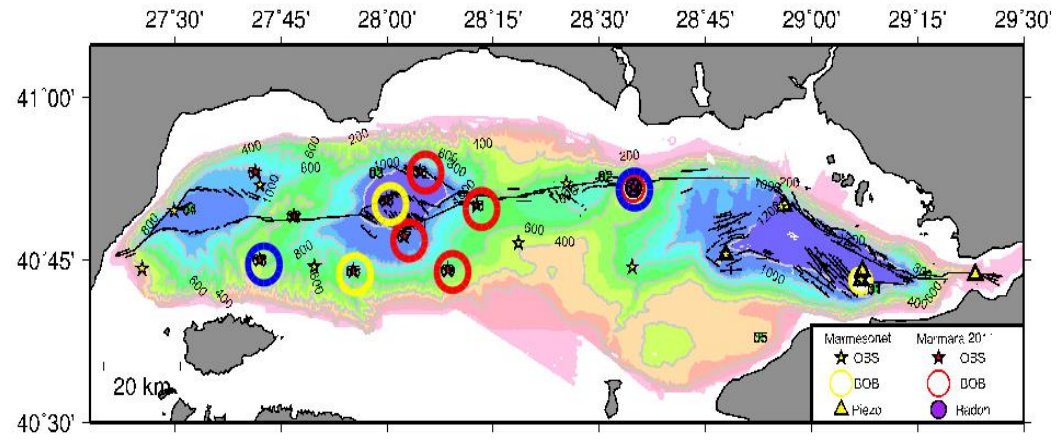

b)

Figure 5.2.3.2: ***a)*** *Correlation matrix between temporal SDE distributions observed on each OBSs of the Marmara 2011 network. X and Y axis are OBS numbers. Colors indicate correlation values.* ***b)*** *Spatial distribution of OBSs with mathematically correlated temporal SDE distributions.*

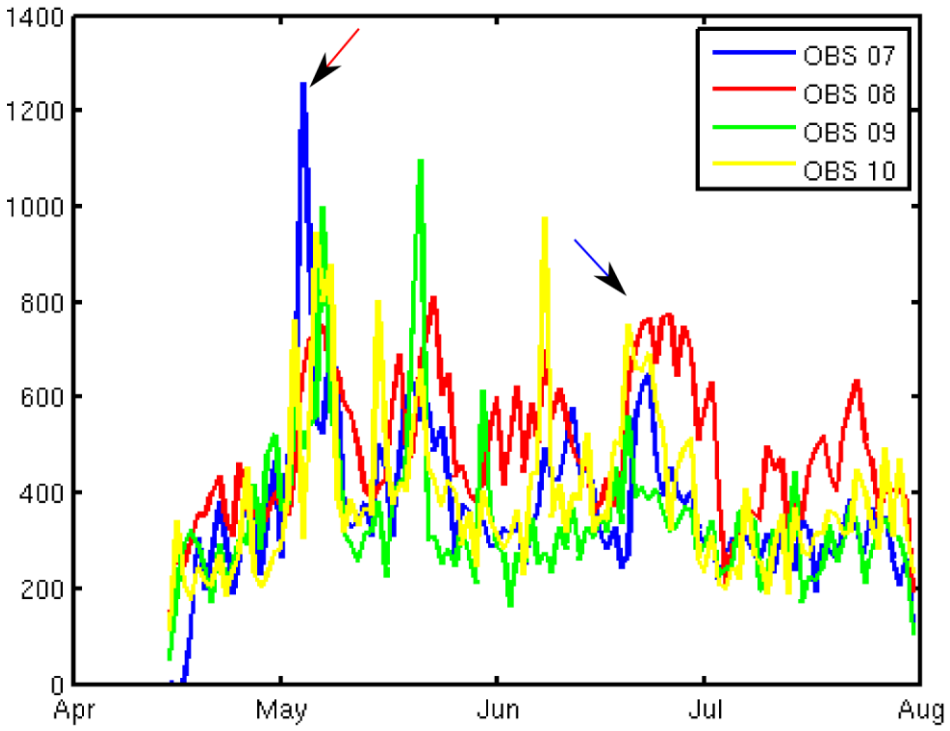

Figure 5.2.3.3.: Daily histograms of OBS 07, 08, 09 and 10 plotted all together. Red and blue arrows show the May 3-8 and the June, 15-30, SDE crisis identified by the visual analysis of the daily histograms (Fig. 5.10). Around May 21 and June 8,, two secondary peak periods are observed on these four OBSs.

Figure 5.2.3.4 shows the micro-seismic events observed from May 15th to May 25th. Two seismic events of Mw>3 happened on May 20th and 21th respectively within the Central

Basin.

Moreover, a micro-seismic crisis on-land and on the shallow southern shelf of the Marmara Sea, southeast of the Central Basin occured from May,19th and May 24th. There is thus a likely correlation between this crisis of seismic micro-events and the SDE crisis recorded on May 21th by the four OBSs (07, 08, 09 and 10) located near or within the Central Basin.

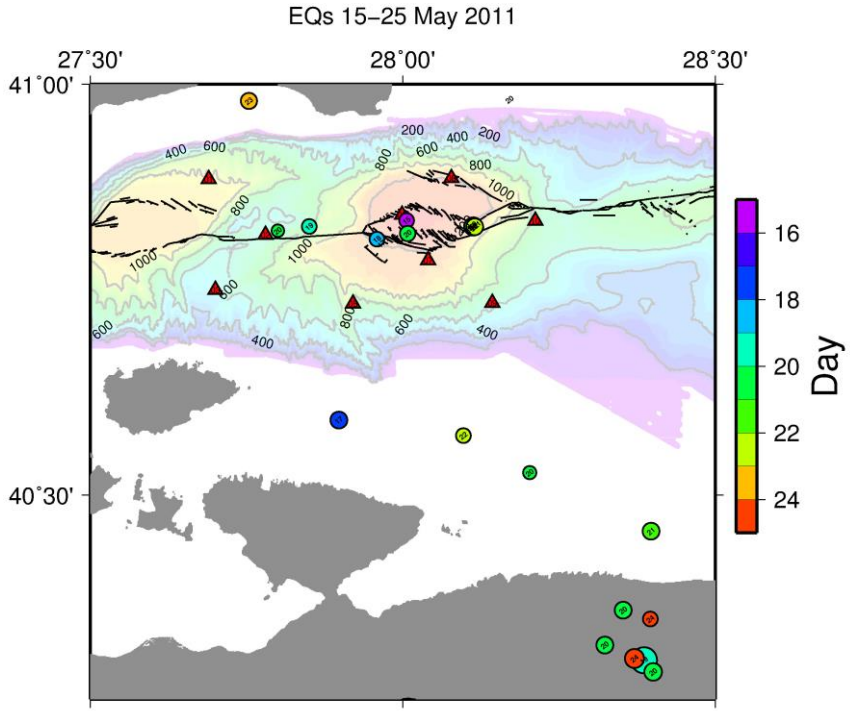

Figure 5.2.3.4: Positions of earthquakes recorded by the Marmara 2011 OBS network between the 15th and 25th of May after the relocation study carried out by E. Cros. Circles represent the earthquakes. The size of the circles represent the magnitudes of earthquakes and the colors represent the dates.

Hourly histograms of four OBSs are analysed to see if there are some simultaneous peak periods on the different OBSs and to check if these peak periods correspond to earthquake occurence times.

On OBSs 07, a SDE crisis is observed on May 20, between 00:00 to 01:00 am. During this period, two seismic events (00:12:12 and 00:23:49 am) of Mw 3.3 and 3.4 are listed and they are both located on land, more than 70 km away from OBS O7. These two earthquakes and several smaller micro-earthquakes were observed on the one hour sismogram of OBS 07.

Clear SDE's were identified before both earthquakes (Fig. 5.2.3.5). The SDE's were also observed during and after the second earthquake (00:23:49 am) (Fig. 5.3.5, b and c). During this small SDE crisis, the SDE's happens as pairs and with a periodicity of around 17 s.

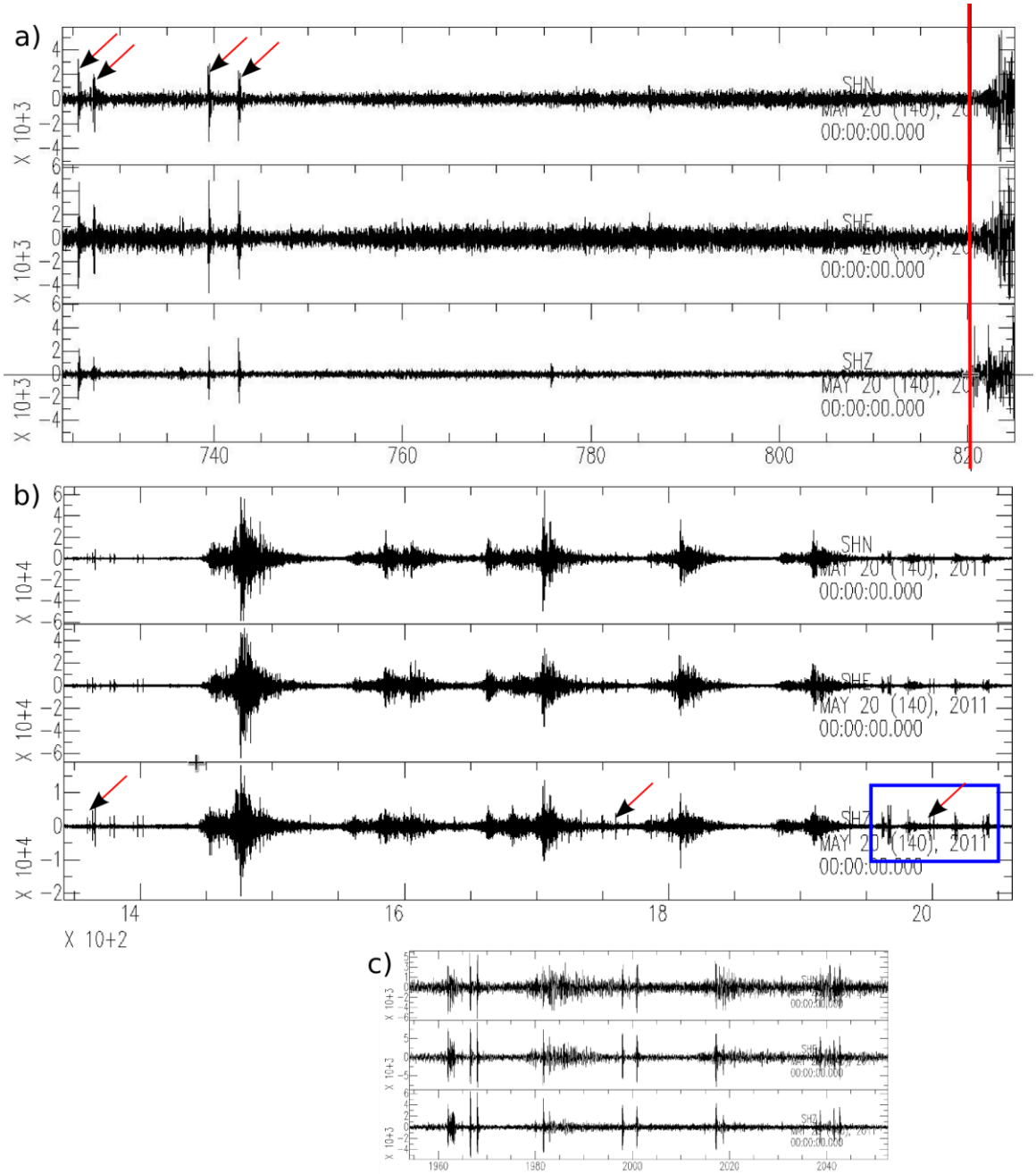

Figure 5.2.3.5: ***a)*** *Red line shows the P wave arrival time of the Mw 3.3, 20th of May, 00:12:12 earthquake recorded by OBS 07. Red arrows show the SDE's before the earthquake.* ***b)*** *The Mw 3.4 earthquake of 20 th of May, 00:23 displayed along with several non listed smaller earthquakes recorded by OBS 07. Red arrows shows the groupes of SDE happenning before, during and after the micro-earthqake crisis. Blue frame shows the location of events represented in c.* ***c)*** *Zoom on the SDE's happining after the seismic events. The SDE's happens as pairs and with a periodicty of 17 s.*

On OBS 07 (May 20, from 00:00 to 01:00), small micro-seismic events which do not appear in the relocated earthquakes list have been identified (Fig. 5.2.3.5 b, Fig. 5.2.3.6). The P and S waves arrival times of these micro-earthquakes are buried by the occurence of SDE's. During this micro-seismic sequence, the SDE's appear also to be periodic with 2 s intervals (Fig. 5.2.3.6)

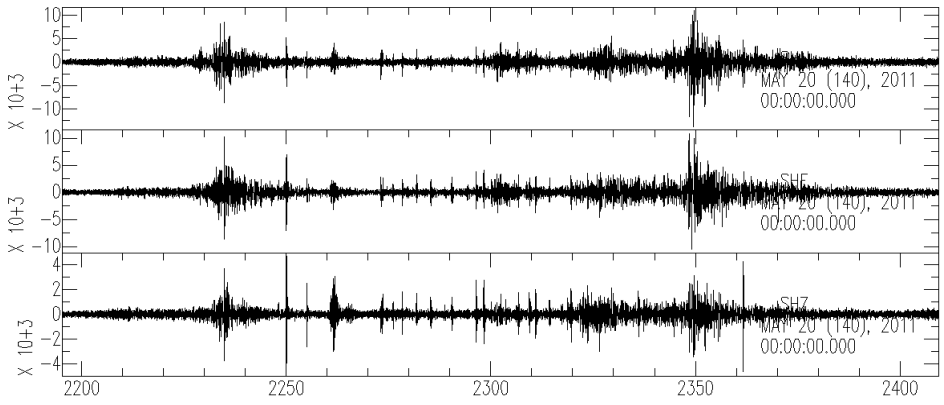

Figure 5.2.3.6: Micro-earthquake sequence observed on OBS 07, on May 20, from 00:00 to 01:00 am. The P and S wave arrivals of the micro-earthquake is buried by the SDE occurence. During this time interval the SDE's occur with a 2 s periodicity.

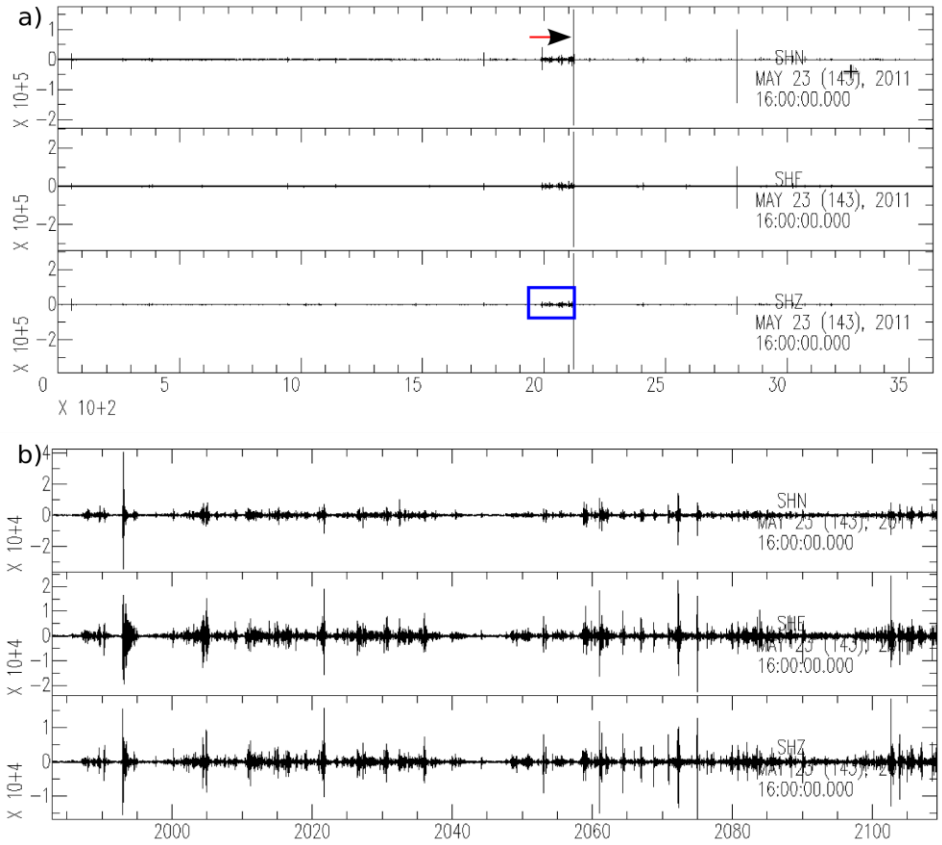

*Figure 5.2.3.6: **a)** One hour record section of 23th of May from 16:00 to 17:00 recorded by OBS 08. No micro-seismic event is observed on this record section. The red arrow shows the large amplitude SDE observed on this section. The blue frame shows the time interval in b. **b)** Zoom on the small amplitude SDE crisis before the large amplitude SDE.*

On OBS 08, an intense SDE activity is observed on the 23th of May between 16:00 and 17:00. Only one seismic event was identified on this OBS on May 23. This event is a Mw 3.1 earthquake that occured at 15:32:10. Figure 5.2.3.6 shows the corresponding section recorded

by OBS 08 between 16:00 and 17:00. No micro-earthqakes were observed during this period but a SDE of large amplitude (~ 10+5) is oberved on the record section. Before the large amplitude SDE, a crisis of small amplitude SDEs was observed, with the same caracteristics as the crisis observed on OBS 07.

On OBS 09, two peak periods of intense SDE activity was observed on May 20, between 07:00 and 08:00 and on May 21, between 11:00 and 12:00.

- One earthquake occurred at 07:35:59 (Figure 5.2.3.7). This event was identified in the local earthquake catalogs and relocated on the northwest of the Central Basin. On OBS 09, many micro-seismic events were observed (e.g. Fig. 5.2.3.7 a and b) that do not appear on the relocated earthquake list, likely due to the occurence of SDEs which prevent the determination of P and S wave arrival times.
- No earthquake was listed in the catalogs during the second period of high SDE activity (between 11:00 and 12:00). Instead, a low magnitude, micro-earthquake was recorded on OBS 09 (Fig. 5.2.3.8).

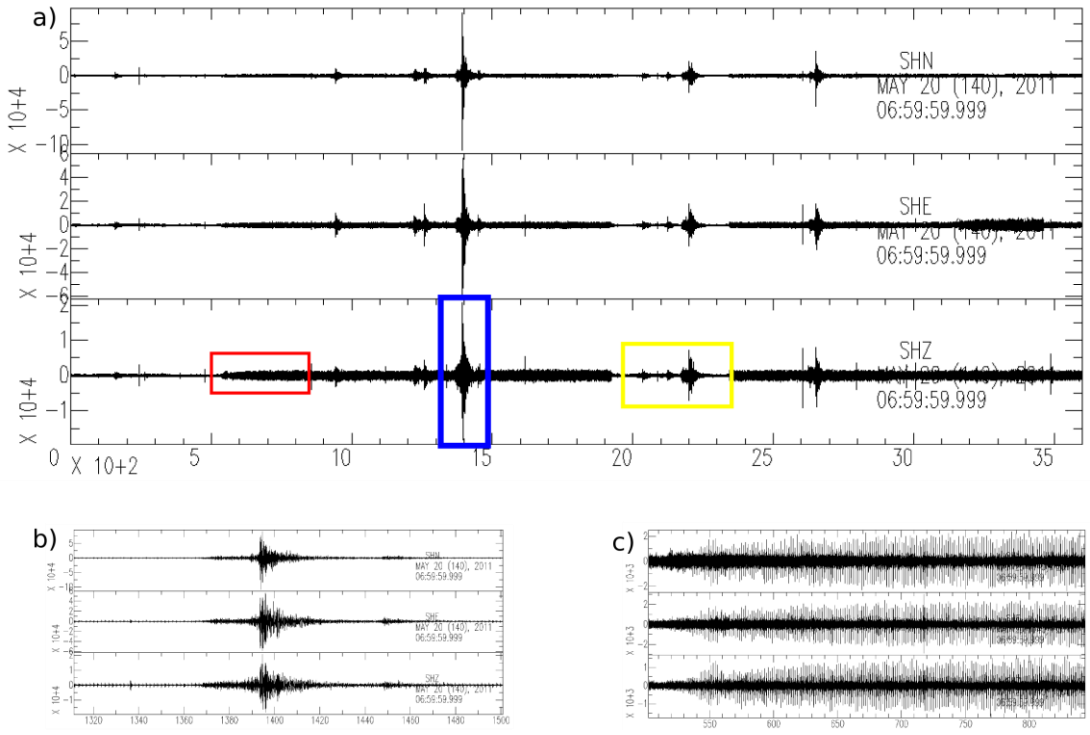

Figure 5.2.3.7: ***a)*** *Section recorded by OBS09 on May 20, from 07:00 to 08:00. Yellow frame shows the listed seismic event of 07:35. The blue frame shows one unlisted seismic event, zoomed in b). Periodic (every 1.65 s) SDEs are identified before and after the seismic event.* ***c)*** *is a zoom on the beggining of the SDE crisis, shown within a red frame in a).*

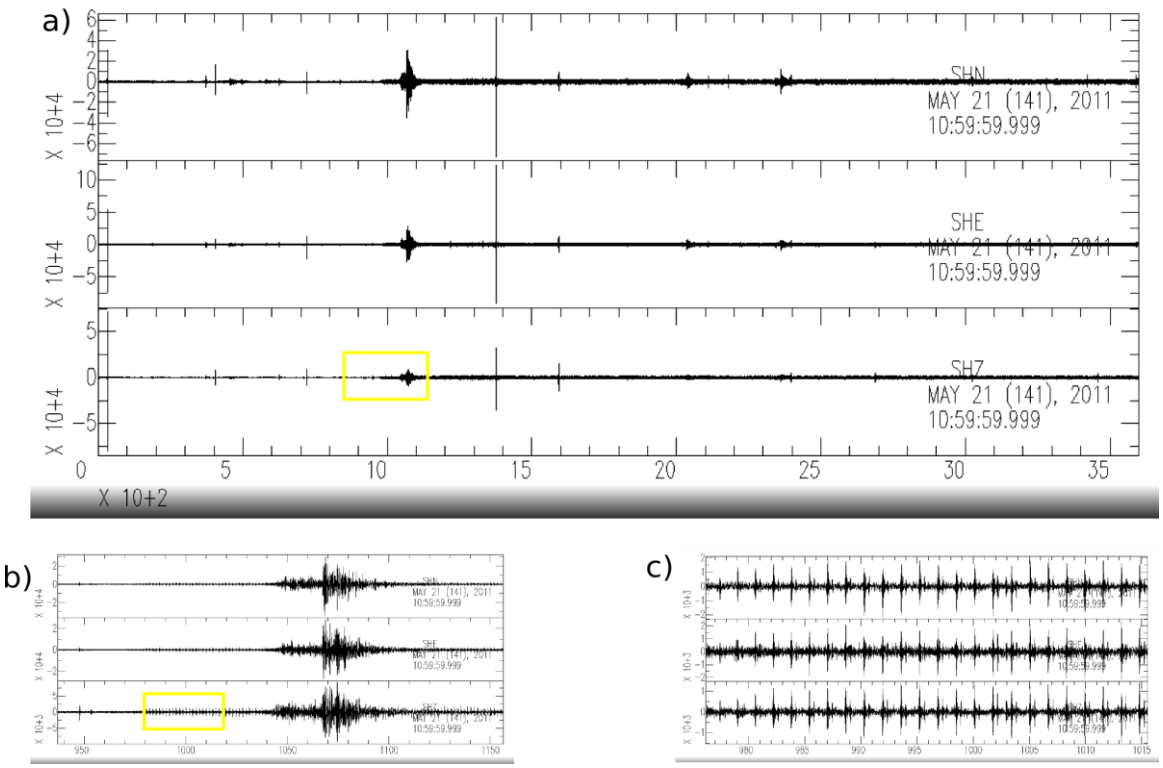

Figure 5.2.3.8: ***a)*** *One hour record section of 21th of May from 11:00 to 12:00 on OBS 09. Yellow frame shows the unlisted seismic event observed on this record section.* ***b)*** *is the zoom on the unlisted event. Very periodic SDE's are identified before and after the seismic event.* ***c)*** *is a zoom on the beggining of the SDE crisis. The SDE's occurs very periodically every ~1.65 s. Red frame in a) shows the time interval of c.*

On OBS 09, during both peak period (Fig. 5.2.3.7 and 5.2.3.8), SDEs happen very periodically, every 1.6 s before and after the earthquakes. The waveform of these signals are different from the ones identified previously on the other OBSs. Their frequency are higher (<39 Hz) and they appear with a first signal similar to the SDEs, then a second one of smaller amplitude, 0.5 s later than the first one. The SDEs occuring during this crisis are very similar to each other. Contrarily to the other SDE's, those observed on OBS 09 are also observed on the hydrophones. The clear periodicity, the high frequency and the similarity between events may suggest an instrumental noise origin for these events which may be related to the earthquake effects. But, these signals are not observed before or after each observed earthquakes. In addition, the amplitude of earthquake signals do not seem to play a role on the occurence of the events observed during the crisis. Moreover, the first particule motion of different events are not always in the same direction indicating a source location change (Fig. 5.2.3.9, bottom).

On OBS 09, nearly none of the SDEs are recorded by the hydrophones, except during this crisis of micro-seismic events crisis. This could be due to a electronic problem on OBS 09. However, we preclude this hypothesis, because during the same period we identified several SDEs that were also recorded on the hydrophones of OBS 06, 07, 08 and 10 (Fig. 5.2.3.10).

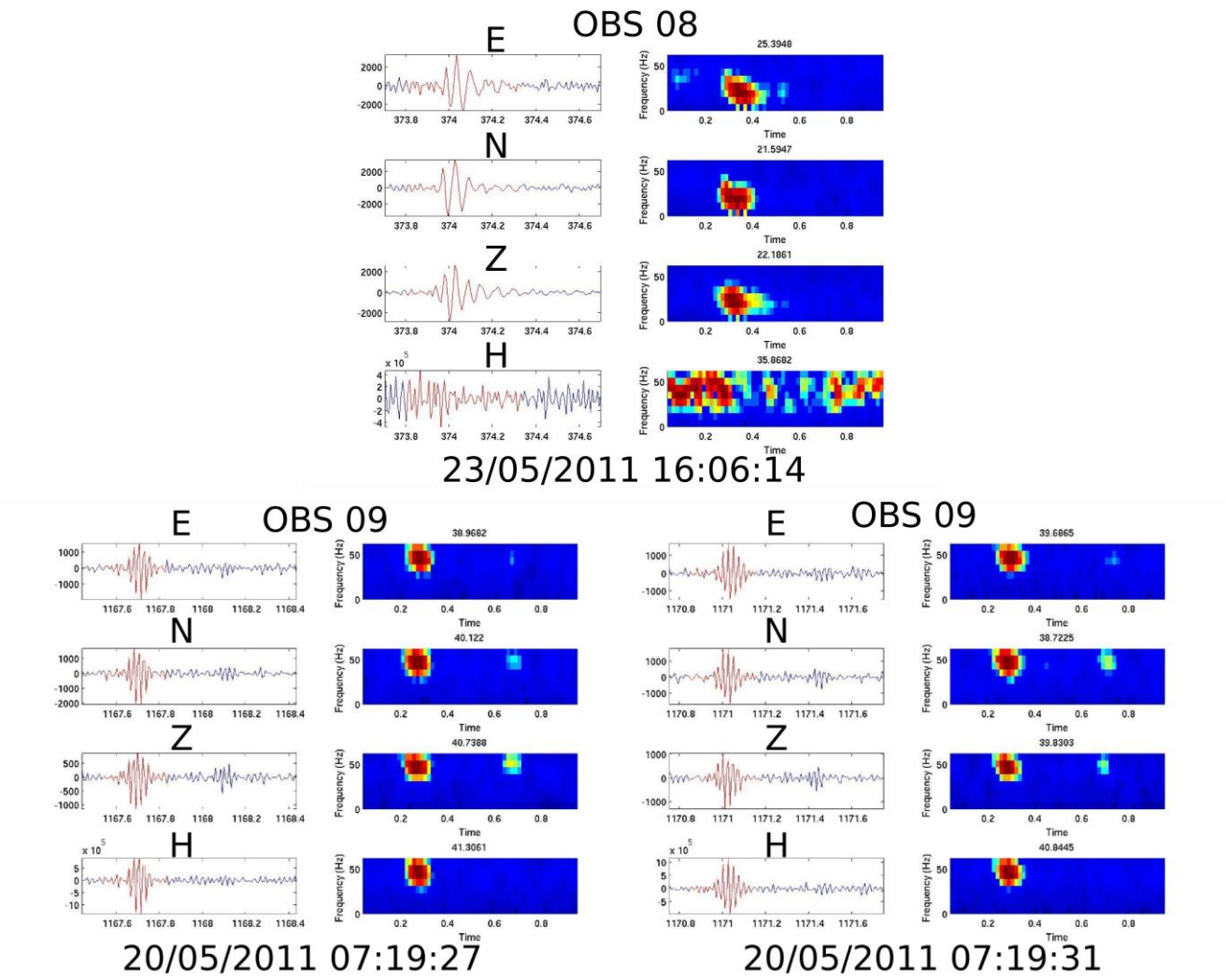

Figure 5.2.3.9: ***Top****: Example of SDE observed on OBS 08 during the crisis of 23th of May.* ***Bottom****: two examples of SDE observed on OBS 09 during the crisis of 20th of May. Note that the SDE's are very near in time, their waveform are very similar but not identical as one may expect for electronical signals.*

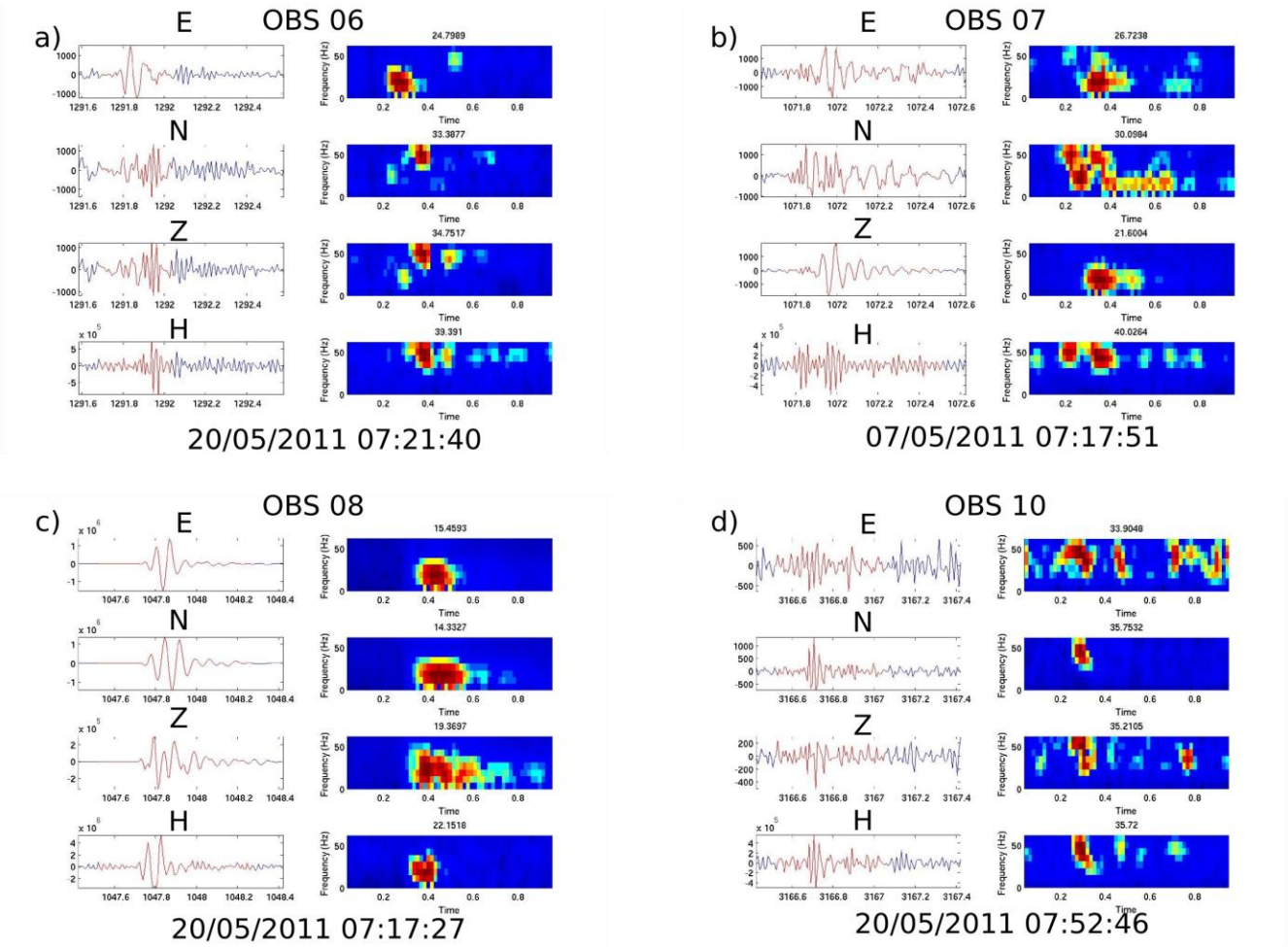

*Figure 5.2.3.10: SDEs observed on various OBS **a)** OBS 06, **b)** OBS 07 **c)** OBS 08 and **d)** OBS 10, simultaneously with the very periodic SDE crisis of 20th of May observed on the OBS 09. Like the SDE's observed on the OBS 09 during the crisis, all shown events are observed also on the hydrophone component.*

On OBS 10, a crisis is observed on May 21, between 8:00 to 10:00. One earthquake (08:29:38) was listed during this period of two hours. This earthqauke does not appear on the KOERI's catalog, but it is identifed thanks to the Marmara 2011 OBS network (Fig. 5.25a).

Like on the previous OBSs, a crisis of periodic SDE was identified on OBS 10 before the micro-seismic event with a period of about 2 s (Fig. 5.25b).

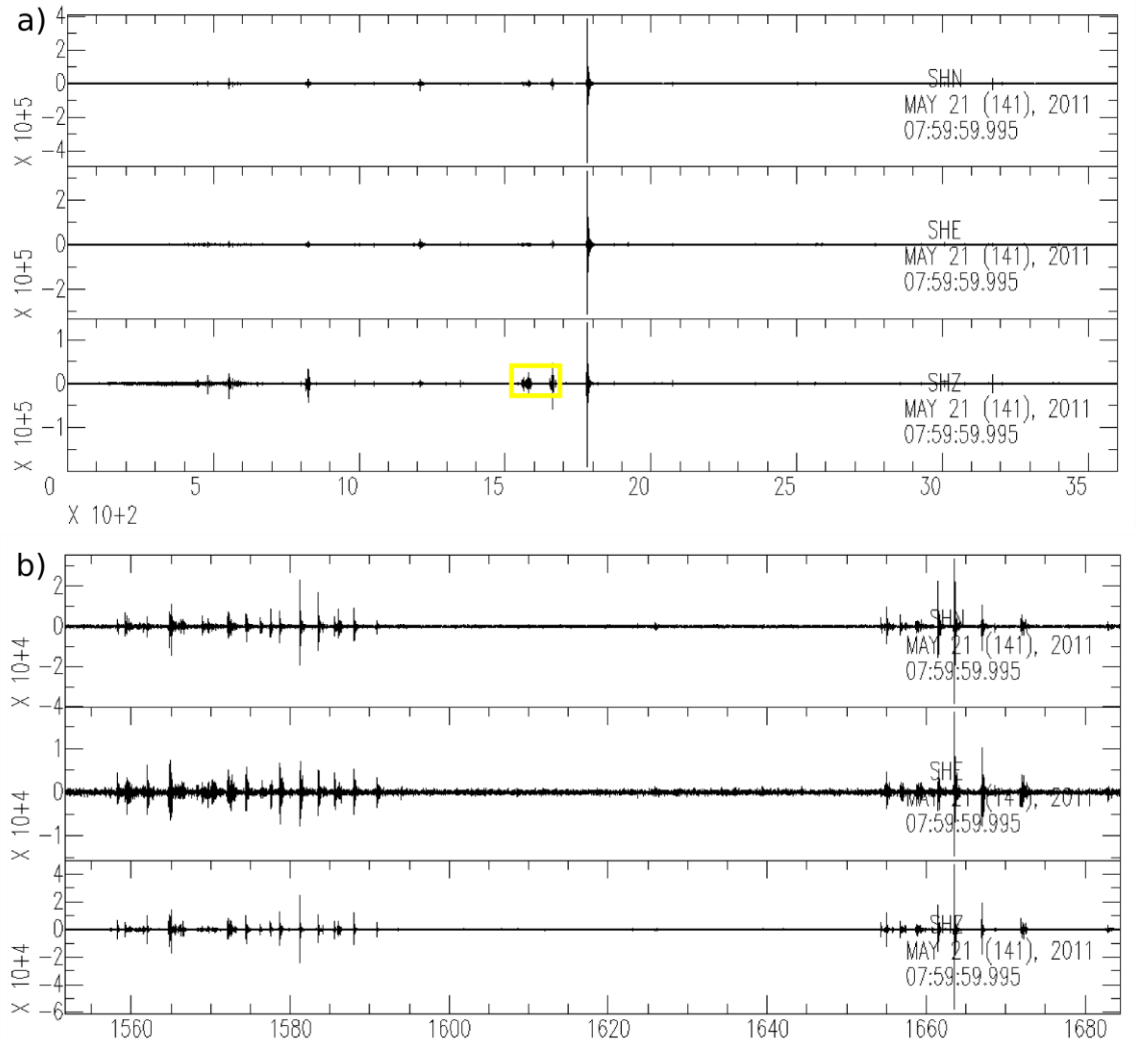

Figure 5.2.3.11: ***a)*** *One hour record section of 21th of May from 08:00 to 09:00 of OBS 10. Yellow frame shows the seismic event identified thanks to the Marmara 2011 network.* ***b)*** *is the zoom on the SDE crisis observed before this seismic event. SDE occur with a periodicity of ~2 s.*

The analysis of the seismograms of the observed SDE peak periods showed a clear relationship between SDE occurence and earthquake occurence. Earthquakes observed simultaneously with the SDE crisis do not necessarily occur at the neigbourhood of the OBSs. They may be located tenths of kilometers away from the OBSs. During the crisis of micro-seismic events, SDEs may occur periodically with time intervals which may be related to the amplitude of the micro-seismic events. However, we need more analysis in order to confirm this hypotesis.

5.2.4 SDE waveforms during crisis

Tary et al., [2012] has observed one specific SDE cluster sequence on one OBS deployed within the Marmara Sea in 2007, during the Marnaut cruise. On this OBS, they observed a swarm of more than 400 SDE in 24 hours and they reported that the waveforms of the observed events are very similar during this swarm. During this crisis, autors have observed that the number of SDEs increases gradually and reaches more than 90 SDEs in 2 hours, 6 hours after the beginning of the crisis (observed background rate was ~ 5 SDEs per hour).

In this study, the STA/LTA code used to detect the SDEs is developped specifically for this purpose and it is different from the one used by Tary et al., 2012. For a similar record duration (~ 3.5 months), Tary et al., have reported very different numbers of SDE's on different OBSs ranging between 915 and 3168. In our study, the number of detected SDE's is higly variable from one OBS to another (34571 to 80813) and it is nearly ten times bigger than the observations of Tary at al., 2013. The reason of this very large difference is not an increase of activity during the survey period, but the difference between two used detection tools and the chosen parameters. Tary et al., did not considerend events with small amplitudes (personal communucation) in order to undersand the general behavior of the SDE's. Here we considered as many events as possible in order to analyse the spatial and temporal distributions of the SDEs. The daily average of the number of SDE occurence on all OBSs of the Marmara 2011 network is ~445 SDEs per day. On the daily distributions very clear SDE crisis were observed on the OBS 01 on the 26th of July with more than 3500 SDE per day and on the OBS 04 on 14th and 27th of June, with more than 2000 SDEs. The average hourly background rate is ~19 SDE per hour. This values varies from ~ 13 SDE per hour on OBS 03 to ~ 33 SDE per hour on the OBS 04.

We identified the swarm periods observed on different OBSs and carried out a principal component analysis (PCA) on these swarms in order to analyse the degree of similarity between the SDEs. The STA/LTA identified SDE's are recorded as temporal series of one second (100 samples with a sampling frequency of 100 Hz). The signals were rotated in the frame of reference of the wave than the covriance matrix was calculated for the events. The characteristic signals have been approached by the eigenvectors and the degree of representativeness of the eigenvectors has been approached with the eigenvalues. Hereafter, the representativeness of each eigenvector will be given as a percentage of total energy ($(\lambda i^2/somme\lambda i^2)$.

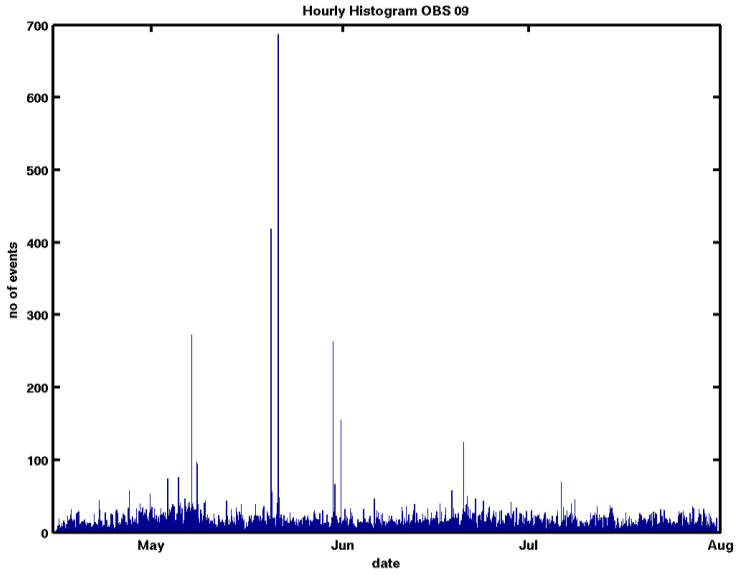

Figure 5.2.4.1: The hourly SDE distribution on the OBS 09. Two clear SDE crisis are observed on the 20th of May at 07:00 with more than 400 SDEs and on the 21th of May at 11:00 with nearly 700 SDE per hour which is the maximum number of SDE observed in one hour during the whole record period.

The maximum number of SDE in one hour is observed on OBS 09, during the swarm of 21th of May introduced in the previous section (Fig. 5.2.4.1). More than 700 SDEs are identified between 11:00 to 12:00. The PCA perfomed with this data set indicates that the first eigenvector has a data representativeness of ~83 % on the x1 component(Fig. 5.2.4.2), suggesting a common source and similar source-receiver ray paths. The relatively low data representativeness of the first eigenvectors of the x2 and x3 components, ~27 and ~31 per cent, respectively, result likely from the presence of coherent arrivals of smaller amplitudes, such as near-field waves, modifying the otherwise linear polarization of these microevents. This high representativeness and the clear periodicity with ~1.6 s between the SDEs may suggest that this swarm has an electronic origin rather than a gas related origin. We preclude this hypothesis, because these events occur before and after some specific earthquakes. If they had an electronic origin, they would occur before and after all micro seismic events and the magnitude of earthquakes migth play a role. No relationship has been identified between the occurence of these periodic signals with the magnitude of the earthquakes.

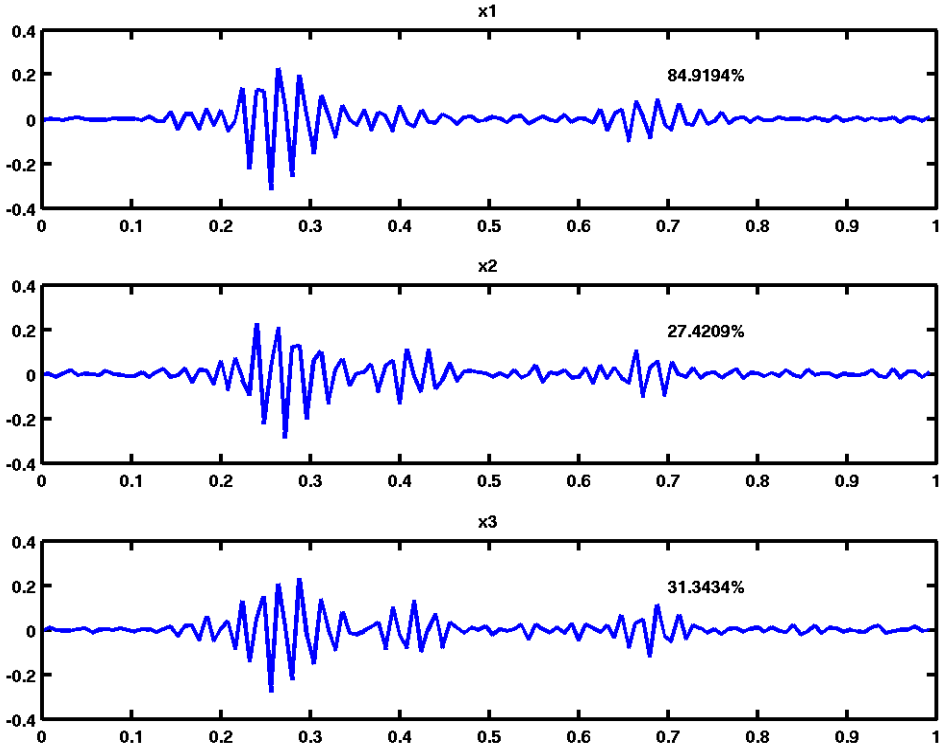

Figure 5.2.4.2: PCA of micro-events constituting the crisis identified on OBS 09 on the 21th of May at 11:00 for the components x1, x2 and x3. Temporal series of the first eigenvectors. The representativeness of each eigenvector is indicated by its eigenvalue given in percentage of the total energy.

The second most important SDE swarm is observed on the OBS 04 on June 15, between 19 and 20:00 pm with nearly 600 SDE per hour (Fig. 5.2.4.3). The observation of the second larger swarm on OBS 04 supports our hypothesis that OBS 04 was located on a gas emission site. The semblance between the SDEs constituting this swarm is less than for the one observed on OBS 09. This may be due to the activity of more than one gas source which have been recorded by the OBS 04.

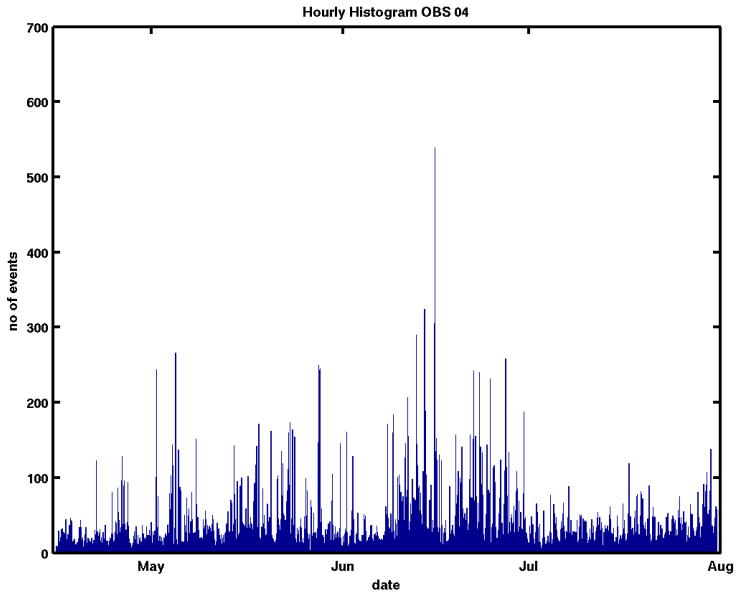

Figure 5.2.4.3: The hourly SDE distribution on OBS 04. A clear SDE crisis is observed on June 15, at 19:00 with more than 500 SDEs.

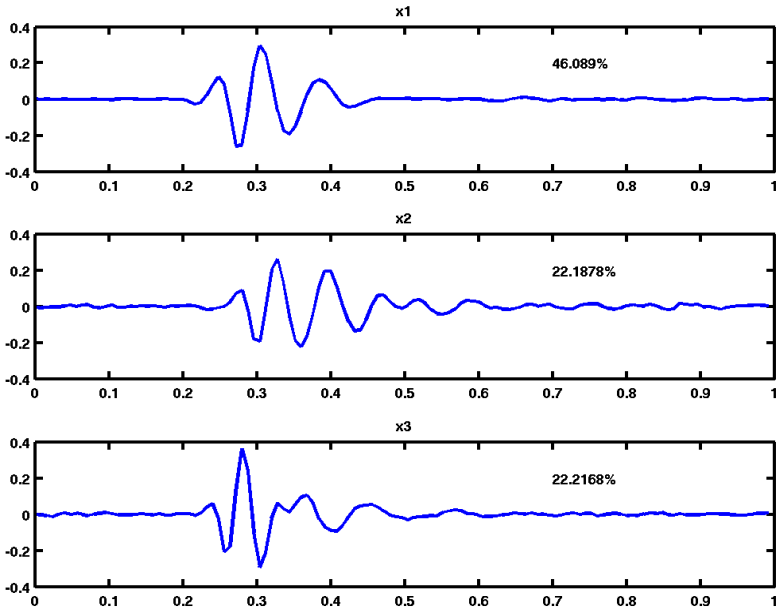

Figure 5.2.4.4: The hourly SDE distribution on the OBS 04. A clear SDE crisis is observed on the 15th of June at 19:00 with more than 500 SDEs.

5.2.5 Combined analysis of SDE and micro-seismic event distributions

An earthquake of magnitude Mw 5.1 occured on the 25th of July at 17:57 pm on the North Anatolian Fault segment which cuts across the Western High (Fig. 5.2.5.1). Following this earthquake a crisis of micro-earthquakes was recorded on all OBSs, until the end of July (the end of Marmara 2011 OBS recording period). Simultaneously, a SDE crisis was observed on

OBS 01, which was located at the northern border of the Tekirdag Basin (see Fig 5.2.5.1 for location). OBS 02 which was located on the Western High, right above the mainshock, stopped recording on the June 16, at 21:00 am, before the micro-seimic crisis. Periodically happening SDE's were observed together with high amplitude SDEs in the hours preceding the recording end AT OBS 02. The reason why OBS 02 stopped recording before the end of the survey may be related to anomalously high gas emissions at this site.

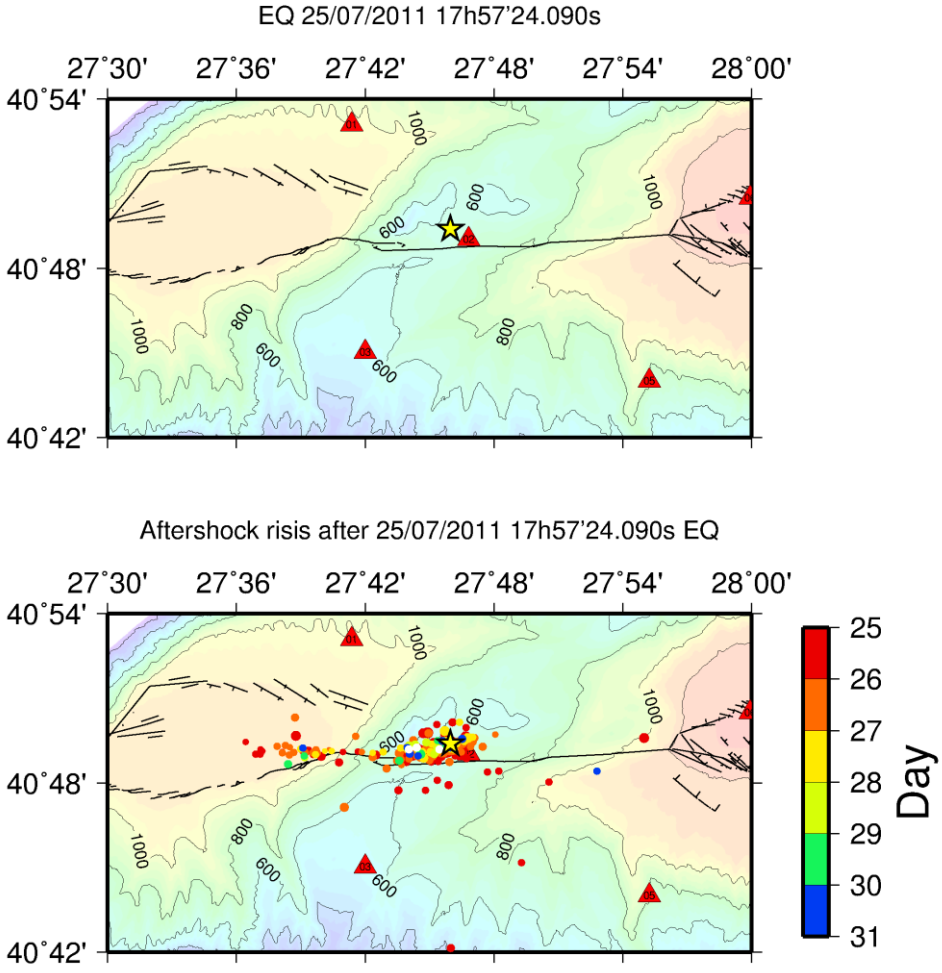

*Figure 5.2.5.1**: Top**: the yellow star shows the location of Mw 5.1 earthquake of 25th of July at 17:57. Red triangles are OBSs of the 2011 network. **Bottom**: the micro-seismic swarm which followed the Mw 5.1 event*

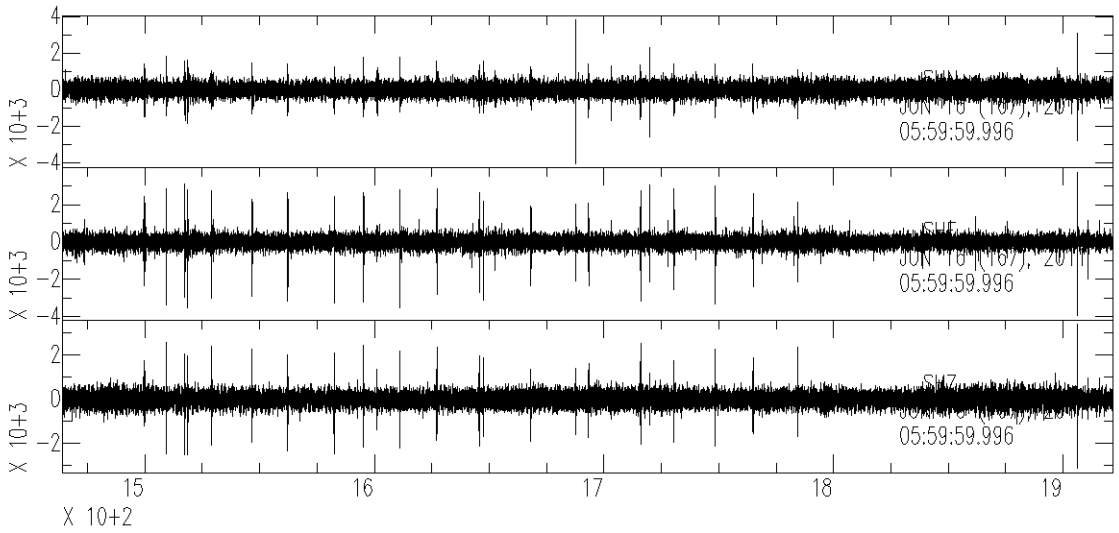

Figure 5.2.5.2: SDE crisis observed on the 16th of June on OBS 02 in the hours (here 06:00 to 07:00 is shown) preceding the break down (at 09:00) of OBS 02.

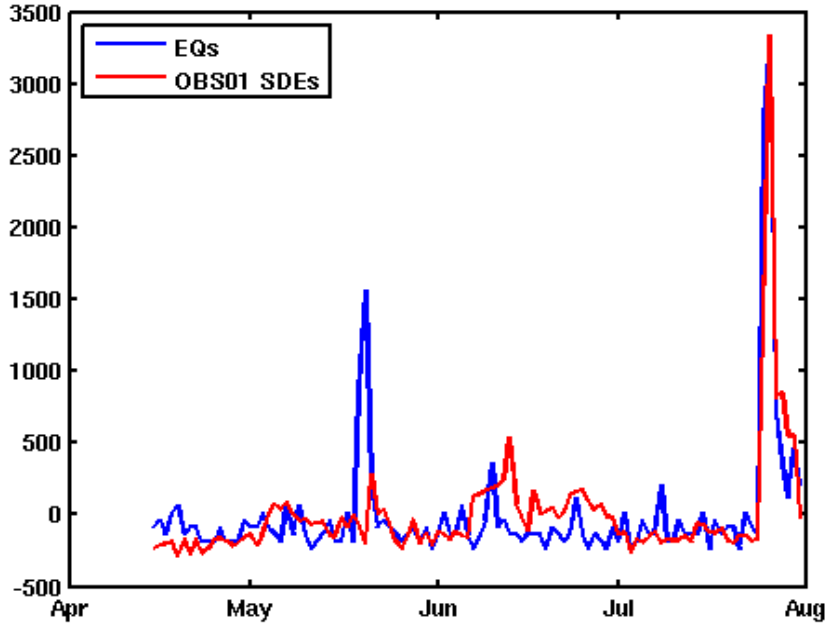

Figure 5.2.5.3: Daily distribution of seismic events identified on the Marmara 2011 OBS network together with the SDE distribution osbserved on OBS 01. In order to easily compare the daily micro-earthquake distribution with the daily SDE distribution, the number of micro-earthquakes have been multiplied by 50.

Fig. 5.2.5.3 shows the daily distribution of seismic events identified on the Marmara 2011 OBS network together with the SDE distribution osbserved on the OBS 01. In order to easily compare the daily micro-earthquake distribution with the daily SDE distribution, the number of micro-earthquakes have been multiplied by 50. The increase in the SDE occurence happens simultaneously with the crisis of micro-eathquakes (Fig. 5.2.5.3) and the SDE occurrence

decrease with the decrease of the micro-earthquake occurence. Such correlation could be related to the STA/LTA code which could identify some earthquakes parts as being SDE's due to the reasons explained before. The SDE's during this crisis has been checked visually and with a principal component analysis. The most representative waveform (the first eigenvector) has the characteristic of SDE's.

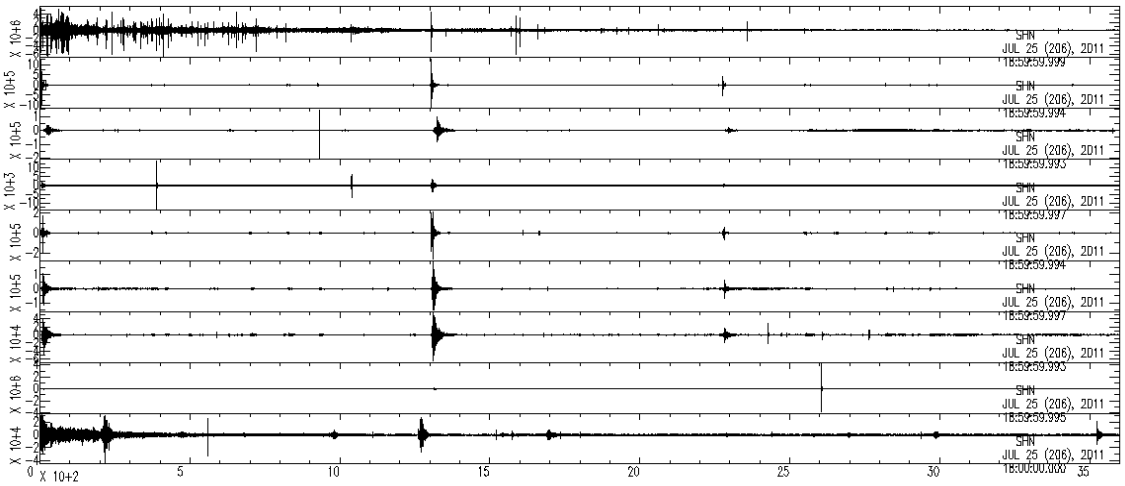

Figure 5.2.5.4: One hour record section of the 25th of July, 20:00 to 21:00 pm. An SDE crisis is observed on OBS 01 whereas no important SDE activity is identified on the other OBSs. Some micro-seismic events are also observed on this record section.

On the daily distribution of the micro-seismic events the second most important peak period is the one observed on the third week of May and this peak corresponds to the SDE crisis observed on the OBSs 07, 08, 09 and 10 which have been discussed previously in the *section 5.4.3.*, together with the correlation observed between these four OBSs on which we observed a SDE swarm simultaneouly with this micro-earthquake swarm.

6. Task 6 Multi-parameter correlation (joint analysis of OBS and acoustic data)

6.1. Joint analysis of seismologic data and acoustic BOB data

Marmesonet (2009)

During the Marmesonet experiment, in 2009, OBS 09 was deployed 150 m to the NE of the BOB module, in the Cinarcik Basin. The OBS data appear to be affected by a characteristic noise of very high amplitude (Fig. 6.1.1). The automatic detection of SDEs on OBS 09, based on STA/LTA, turned out to be inefficient, due to the high background noise level. The attempt of manual picking was also inefficient, likely due to a high level of man-made noise.

In the Marmara Sea, the Cinarcik Basin zone is used as ship parking and testing area. The noise observed on the OBSs located within this basin could be due to shipping noise which usually varies between 0 to 200 Hz depending on ship size and speed (bigger ships having larger helices and lower revolution per minutes, result in bas frequency noises and vice versa). On the OBSs which are not located within the Cinarcik Basin, the characteristic noise explained above does not affect the signal and enables the micro-event identification to be done manually, without any problem (Fig. 6.1.1).

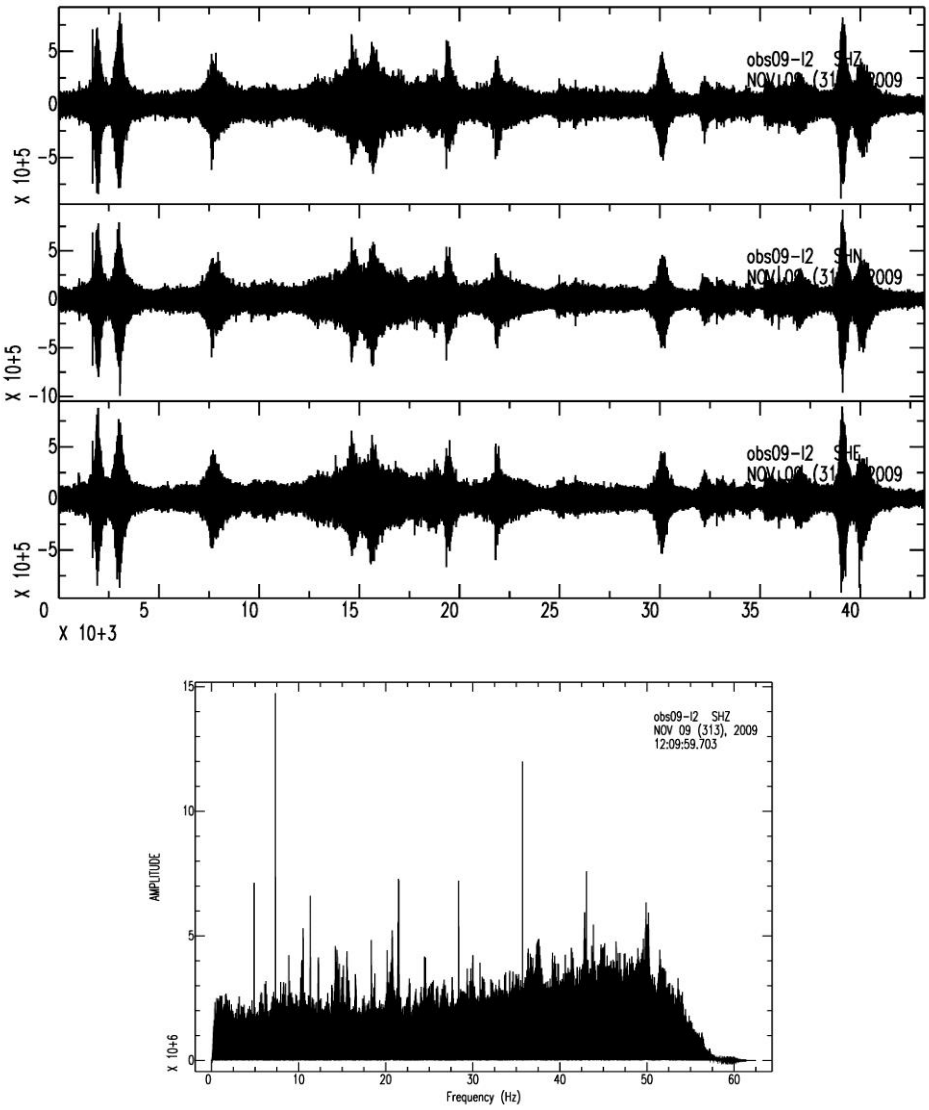

*Figure 6.1.1 :**a)** 12 h of data recorded at the Cinarcik Basin, 150 m NE of BOB, by the three geophone components of OBS 09. **b)** the corresponding spectrogram**.***

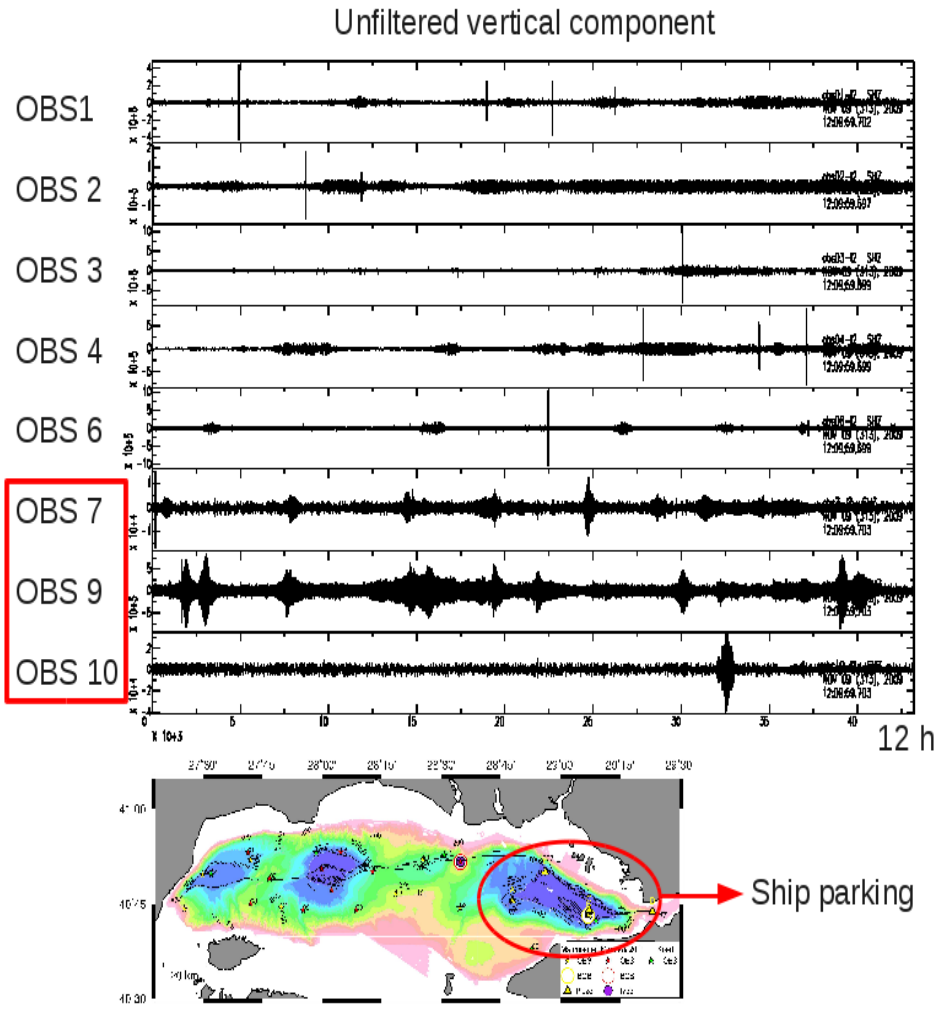

Figure 6.1.2) ***a)*** *Same 12 h record period than on Figure 6.1.1, displayed for the vertical component of all OBSs of the Marmesonet network. All OBSs located within the Cinarcik Basin (OBS 07, 09 and 10) are affected by similar (but not same) characteristic seismic noise.*

b) *Zoom on a 1 min long recording period on the vertical component of all OBSs of the Marmesonet network.*

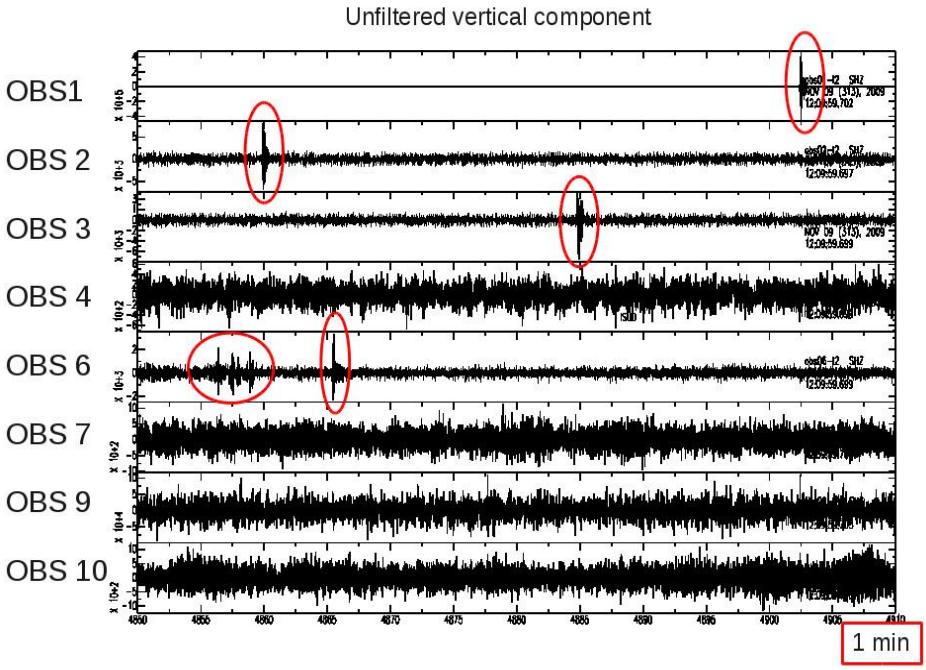

Marmara 2011

The identification of SDEs first has been done manually for the record period of BOB Marmara 2011 on OBS 04, which was deployed during the Marmara 2011 survey on the Central High, within the area insonified by the BOB module. OBS 04 was located 46 m north of BOB (based on the echo-integration results), within sector 10. The echograms recorded over 5 cycles within sector (6.1.3) suggest the presence of a bubble source beneath the OBS.

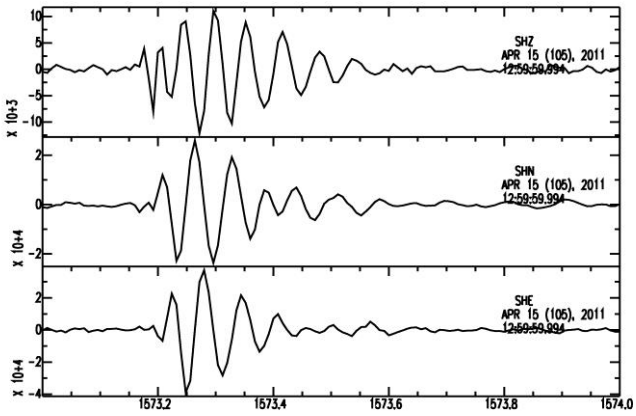

a)

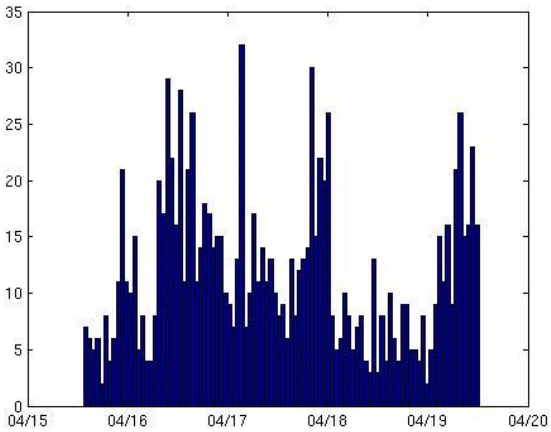

b)

Figure 6.1.3: ***a)*** *Example of Short Duration Event recorded by OBS 04 during the recod period of BOB.* ***b)*** *Histogram showing the distribution of the events identified on OBS 04 during the period when BOB was recording.*

Figure 6.1.3 shows an example of a manually detected SDE, recorded on OBS 04 during the record period of BOB. Characteristic SDEs detected on OBS 04 are similar to those described

by *Tary et al., [2012]*. OBS04 records started on April 15th, 2011, for a duration of 4 months. BOB recorded data from April 12th to April 19th, 2011. OBS 04 and BOB thus recorded simultaneously data during only 4 days, from April 15th to April 19th. During these 4 days, a total of 1101 SDEs (manually identified) were recorded by OBS 04. However, it is not really possible to analyse simultaneously the flow rates associated to the gas emission sites identified on BOB acoustic data, and the temporal distribution of SDE's identified on OBS 04. The OBS acquires a continuous time series with events that may be located on a circle centred around the OBS. In contrast, in its present configuration, the BOB module acquires during limited durations (of 1 hour in the case of Marmara 2011) over a volume covered by the beam of 7° and on 80 m (after 80 m, the signal/noise become too small to detect the gas bubble).

During the common record period of 4 days, there is thus only 4 hours during which the BOB was oriented towards the OBS. These 4 hours correspond to cycles 4 to 7 of sector 10. However as explained before, due to a tecnical problem, the data for the cycles 5 and 7 could not been reduced for this sector. Hence, the common record period of two instruments is only 2 hours (April 15th 21:00 to 22:00 and April 17th 21:00 to 22:00) corresponding to cycle 4 and 6, of the sector 10.

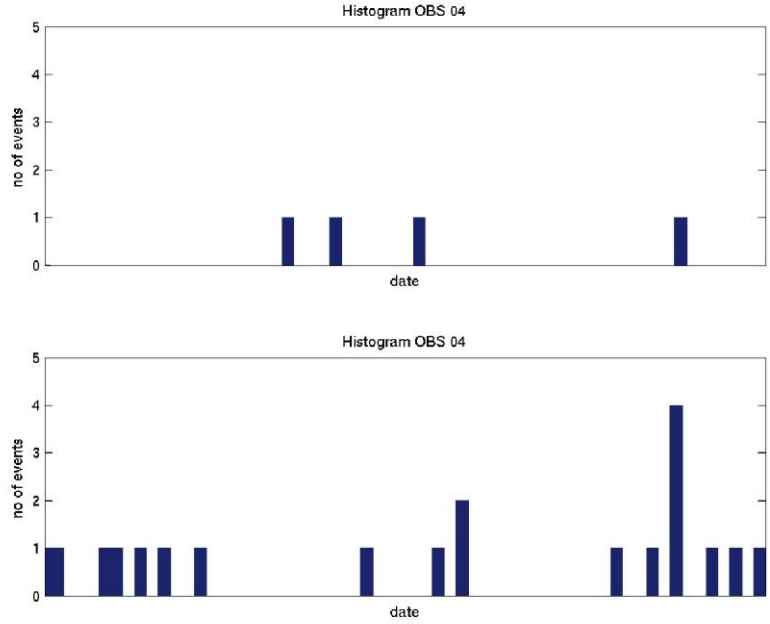

Figure 6.1.4: The hourly distribution of SDE's automatically identified on OBS 04 during April 15th 21:00 to 22:00 and during April 17th 21:00 to 22:00.

The numbers of SDEs identified (automatically) during the two hours of joint recording are shown on Figure 6.1.4. During cycle 4, only 4 SDE's have been identified whereas during cycle 6, a total of 21 SDE's have been observed. This observation is coherent with the

acoustic data which shows an increase of gas emission on cycle 6 with respect to the one observed on the cycle 4.

Since the OBS records all events around itself, we could also compare the temporal SDE distribution with a total flow rate wich could be computed for the whole record period of the BOB however, this unfortuanely is not possible to compute since the acoustic data from different sectors are not simultaneous. Therefore, this study shows the need to design an acoustic system which will acquire a continuous time series from a larger insonified volume.

The alternative solution which would allow to compare the SDE distribution with the flow rates computed by using the BOB acoustic data would be to relocate SDEs thanks to a triangulation and to compare the flow rates computed for one sector only with SDE's located within this insonified area. Since SDEs are very local events which are not recorded on distant OBSs, such study would require at least three very densly spaced OBSs.

6.2. Joint analysis of seismologic data and acoustic multibeam data

Refer to *Dupré et al [2015]* and to *Bayrakci et al [2014]*.

6.3 Joint analysis of piezometric data and seismological data

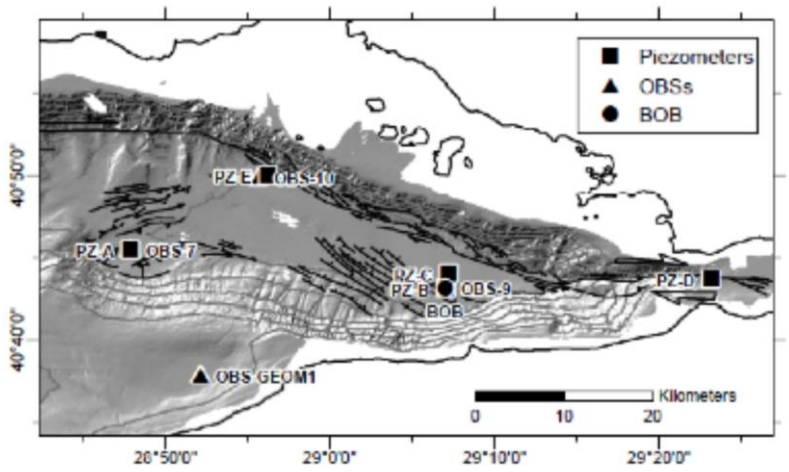

Figure 6.3.0 Location of piezometers (black squares), OBSs (black triangles) and BOB (acoustic detector of bubbles in the water column, black dot) deployed in the Çinarcik Basin during the Marmesonet cruise.

PZA

Piezometer PZA was located at the southwestern border of the Cinarcik Basin, at the neighborhood of OBS 07, recording pressure and temperature variations during 153 days between 27th of September 2009 and 27th of February 2010. Correction for offset was performed and anomalous values we removed. Four pressure variations were observed on this piezometer during the whole record period:

- A decrease in pore pressure (from 7.25 kP to 6.5 kPa) was observed on September, 30, 2009 at 11:00 pm, on sensore located at 3.84 m sbelow seafloor (shown in green on Fig. 6.3.1). OBS recordings started not before October 1st, 2009. Earthquake catalogs (e.g. from KOERI) do not show any unusual increase in the number of earthquakes within less than ~ 200 x 200 km away from PZA (Fig. 6.3.2).
- A smooth decrease in pore pressure (from 1.6 kPa to 0.6 kPa) was recorded on October 12th, 2009, at 09:00 am (Fig. 6.3.3) by the sensor located at 5.39 m below sediment surface. No simultaneous earthquake, nor no simultaneous temperature variation were observed along with the pressure variation. On the other hand, an increase in SDE occurence was observed on the nearby OBS 07 during the 24 hours that preceded the pressure drop.

- A transient, high frequency pore pressure variation occurred on October 21st, 2009, 22:16, in response to a micro-earthquake that was clearly recorded on the nearby OBS 07.

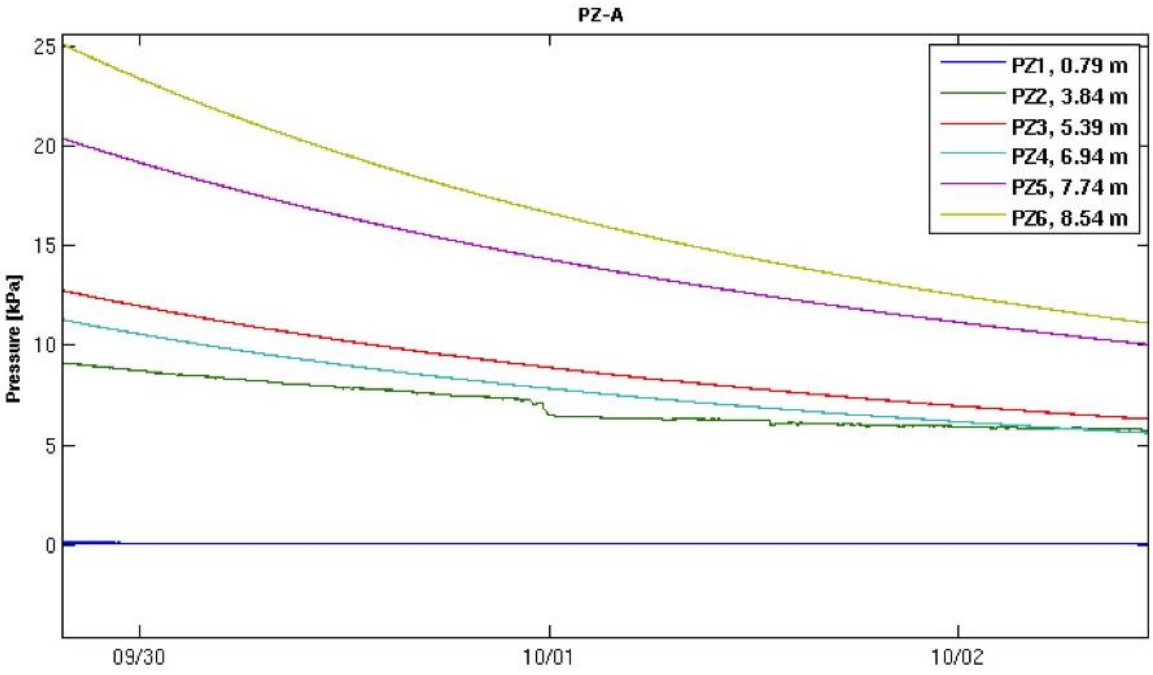

Figure 6.3.1 Differential pore pressure observed on PZA, between September, 27th 2009 and February, 27th, 2010

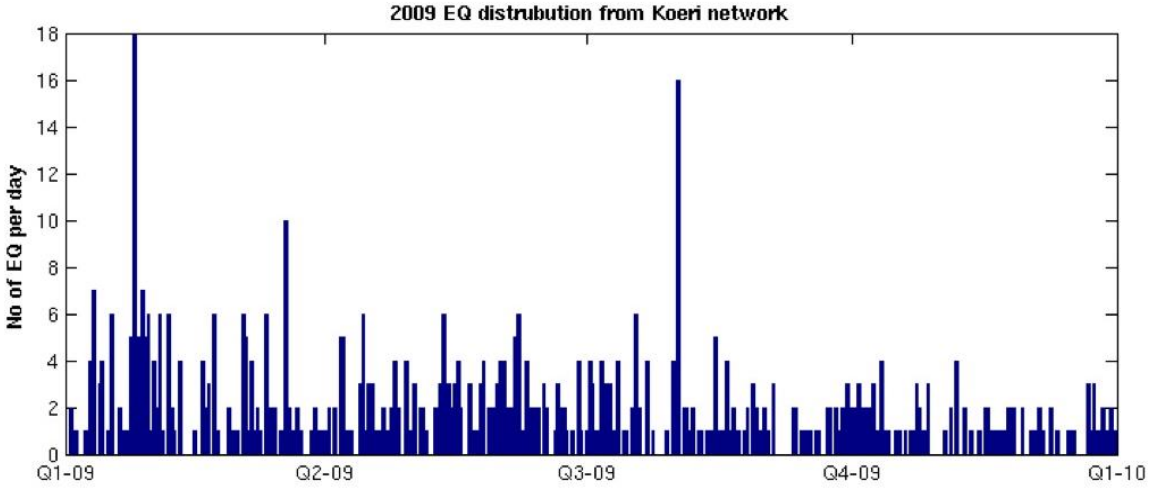

Figure 6.3.2: Daily distribution of Marmara Sea Region earthquakes (source: KOERI earthquake catalog). The pressure variation observed on September 30th does not correspond to an increase of the number of earthquakes.

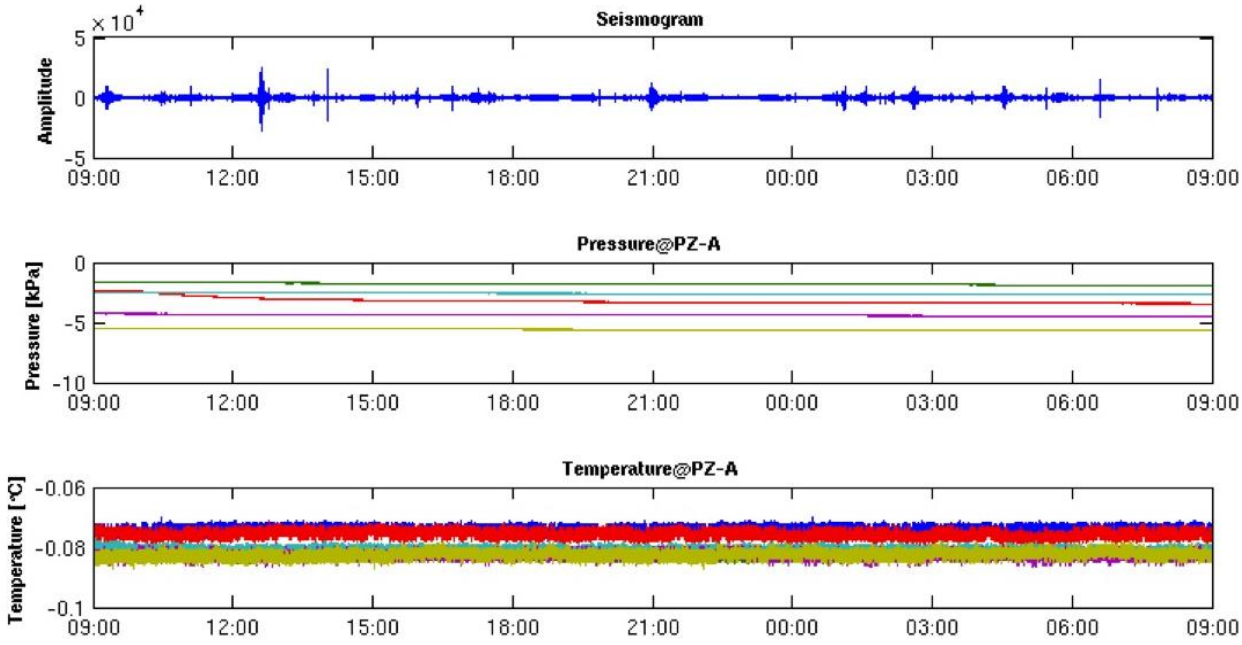

Figure 6.3.3: 24 hours seismologic (top) and piezometric (pressure, middle and temperature, bottom) records recorded by OBS 07 and nearby PZA on October 12th, 2009.

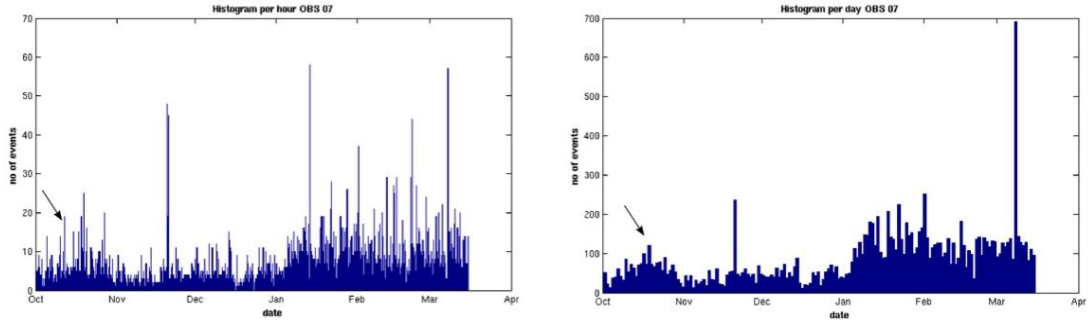

Figure 6.3.4: Hourly and daily SDE distributions on OBS 07.

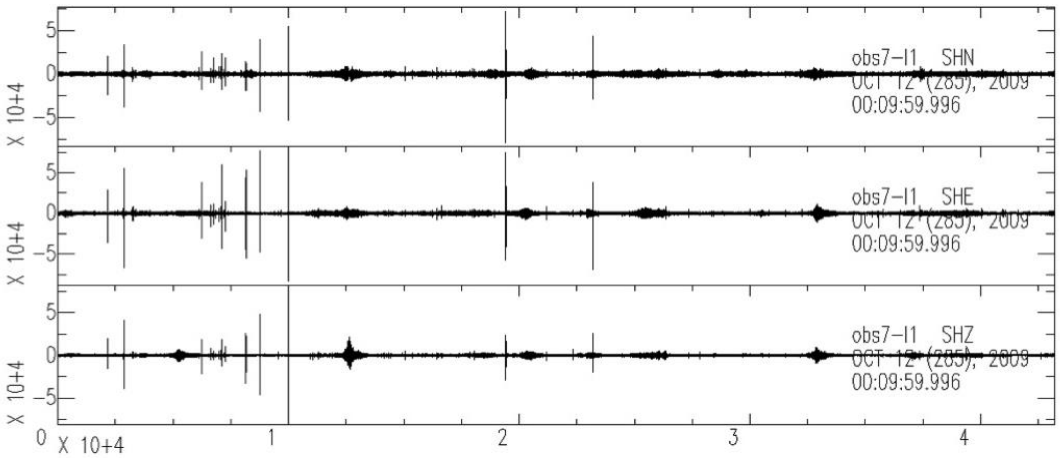

Figure. 6.3.5 Crisis of SDE events recorded on OBS07, on October 12th, 2009, between 02:00 to 03:00.

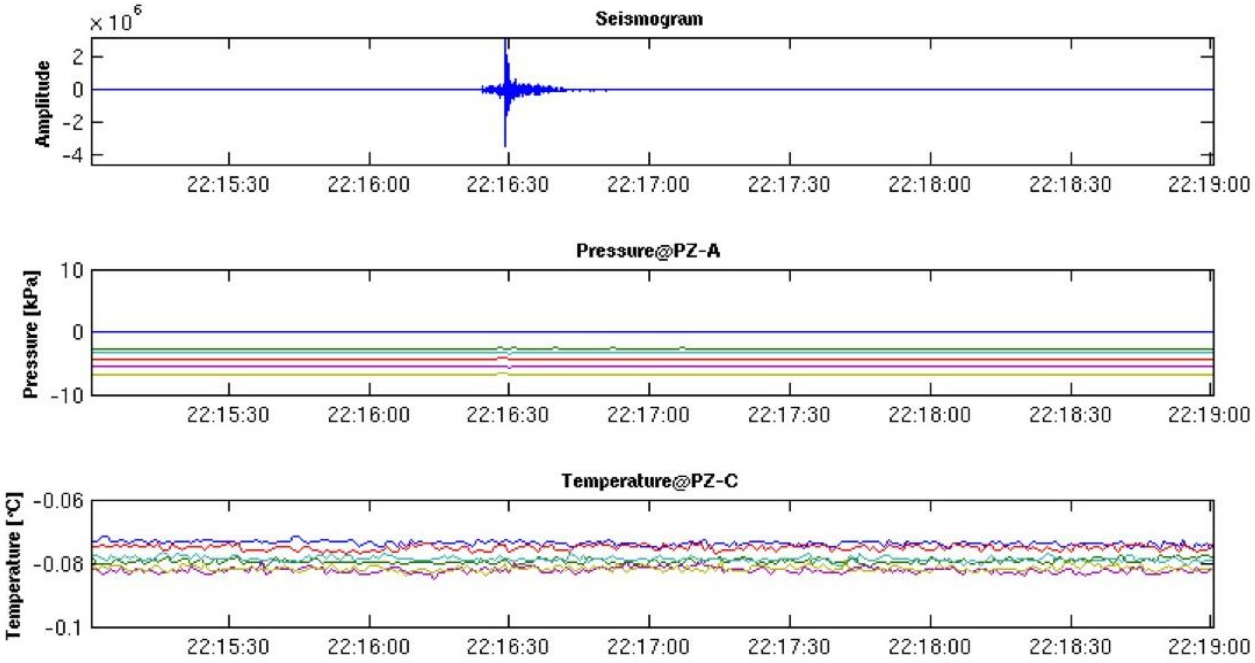

Figure 6.3.6: Tiny pressure variation on PZA piezometer in response to a micro-earthquake on October 2009 at 22:16.

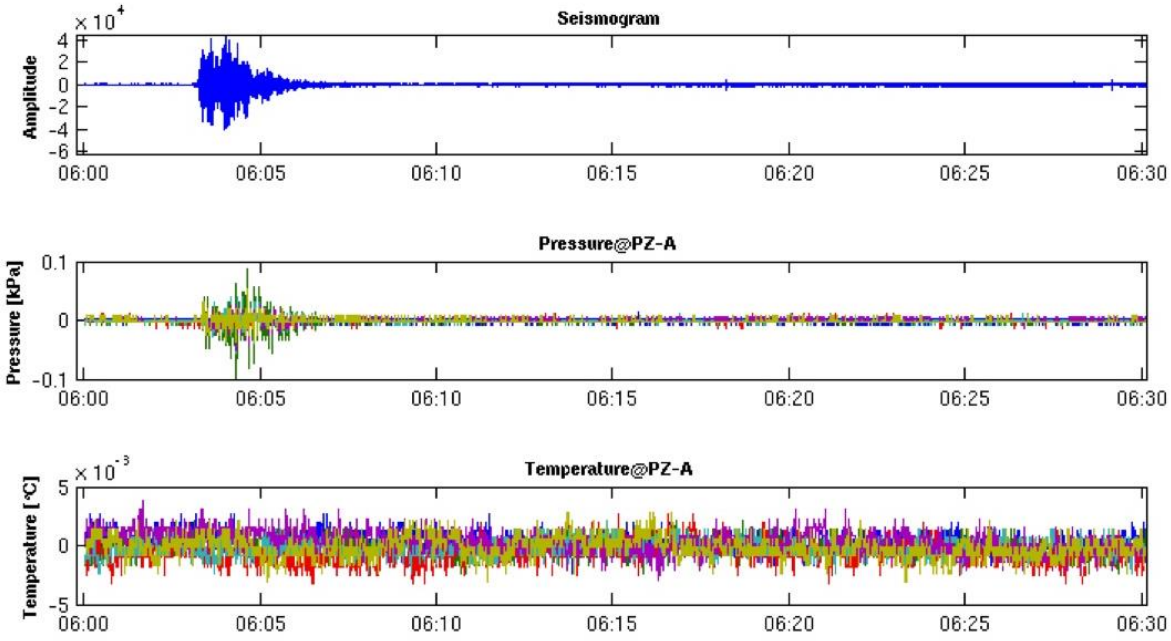

Figure 6.3.7: Pore pressure variation recorded at PZA in response to a 5.2 mb regional earthquake that occurred on December 4th, 2009, recorded on OB 07.

Earthquakes involve variations in static stress near the fault (near-field), and in dynamic stress due to seismic waves propagation (intermediate- and far-field). Depending on the level of stress increase, the porous media will deform either elastically or plastically. No permanent deformation or pore pressure build-up occurred at any depth (in both earthquake cases), showing a purely elastic response of the system piezometers sediments. Due to higher permeability in the first meter of sediments, the first sensor at 0.79 m (in blue on Fig. 6.3.6 and 6.3.7) below sea floor did not record the earthquake.

The fast Fourier transform of the time-series acquired by all sensors of the PZA did not show a periodicity related with tides. Since the Marmara Sea is surrounded by land, tidal effects are small and observed mostly within the neighborhood of straights, in which case tidal variations are smaller than the sensitivity limit of piezometers.

PZB

Piezometer PZB was deployed at the southern border of the Cinarcik Basin, close to the BOB module and to OBS 09. Unfortunately, PZB stopped recording after 3 days of recording, possibly due to the extensive bubbling at this location. Recording at OBS 09 starts on October 15th, 2009, thus no simultaneous seismologic data is available at this site.

PZC

Piezometer PZC was deployed on the southeastern part of the Cinarcik Basin, close to the BOB module, to OBS 09 and to PZB. Pressure variations were observed:

- on all sensors on november 11th, 2009, at 02:10 pm (Fig. 6.3.8), simultaneously with an earthquake, which is not reported in KOERI's earthquake catalog.
- on November 16th, 2009 (Fig. 6.3.9) on all sensors at 05:07 pm and at 06:46 pm. The latter event at 06:46 pm occurred in response to a local micro-earthquake, recorded on a few, but not all OBSs (Fig. 6.3.10).
- on January 2nd, 2010, on all sensors, in response to a local micro-earthquake, having the same specific characteristics as previously described (with no distinct P and S arrivals).

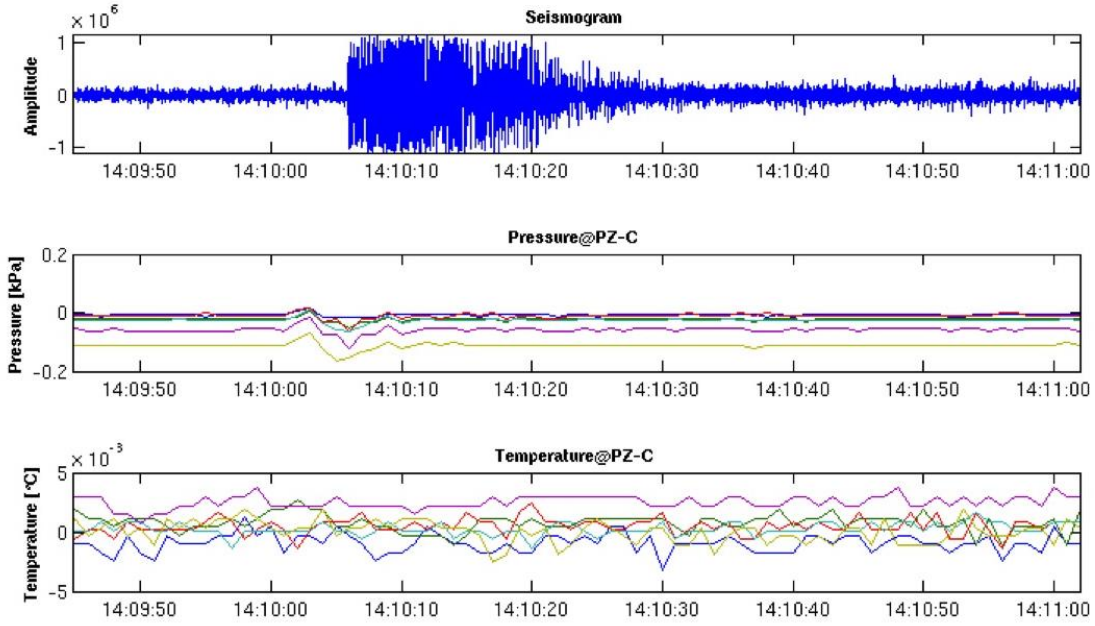

Figure 6.3.8:Pressure and temperature variations observed on November 11th, 2009 at 02:10 pm and the corresponding seismogram.

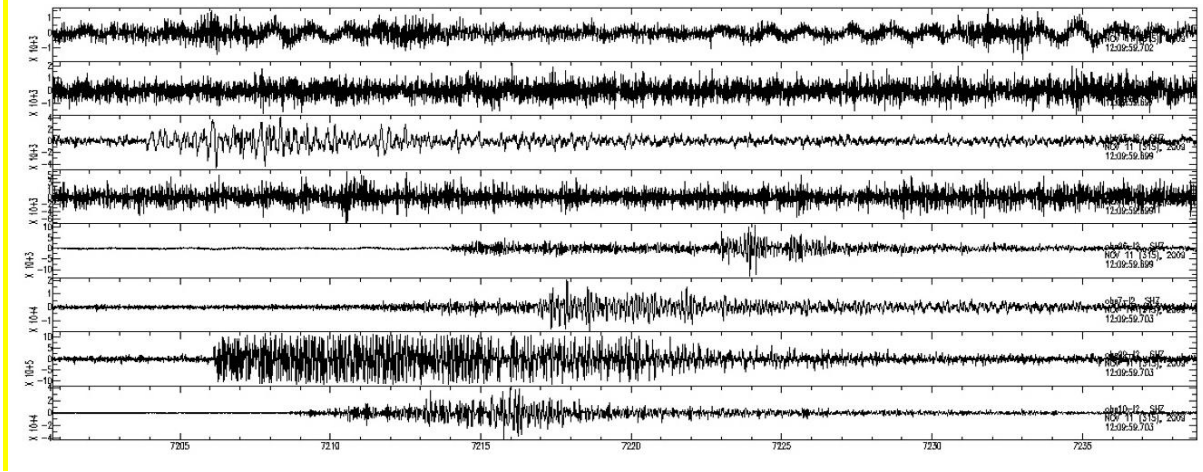

Figure 6.3.9: The uncatalogued earthquake observed on the OBSs on November 11th, 2009 at 02:10.

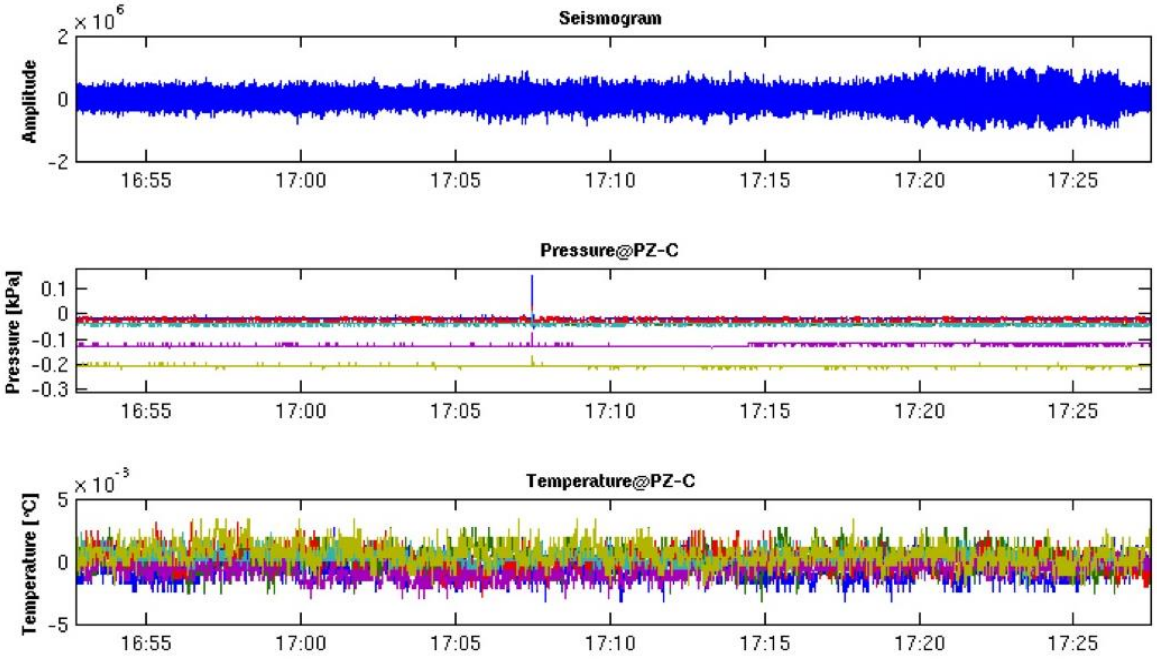

Figure 6.3.10:Pore pressure micro-variations and temperature, recorded on PZC on November 16th, 2009 at 17.07 along with the seismic signal.

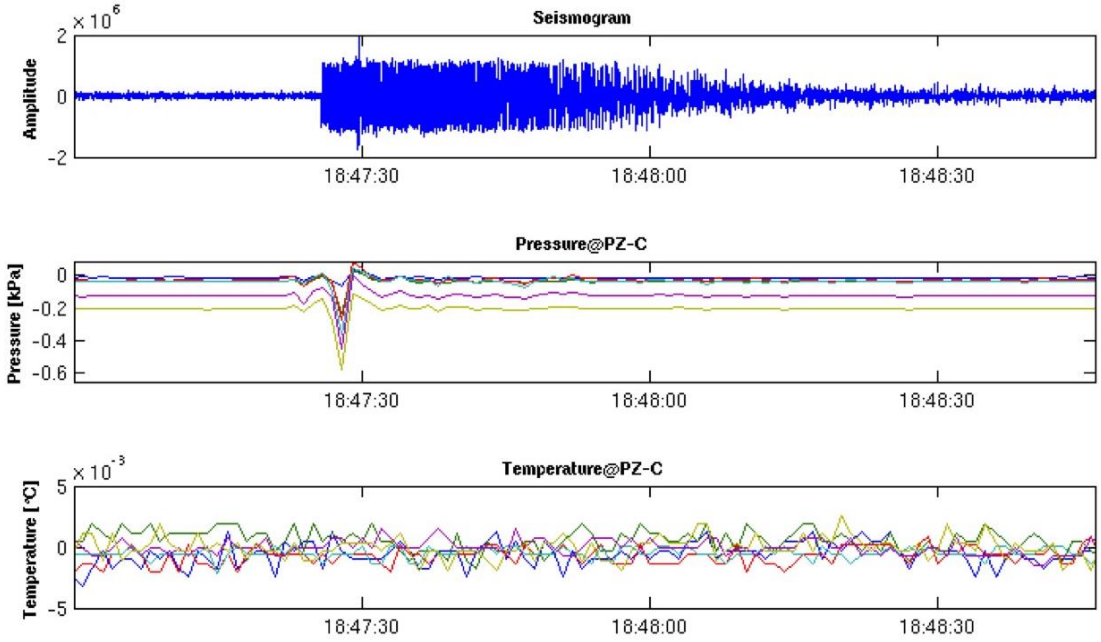

Figure 6.3.11: Pore pressure variation recorded on November 16th, 2009 at 18:46 in response to a local, uncatalogued, micro-event. and corresponding seismogram and temperature measurements.

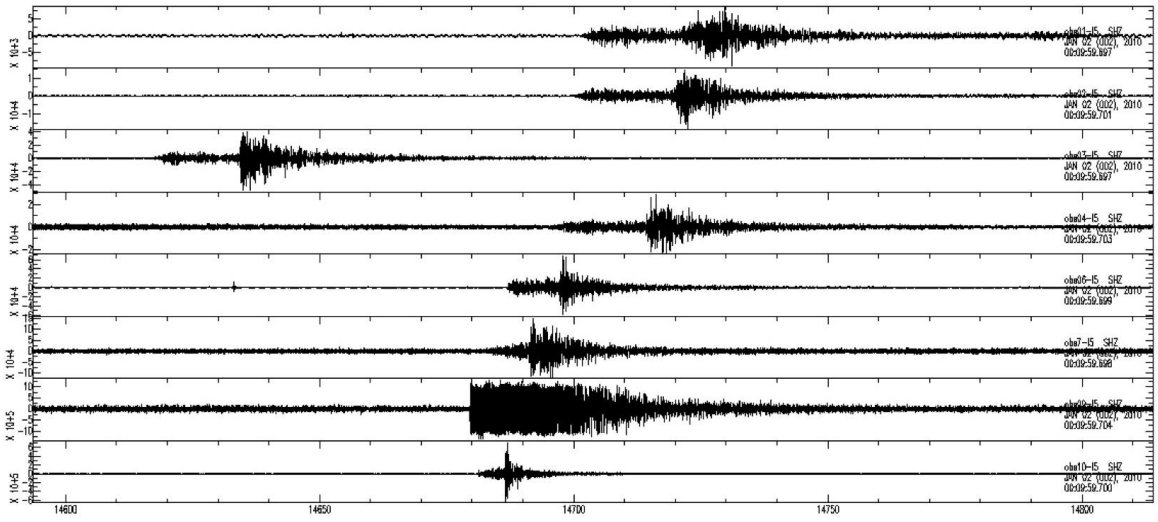

Figure 6.3.12: Uncatalogued earthquake as recorded on the OBSs on November 16th, 2009 at 18:46.

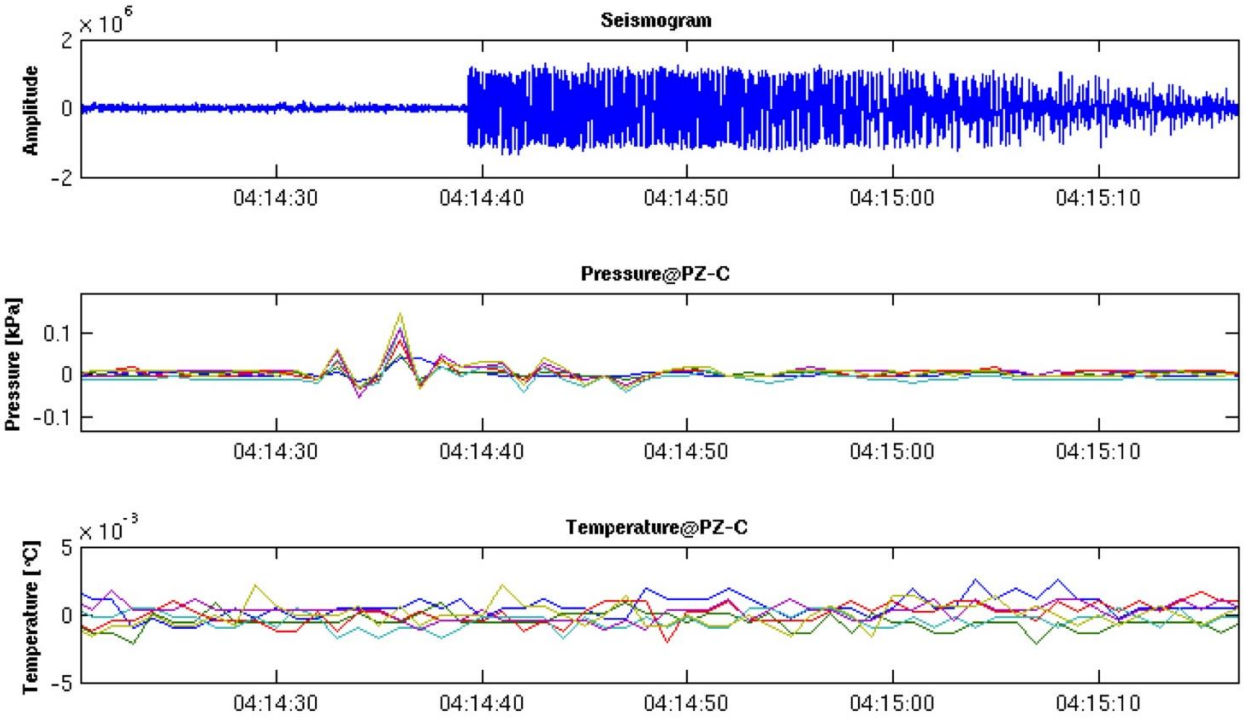

Figure 6.3.13: Pressure variation observed on January 2nd at 04:14 and corresponding seismogram and temperature measurements. An uncatalogued earthquake is observed simultaneously.

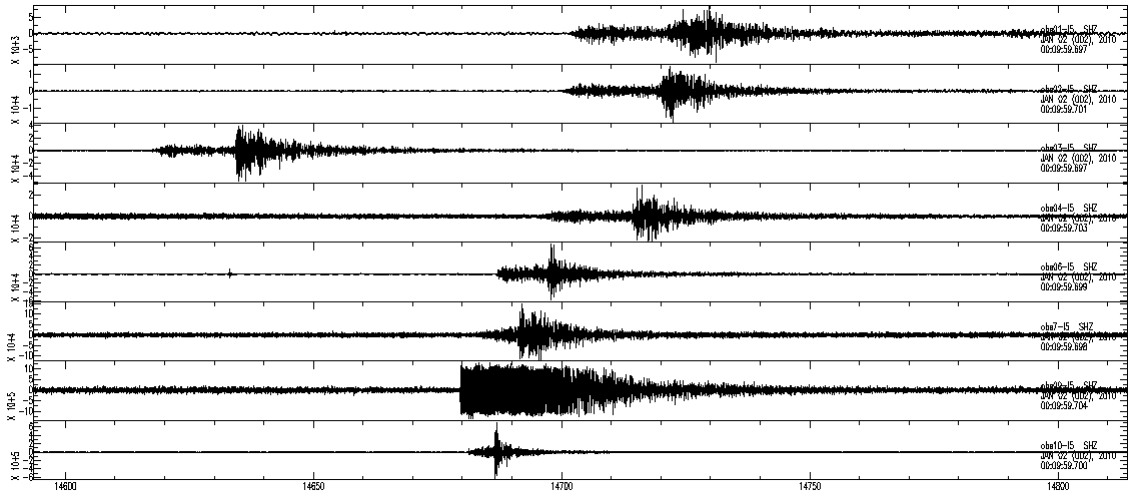

Figure 6.3.14: Uncatalogued earthquake as recorded by the OBSs on november 16th, 2009 at 18:46.

PZD

Piezometer PZD was located at the Gulf of Izmit. No OBS was located at the neighborhood of this piezometer. Pressure variations were recorded on PZD, in response to micro-earthquakes that were clearly recorded on OBS 09 and OBS 07 (Fig. 6.3.15 to 6.3.18).

PZE

The piezometer PZE was located at the northern border of the Cinarcik Basin, near by OBS 10. Unfortunately it stopped recording on the 10th of October, at the end of eleven days, before the begging of OBS recordings. No pressure variation was observed on this piezometer in the record period of 10 days.

Conclusions of piezometer data analysis

During this systematic analysis of Marmesonet 2009 experiment, most observed pressure variations appear to be linked to local earthquakes and recorded on all sensors. There is only one case of pressure variation related to a SDE swarm. In contrast to the other cases this pressure variation is observed as a pressure decrease only on the sensor located at 5.39 m bsf. The amplitude of this variation is ~1kPa, much higher than the amplitude of the seismic-induced, pore-pressure transients.

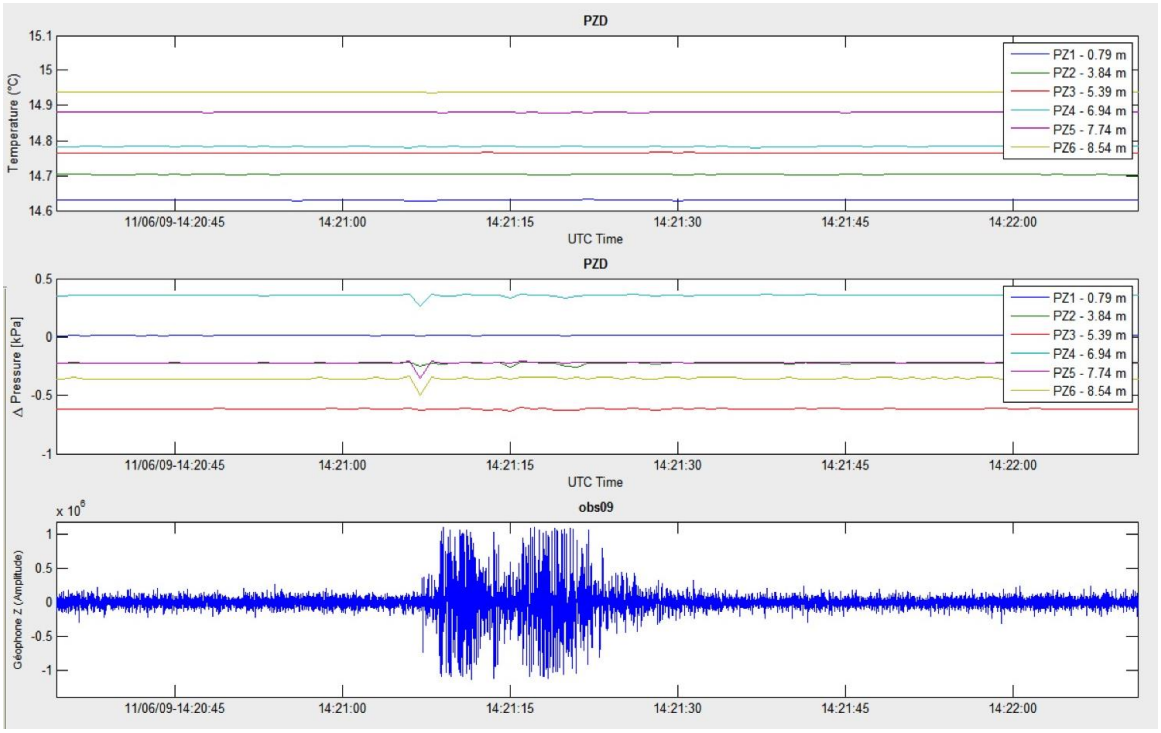

Figure 6.3.15: Temperature and pressure variation recorded at PZD along with ground velocity recorded on OBS 09, on November 6th 2009, at 14:22.

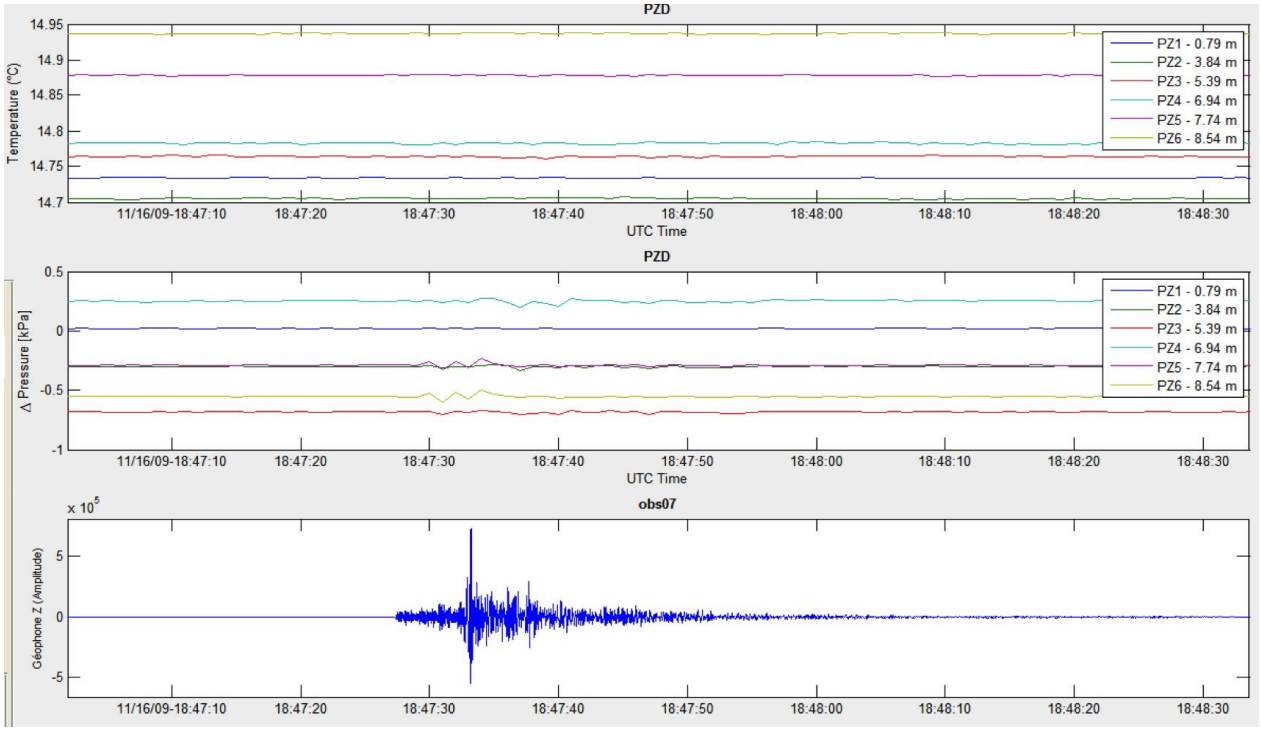

Figure 6.3.16: Temperature and pressure variation recorded at PZD along with ground velocity recorded on OBS 07, on November 16th 2009, at 18:47.

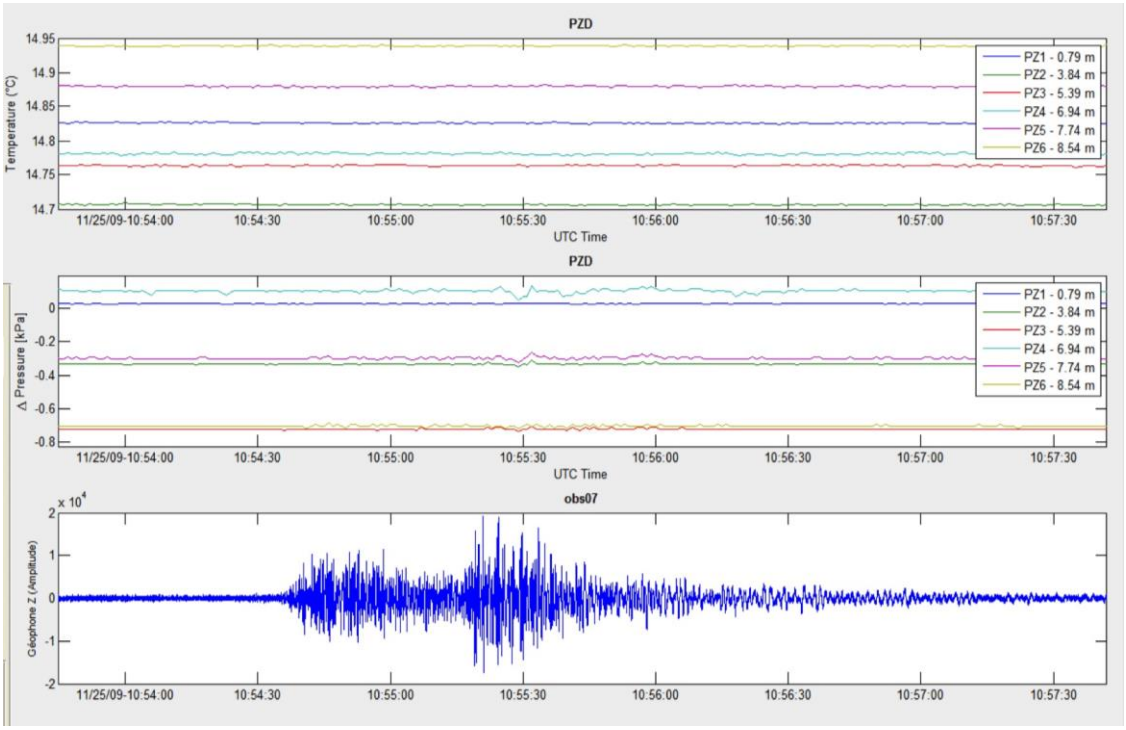

Figure 6.3.17: Temperature and pressure variation recorded at PZD along with ground velocity recorded on OBS 07, on November 25th 2009, at 10:54.

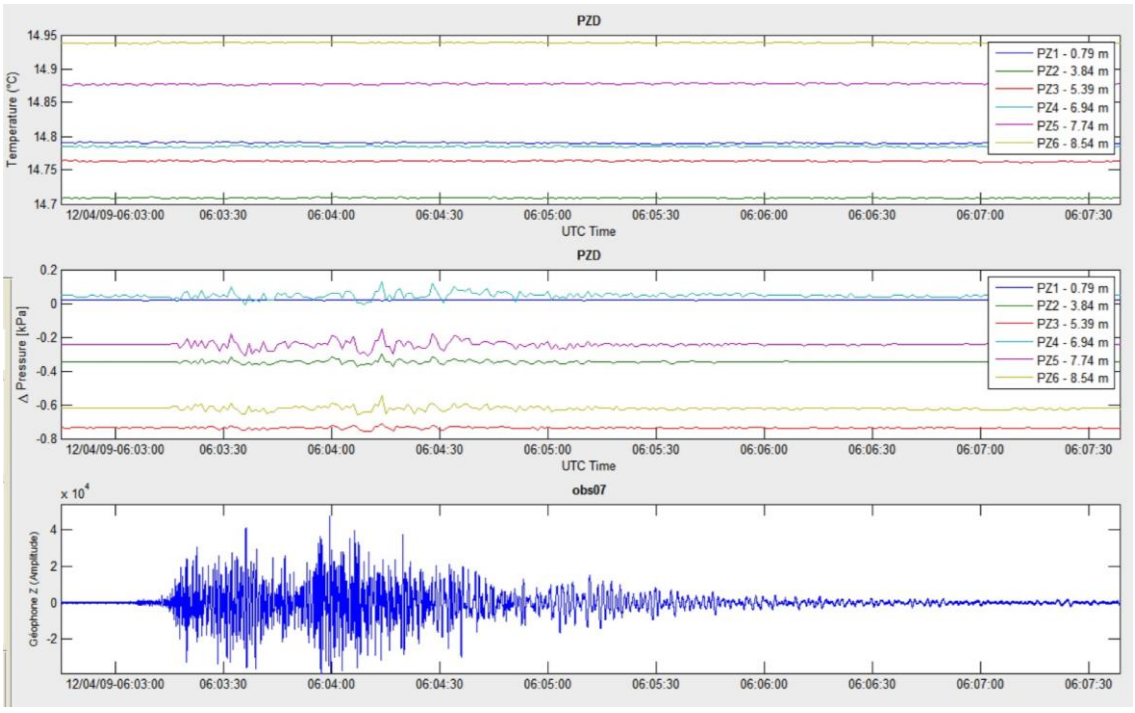

Figure 6.3.18: Temperature and pressure variation recorded at PZD along with ground velocity recorded on OBS 07, on December 4th, 2009, at 06:03.

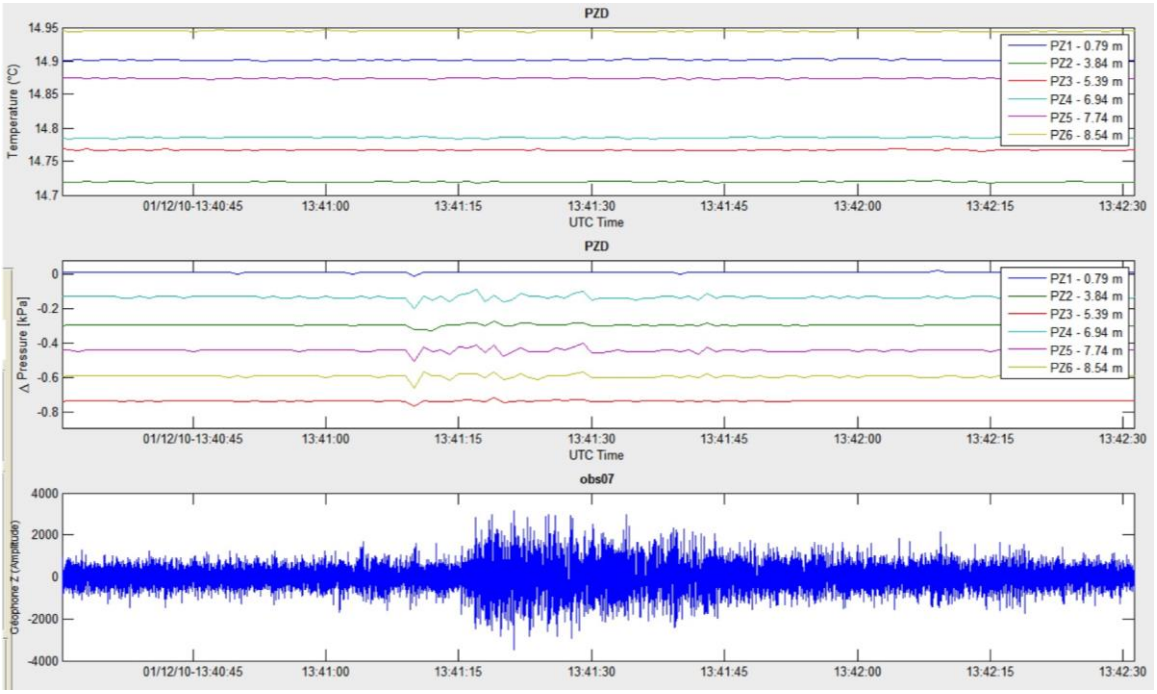

Figure. 6.3.19: Temperature and pressure variation recorded at PZD along with ground velocity recorded on OBS 07, on January 10th, 2010 at 13:41.

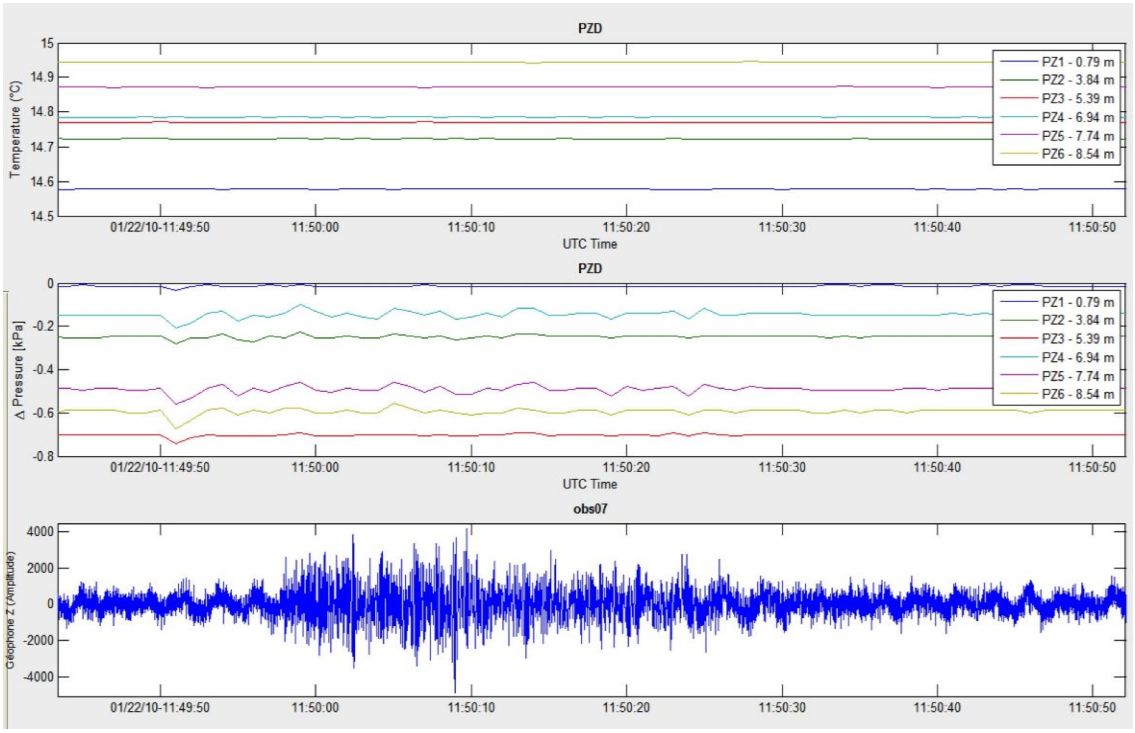

Figure 6.3.20: Temperature and pressure variation recorded at PZD along with ground velocity recorded on OBS 07, on January 22th, 2010 at 11:48.

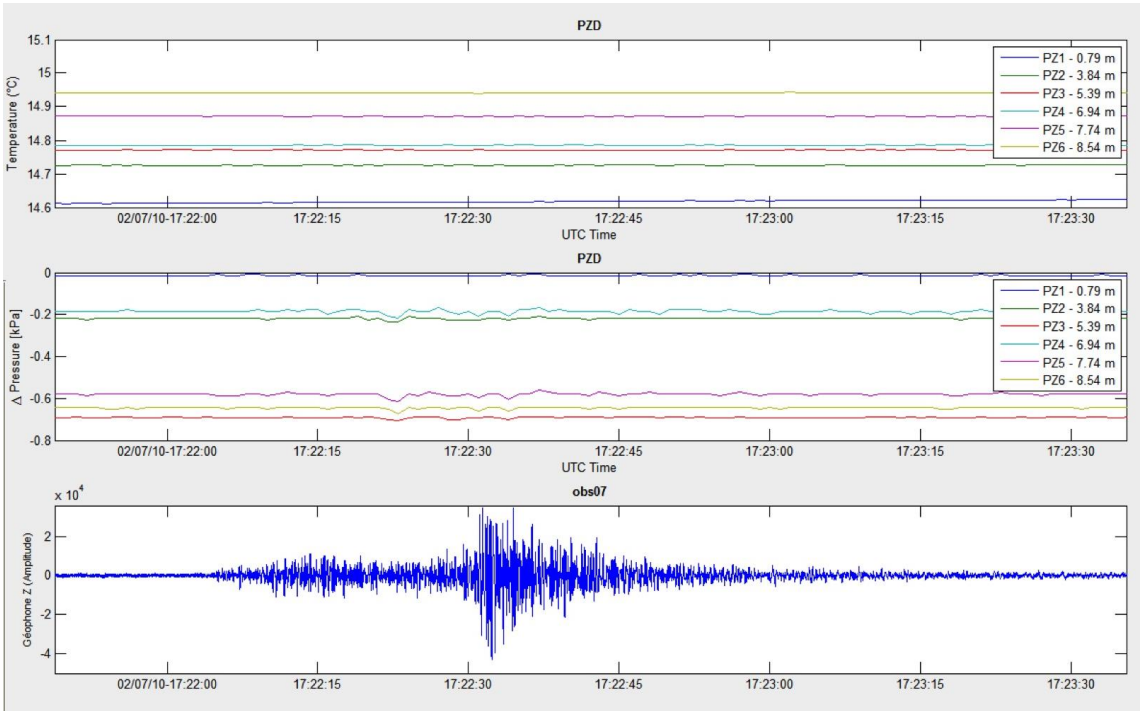

Figure 6.3.21: Temperature and pressure variation recorded at PZD along with ground velocity recorded on OBS 07, on February 7th, 2010 at 11:48.

7. Task7. Analysis of bottom pressure records

7.1 Fourier analysis of pressure records

A matlab function was designed to help visualize and analyze pressure records from various sources and varying sampling rate and is available on demand. The power spectrum is determined over a time window specified by the user. In order to avoid spurious oscillations in the spectrum a Gaussian apodization is applied to the signal in the selected window. A fast Fourier transform is then applied to the signal and the power spectrum computed and plotted. The part of the spectrum of interest may then be selected and spectral domain filtering applied to the data within the window:

[] = fft_window (filename, irec, nrec, center_hour, width)_

filename designates the data file to be processed. The file format is double precision binary matrix in column order with nrec lines and no header. The first line of the matrix is the time in hours. Synchronized data time series are on the following lines; irec is the line number of the time series to be processed; center_hour is the center of the time window; width is the full width at half maximum of the Gaussian defining the time window. The FFT will be performed on a window at least twice the width of the Gaussian.

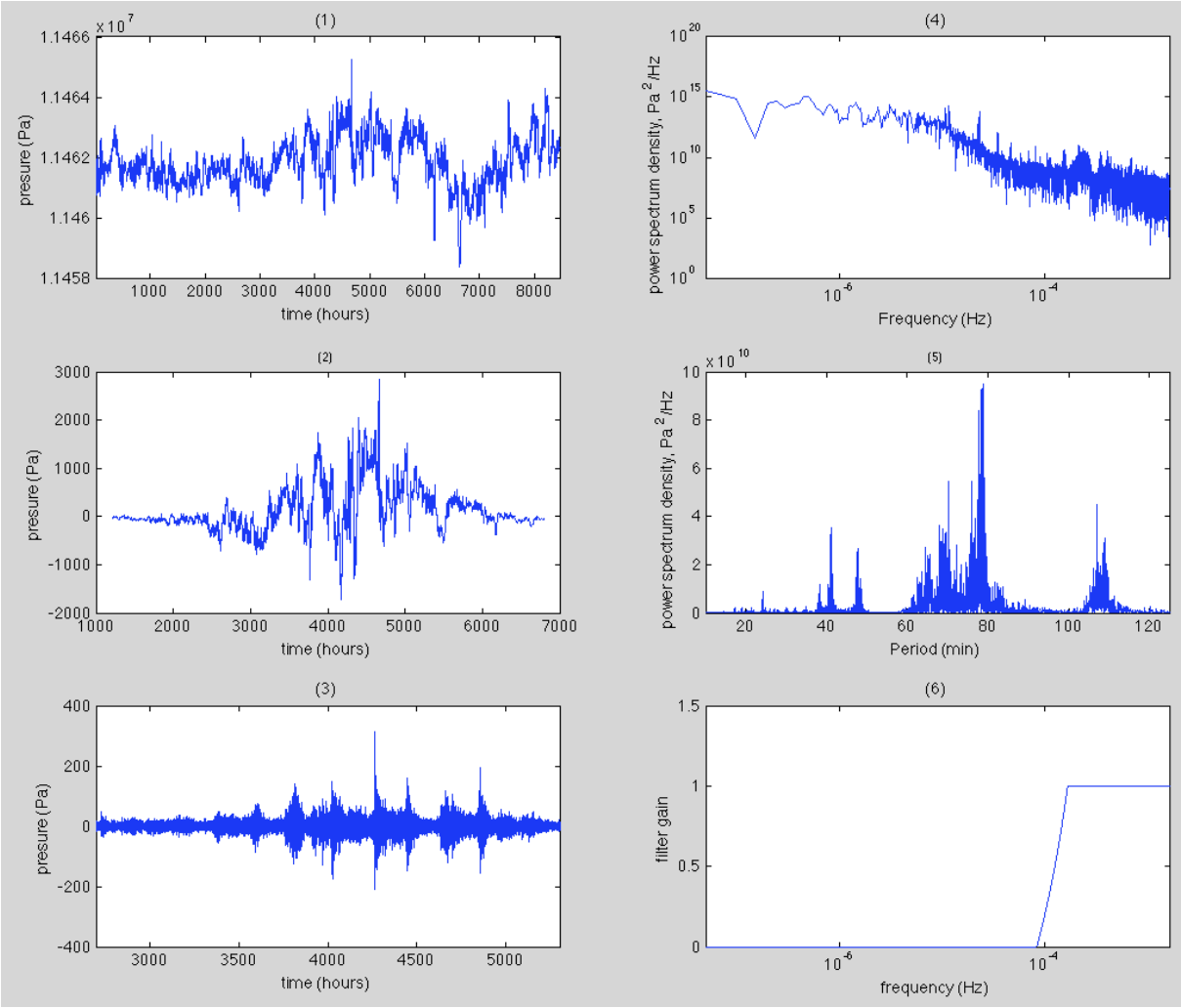

Figure 7.1.1 : example of output of fft_window applied to Tekirdag BPR data. 1) raw signal recorded between 17/05/2007 and 03/05/2007 2) windowed signal, window is centered at 4000 hour and the signal is weighted with a Gaussian function 1300 hour wide at half maximum 3) high pass filtered signal 4) full power spectrum calculated from windowed signal 5) power spectrum plotted as a function of period in the 10 to 125 minutes range 6) high pass filter applied in the spectral domain

7.1 Analysis of absolute pressure records

The bottom pressure record acquired in Tekirdag Basin over a one year period displays a chaotic signal with a range of variations of 60 hPa that likely represent regional atmospheric pressure variations. The seasonal variation of average atmospheric pressure is not more than 10-15 hPa in Istanbul, but the 60 cm (60 hPa) amplitude represents the variation between highest anticyclonic conditions (c.a. 1025 hPa) and the lowest pressure measured during a storm (c.a. 965 hPa)

. Tides are, however, present in the power spectrum with one main peak at 23.9 hour corresponding to diurnal tidal harmonics K1 and a smaller one at 25.883 corresponding O1, as

well as smaller peaks at 12 hours and 12.427 hours corresponding to semi-diurnal harmonics S2 and M2. Tides vary between diurnal and semi-diurnal regime and maximum tide amplitudes (between highest and lowest diurnal tides) is 11 hPa (11 cm). When a high pass filter with a cut off frequency of 8.3 10-5 Hz (200 minutes period) is applied, bursts of oscillations with an amplitude of a few hPa (corresponding to a few cm of hydraulic head) become prominent. These bursts were more frequent and with higher amplitude in autumn (October-November) and spring (March-April).

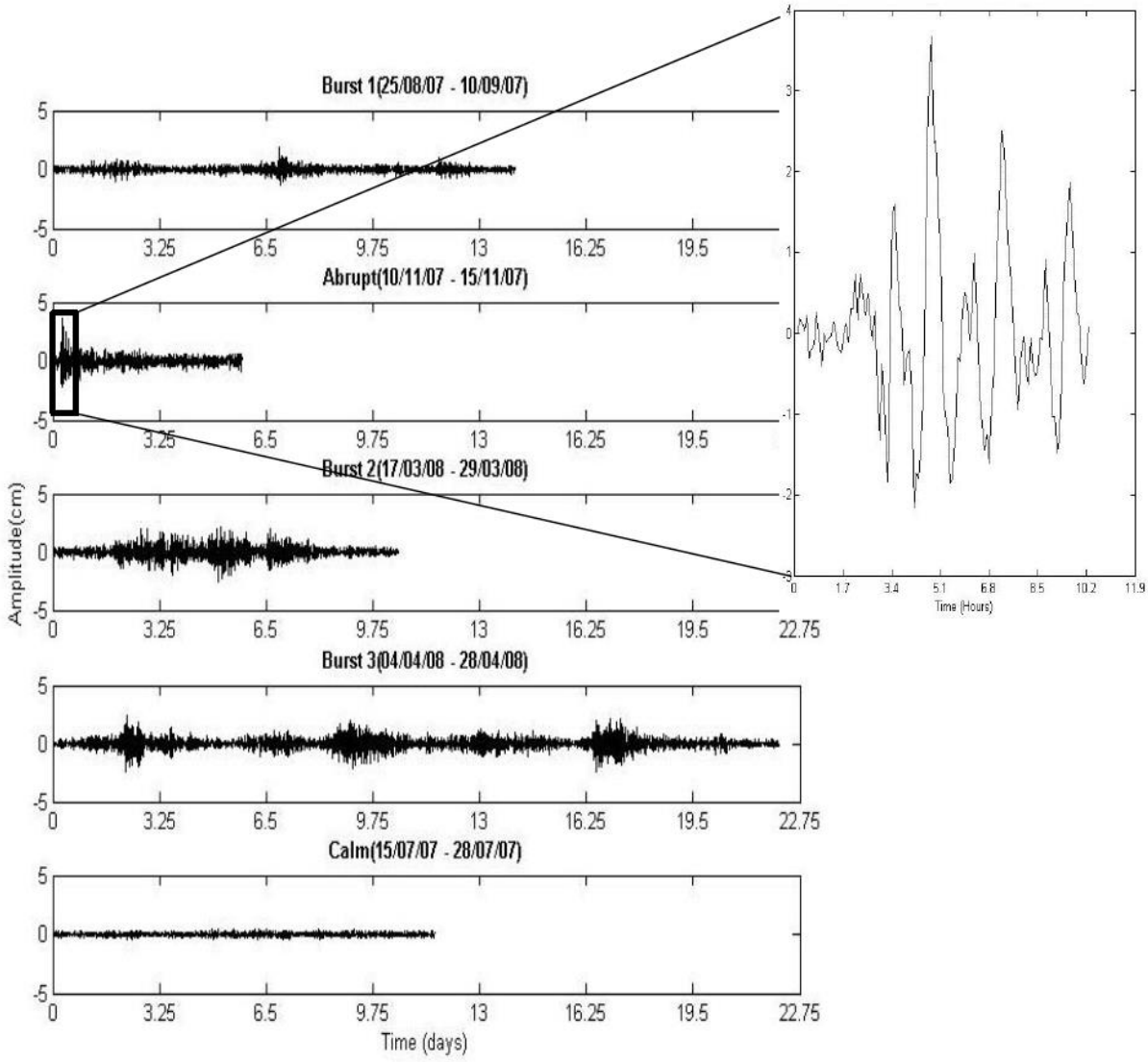

Figure 7.1.1: High passed (maximum period 200 minutes) bottom pressure records from Tekirdag Basin, showing burst of oscillation of a few cm (hPa) amplitude and compared with a quiet interval in the signal. The event on 10/11/07 has notably abrupt onset and a main oscillation frequency of 78 minutes.

Fourier transform was applied to time windows of several days in order to calculate amplitude spectra (Figure 7.1.2). The spectra obtained display sharp peaks at periods 24, 38, 41, 78 and 110 minutes. The amplitudes of the peaks vary between successive bursts of oscillation, but

the frequency at the peak remains constant. This suggests that the characteristic frequencies correspond to resonant frequencies of normal mode oscillations in the Sea of Marmara. The trigger of the oscillations, here, is likely atmospheric, possibly by coupling with wind energy, as the higher amplitudes observed in autumn and spring would suggest. Landslides and earthquakes in the Sea of Marmara may excite the same modes of oscillation.

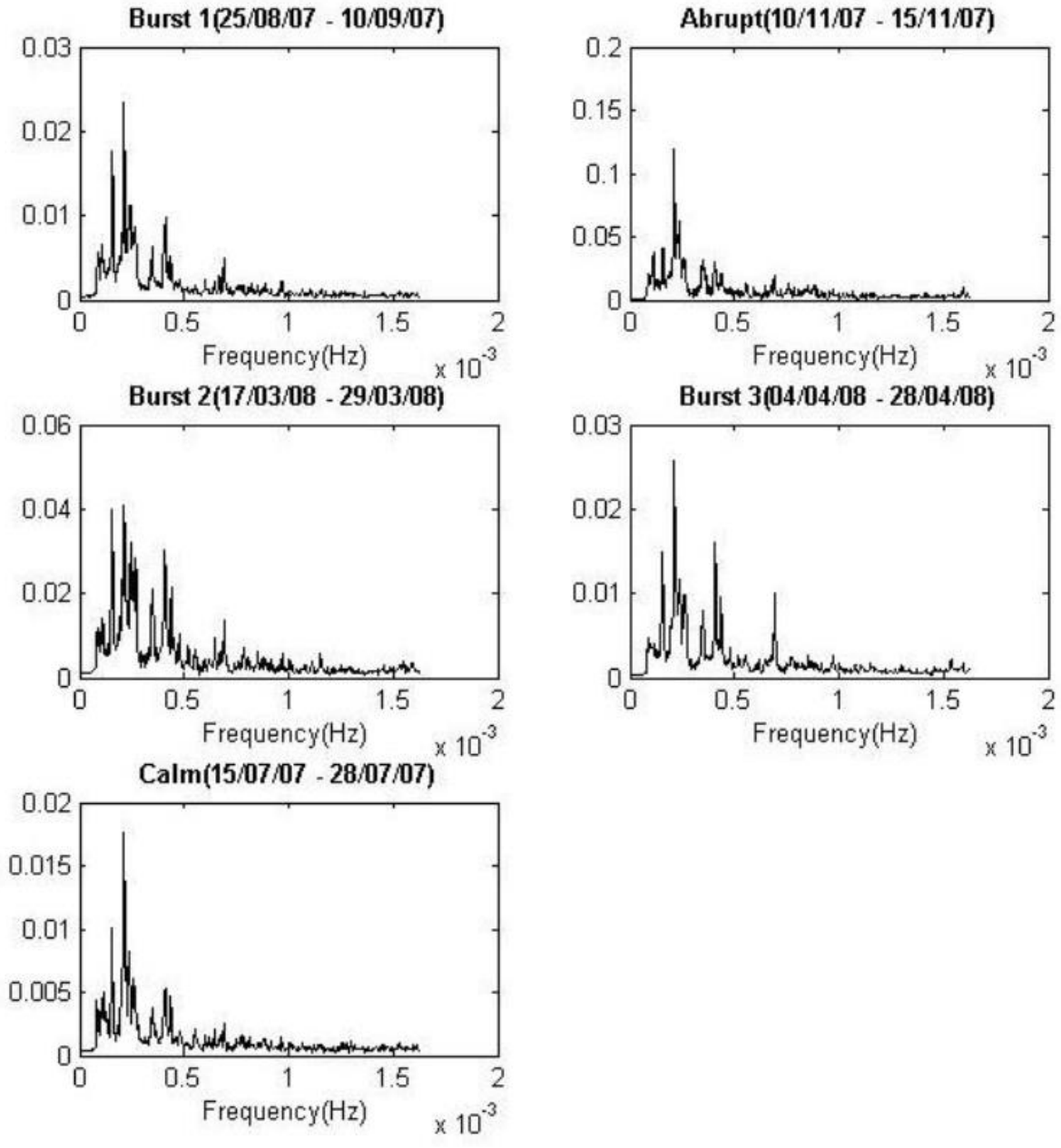

Figure 7.1.2 : Power spectra of selected time windows (in hPa^2/Hz). Note the presence of sharp peaks interpreted as normal mode resonance frequencies of the Sea of Marmara.

7.2. Differential pressure gauge data

The ambient noise recorded on the Differential Pressure Gauge (DPG) from the KOERI

observatories comprises a high frequency component above about 0.1 Hz corresponding to microseismic noise, and a low frequency component corresponding to low frequency gravity waves affecting the water column, as generally observed in the ocean (Cox et al., 1985). The maximum frequency of gravity waves recorded at the seafloor depends on the water depth (e.g. Becel et al., 2011). For the Central Basin and Tekirdag Basin stations, set at about 1100 m water depth, the cut off frequency is at 0.03-0.04 Hz (about 30 s period). For the Imrali Basin station at about 300 m water depth, the cut off frequency is around 0.07 Hz (15 s). These cut off frequencies are consistent with theoretical wave base depth (d), which is about half of the wavelength and thus related to the period (T) as $d = (g/4\pi) T^2$. The microseismic noise in the 0.1 Hz to 2 Hz range is mostly caused by the interaction of sea waves with the seafloor on the continental shelf (Cox et al., 1984; Becel et al., 2013) but the passing waves from local earthquakes were also recorded. A magnitude 5.1 earthquake, which occurred July 25th, 2011 below the Western High, is recorded as an oscillatory signal on all three Sea Bottom Observatories with maximum energy in the 2-to-6 s period range. The maximum amplitude exceeds 2 kPa on the nearest stations in the Central Basin and Tekirdag Basin, located 15-20 km from the epicenter. A low frequency oscillation appears to follow the earthquake (figure 7.2.1) but its frequency is outside of the theoretical bandwidth of the sensor. It thus remains unclear whether this signal is noise of related to water column movements. The response of DPG sensors at low frequency is mechanically limited with a capillary shunt, which function is to prevent pressure build up caused by temperature variations from damaging the sensor (figure 7.2.1). It follows that such sensors are not optimal to study the coupling between earthquake and tsunami.

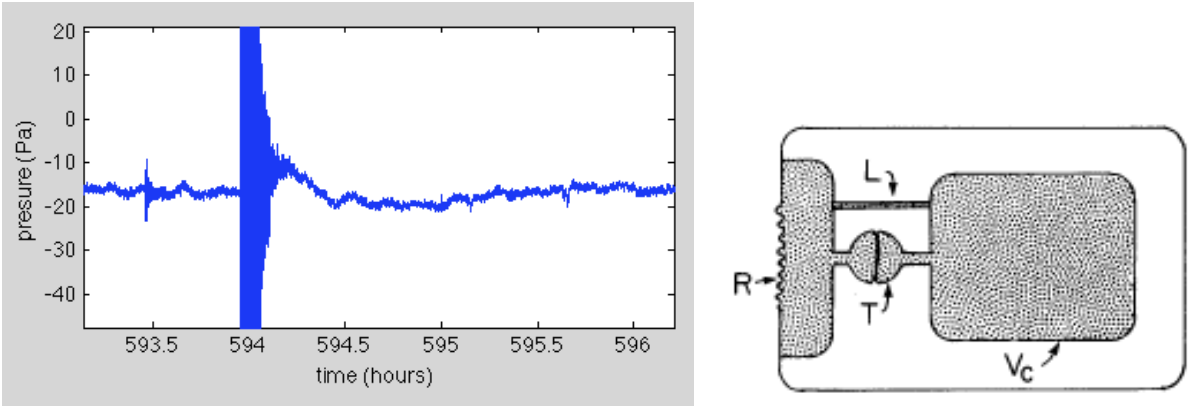

Figure 7.2.1: (Left) Pressure record of July 25th magnitude 5.1 earthquake, located below the western high, from DPG located in Tekirdag Basin (KOERI SBO 1356). (Right) Sketch of DPG (from Cox et al., 1985), R is membrane, Vc is pressure reference volume, T in sensor, L is capillary shunt limiting maximum period to 9 minutes.

7.3 Discussion

Seiche oscillations triggered by atmospheric perturbations can be detected with bottom pressure recorders. Coastal records appear to be affected by local resonance effects and, in the Sea of Marmara, by free oscillations of the Bosphorus and Dardanelles straights (Alpar and Yüce al., 1998). Pressure records of the tsunami alert system in the Sea of Marmara are available but retain noise from aliased sea waves that cannot be filtered out. It is thus unclear whether coastal records can be used to constrain basin modes of oscillations. A Digiquartz pressure sensor had been deployed for almost a year at the bottom of Tekidag basin in 2007 and burst of small amplitude pressure oscillations were observed. Power spectra display a prominent peak at 78 minutes and smaller ones at 41, 38 and 24 minutes. These preliminary results could be consistent with the lowest free oscillation frequencies estimated with tsunami models in the Sea of Marmara (72, 36, 25 minutes; Yalciner and Pelinovsky, 2007).

Several characteristics of turbidites observed in lakes or bowl-shaped basins have been explained by water column oscillations (seiche) (McHugh et al., 2011; Beck et al., 2007). Such deposits often consist of a basal coarse turbidite layer with multiple and lenticular sand/silt laminations and beds indicative of oscillatory current, followed by a homogeneous mud deposited from a large cloud of suspended fine particles. In theory, this opens the possibility of using hydrodynamic models to relate some characteristics of turbidite-homogenite deposits (volumes and distribution of sediment, grain size, number of sand layers) with characteristics of the tsunami events that shaped them (mode, amplitude, traction on the basin floor, number of oscillations) (e.g. Pritchard and Hogg, 2003; Jordi et al., 2008). One key question we will address is the scale dependence of these processes. Turbidite-homogeneite (TH) thickeness in the Sea of Marmara range from 10 cm to 10 m thickness. How would this translate in term of tsunami amplitude? Is seiche oscillation the likely process of TH deposition throughout the observed range of event size?

Currently available records are insufficient to answer these questions. A magnitude 5.1 earthquake, that may have induced some hydrodynamic effects, occurred during KOERI Sea Bottom Observatories (SBO), but the low frequency cut off DPG data is higher than the frequency of resonant water column oscillations. Monitoring the hydrodynamic response to earthquake and landslides would require the deployment of bottom pressure recorders with high accuracy (10 Pa) in the 10 mHz to 0.1 mHz range.

8. Conclusions

This study is a first step that provides significant progress towards the characterization of episodes of gas accumulation and release in shallow sediment layers, based on the combined interpretation of multi-parameter datasets.

A work flow was established for the acoustic data provided by BOB, that allows: i) the transformation of raw data in HAC format; ii) the visual analysis of echograms; iii) the computation of echo-integrations; iv) the representation of the echo-integration results (MVBS values) as polar diagrams on a georeferenced frame; v) the identification of gas bubbles sources and the analysis of their spatial and temporal variability; vi) the computation of gas bubbles flow rates.

In parallel, a software was developed to process and visualize different datasets from different sensors (except BOB data) simultaneously, over a large variety of time-scales, from a few seconds to a few days.

The data analysis carried out in the present study shows:

1. BOB is a powerful tool to detect gas bubble emissions, within a radius (~a few tens of meters) that directly depends on the acoustic frequency. The echo-integration method allows the characterization (flow rate, source location, etc) of gas emissions.
   - Gas bubble emissions at a given site may be continuous (over the duration of the survey) or transient, at a variety of time scales (minutes, hours, days).
   - In active tectonic settings (e.g. in the Cinarçik Basin), gas emission sites tend to follow tectonic lineations. Other factors, related to the sediment cover, also control gas emissions (e.g. in the Central High).

2. Seafloor monitoring using collocated OBS and acoustic gas bubble recorders (BOB) represent a very promising way to directly monitor gas related processes within the uppermost sediment layers:
   - Short-Duration Events (SDEs), having a duration of less than 1 second, are commonly observed on the OBS records (50 000 in average over the 3 months recording period).
   - The joint analysis of OBS data and BOB data confirms previous interpretations, that SDEs are directly related to gas bubble emissions from the seafloor.
   - Individual SDEs are not correlated from one OBS to the other. In contrast, crisis of SDEs have been simultaneously recorded on distant (> 20 km OBSs).
   - Crisis of SDEs may occur remotely (at distances of up to 10 km), in response to earthquakes of moderate magnitude (M~3 - 4). Seismic ground shaking is thus suspected to trigger gas outbursts from the seafloor.
   - However, the relevance of SDEs for geohazards monitoring is still not established. Additional work is required to know if the observed gas emissions are really significant or if they are simply a part of the background gas emission activity.

3. The piezometers have clearly recorded variations in sediment pore pressure triggered by transient, seismic signals. One case of correlation was also observed between the occurrence of SDEs and pore pressure decrease recorded at 5 m below seafloor. The quantitative relation between ground motions and pore pressure variations requires further investigation, through additional data acquisition and numerical modelling.

4. The present study suggests the following recommendations:
   - Multibeam, bathymetric surveys -on a regular, monthly or yearly basis- are strongly recommended to complement local BOB surveys, not only to determine the geographical distribution of gas emissions sources beyond the BOB acoustic range, but also to assess the temporal variability of gas emissions at the scale of months or years.
   - Sea-bottom currents may strongly affect the acoustic energy that is backscattered by the gas emission sources. Hence, current measurements are very much needed to help interpret the BOB echo-integration results.
   - With the present version of BOB, flow rates can be computed accurately only if the gas bubbles emitted by the source are all located within the insonified area of 7°. An acoustic system allowing the continuous insonification of a volume larger than the actual 7° is needed to compute the flow rates of wider sources. This may be done by replacing the actual split-beam echosounder of BOB with a multi-beam echo-sounder. Or, several split-beam echo-sounders may be used to insonify a larger area. Either solution will also greatly improve the joint analysis of acoustic and seismologic data.
   - Precise positioning (through a DP system) is needed for BOB and OBS deployments.

5. The Sea of Mamara is a unique natural laboratory to study degassing processes from the seafloor in response to seismic ground motions.
6. The acquisition of bottom pressure records in the 10 mHz to 0.1 mHz range within the deep basins is required for a better understanding of tsunami triggering in the Sea of Marmara and of the hydrodynamic processes shaping the turbidite-homogenites constituting the marine paleoseismological record. The currently available records are insufficient. Differential pressure gauges (DPG) that were deployed with Sea Bottom Observatory stations are not sufficiently sensitive above 2 mHz and the deployment of high accuracy (10 Pa) absolute pressure sensors is recommended.